al-Farabi Kazakh National University

UDC: 54.052, 54.058

SEITZHANOVA MAKPAL AZIZOVNA

Synthesis and application of membrane technology for desalination of seawater

6D074000 – Nanomaterials and nanotechnology

Dissertation submitted in partial fulfillment of the requirements for the degree of Doctor of Philosophy (PhD)

Scientific supervisors:

Doctor of Chemical Sciences, Professor,
Institute of Combustion Problems,
Z.A. Mansurov;

Ph.D. in Fundamental and Applied Physics,
University of Naples Federico II,
Roberto Di Capua;

Republic of Kazakhstan
Almaty, 2020

CONTENTS

NORMATIVE REFERENCES

In the present thesis, the following references for standards used:

State Standard 7.1-2003. Bibliographic record. Bibliographic description. General requirements and rules.

State Standard 7.32-2001. Report on scientific - research work. Structure and rules for formulation.

State Standard 12.1.008-76. Occupational safety standards system. Biological security. General requirements. Specifications.

State Standard 3885-73. Reagents and very pure substances. Sampling, packing, packing and marking.

State Standard 6709-72. Distilled water.

State Standard 8.417-81. State system for ensuring uniformity of measurements. Units of physical quantities.

State Standard 1770-74. Laboratory glassware measuring. Cylinders, beakers, flasks, test tubes. General technical conditions.

NOTATIONS AND ABBRIVIATIONS

AFM	– atomic force microscopy
CNT	– carbon nanotube
CRH	– carbonized rice husk
DI	– deionized
DMF	– dimethyl formamide
ED	– electrodialysis
FO	– forward osmosis
FTIR	– fourier-transform infrared spectroscope
GO	– graphene oxide
ICP-MS	– inductively coupled plasma - mass spectrometer
MED	– multiple-effect distillation
VC	– vapor-compression
MSF	– multi-stage flash distillation
NF	– nanofiltration
NMP	– N-Methyl-2-pyrrolidone
PEI	– polyethylimmide
PVA	– polyvinyl alcohol
PVDF	– polyvinylidene difluoride
PVP	– polyvinylpyrrolidone
RH	– rice husk
RO	– reverse osmosis
SEM	– scanning electron microscopy
SWRO	– seawater reverse osmosis
TEM	– transmission electron microscopy
TGA	– thermogravimetric analysis
UF	– ultrafiltration
XRD	– X-ray diffractometer

INTRODUCTION

General characteristics of the work

The work deals with obtaining of graphene based membranes from rice husk and application of these materials for desalination of seawater. The graphene based membranes were obtained by vacuum filtration and immersion precipitation method. The physical and chemical properties of membranes were studied. The desalination properties of membranes were successfully tested for the following salts: NaCl, KCl, $MgCl_2$, $CaSO_4$ and $MgSO_4$.

Actuality of the theme

According to the estimates of the Asian Development Bank, the average volume of drinking water supplied to the population is decreasing at a rate of 3-5% per year due to the continuing deterioration of the existing infrastructure. One of the most promising approaches to solving the problem of water scarcity is the desalinization (desalination) method, which can provide high-quality water without harming natural freshwater ecosystems. Sea water makes up 97.5% of all water on the planet. To date, desalination of sea water has been carried out mainly with the help of multi-stage distillation and reverse osmosis. These types of desalination plants consume large amounts of heat and electricity, resulting in a significant amount of greenhouse gases. Desalination of sea water on a large scale, more than 50% of the total volume, is provided by reverse osmosis systems, due to technical efficiency. However, this technology requires high capital costs, which complicates its widespread use.

In this regard, the relevance of the research topic of the doctoral dissertation on the development of a method for producing new graphene membranes from rice husks and the study of their physicochemical and desalination properties is undoubtedly relevant.

The purpose of research: The purpose of this work is to obtain graphene materials from rice husks by thermochemical activation and their use in the making of nanoporous membranes for desalination of seawater. To achieve this goal, the following tasks were accomplishment:

1) Obtaining graphene materials from rice husk. Development of optimal conditions for carbonization and activation, selection of the composition for obtaining nanoporous graphenes from rice husk;

2) Study of the physicochemical properties of the obtained graphene materials;

3) Production of membranes from the obtained graphene;

4) Study of the desalination properties of graphene membranes for various salts using membrane technology.

The main provisions for the defense of the thesis:

1. Carbonization of rice husk and activating agent at a ratio of 1:5 (g/g) results in a 4-5-layer graphene structure. It was found that such an activation ratio of 1: 5 is optimal and provides a higher graphene content than other ratios of rice husk and activating agent.

2. FTIR results showed that the functionalization of graphene with sulfuric acid for 24 hours leads to the introduction of sulfonic groups in the membrane.

3. Graphene membranes obtained from rice husk by vacuum filtration desalinate seawater to 99%.

The object of research: rice husk, graphene oxide, graphene oxide membranes.

The subject of research: Obtaining graphene materials by pre-carbonization followed by chemical activation of rice husk, and evaluate the characteristics of the material for possible use in the desalination process. Analyze the ability of graphene-based membranes to convert salt water into pure water using suitable membrane technology.

Scientific novelty of research:

For the first time, the following results were obtained:

– A new simpler and more environmentally friendly method is proposed for producing graphene materials from rice husks by carbonation and chemical activation. Graphene materials were obtained and investigated.

– The maximum specific surface area of graphene materials determined by the BET method was 2818 m^2/g. The study of the surface and sorption properties of materials obtained under various conditions using modern methods made it possible to identify patterns of synthesis of graphene materials depending on temperature (850°C) and time (2 h) of carbonization and chemical activation with KOH (1/4 and 1/5).

– Physico-chemical studies of synthesized graphene membranes based on rice husks showed the possibility of obtaining new nanoporous membranes for desalinization (desalination, desalination) of seawater.

The theoretical significance. The main regularities of synthesis of membranes based on graphene and graphene oxide by vacuum filtration and immersion precipitation were established.

The practical significance.

- For the first time, graphene materials from rice husks in Kazakhstan were obtained.

- The optimal conditions for manufacturing membranes by vacuum filtration from graphene materials obtained from rice husks were determined.

- Membrane flows and deviations of five saline fluids (NaCl, KCl, $MgCl_2$, $CaSO_4$ and $MgSO_4$) were tested using a conventional filtration system at room temperature. It was revealed that membranes based on graphene materials obtained from rice husks desalinate sea water to 99%.

Reliability of the results

The validity of the conclusions and the reliability of the results are due to the use of a wide range of modern physicochemical methods: X-ray diffraction, scanning electron microscopy, transmission electron microscopy, Raman spectroscopy, IF-spectroscopy, thermogravimetric analysis, atomic absorption flame emission spectrophotometer.

Conclusions on the basis of the obtained experimental data:

1. Received graphene materials from rice husks. It was found that carbonization / activation of rice husk leads to the formation of a mixture of graphene layers and amorphous carbon. With the optimal ratio of rice husk and activating reagent (1:5), the relative amount of graphene component increases. The results of Raman spectroscopy

indicate that in the samples Gr(1/5) and Gr(1/4) the ratio I_G/I_{2D} is close to 1.56 ± 0.10, which corresponds to the 4-5 layer state of the graphene film.

2. It was found that the obtained graphene material is highly porous with an average pore size <100 nm, contains 80-90% carbon and has a specific surface area of 2500-3000 m^2/g.

3. Graphene membranes deposited on a cellulose acetate membrane were obtained by vacuum filtration and immersion deposition. It was found that the membranes obtained by vacuum filtration have a more microporous and nanoporous structure with a dense upper layer and water permeability of 4, 5 and 30 ml/min compared with membranes obtained by immersion deposition.

4. Desalination properties of graphene membranes were tested for salts of NaCl, KCl, $MgCl_2$, $CaSO_4$ and $MgSO_4$. It was revealed that after filtration of salt solutions through graphene membranes, their concentration decreases to 99.5% (NaCl), 99.8% (KCl), 99.5% ($MgCl_2$), 77.6% ($CaSO_4$) and 99.3% ($MgSO_4$).

Relation to the plan of state research programs

This dissertational work was carried out without any framework.

Approbation of thesis

The materials of the thesis were reported and discussed at various international conferences and symposiums:

- 3rd International Conference on Desalination using Membrane Technology (Palacio de Congresos de Canarias, Las Palmas, Gran Canaria, Spain, 2-5 April 2017);
- Conference of Students and Young Scientists "Problems of Technological Combustion" (Al-Farabi Kazakh National University, Almaty, Kazakhstan, December 22, 2016);
- II Conference of Students and Young Scientists "Chemical Physics and Nanomaterials" (Al-Farabi Kazakh National University, Almaty, Kazakhstan, March 10, 2017);
- 3rd International Conference on Surfaces, Coatings and Nanostructured Materials – ASIA (City University of Hong Kong, Hong Kong SAR, PR China, 4-7 December 2017);
- Conference of students and young scientists dedicated to the 30th anniversary of the establishment of the Institute of Problems of Combustion (Almaty, Kazakhstan, November 30, 2017);
- III Conference of students and young scientists “Chemical physics and nanomaterials” (Almaty, Kazakhstan, 15 March 2018 and 19 March 2019).

The personal contribution of author is in carrying out experiments, summarizing and interpreting the obtained results, writing articles and reports.

Publications. The results of the thesis are reflected in 16 scientific papers, including:

- 1 scientific articles, published in journals having an impact factor according to the Scopus data base;
- 3 scientific articles, published in journals recommended by the Committee for Control in the Sphere of Education and Science of the Ministry of Education and Science of the Republic of Kazakhstan;

- 11 oral abstract presentations at international conferences and symposia;
- 1 innovative patent of the Republic of Kazakhstan for a utility model.

Volume and structure of the thesis. The thesis is presented in 85 pages and includes 49 Figures, 14 Tables, 5 formulas. The work consists of introduction, literature review, description of objects and methods of research, results and discussion, conclusion and list of references including 112 names.

1 LITERATURE REVIEW

1.1 Sea water

The global problem of humanity is the problem of obtaining fresh water. Freshwater scarcity is felt in more than 40 countries located in the arid regions of the globe, and accounts for about 60% of the earth's surface. World water consumption at the beginning of the XXI century reached 120-150*10^9 m^3 per year. The growing global shortage of fresh water can be offset by desalination of salty (salinity greater than 10 g/l) and brackish (2-10 g/l) ocean, marine and groundwater.

Fresh water is a valuable component of seawater. The shortage of fresh water is increasingly felt in industrialized countries such as the United States and Japan, where the need for fresh water for household needs, agriculture and industry exceeds the available reserves. In countries such as Israel or Kuwait, where rainfall is very low, freshwater supplies do not meet its needs, which are growing due to the modernization of the economy and population growth. In the future, humanity will face the need to consider the oceans as an alternative source of water.

A huge layer of salt water, covering most of the Earth, is a single whole and has an approximately constant composition. The ocean is huge and production reaches 1.35 billion cubic meters. It covers about 72% of the Earth’s surface. Almost all water on Earth (97%) is in the oceans. About 2.1% of the water is concentrated in polar ice and glaciers. All fresh water in lakes, rivers and in groundwater is only 0.6%. The remaining 0.1% of the water consists of salt water from wells and living water [1].

Sea water is often called salty. The salinity of seawater is the mass (in grams) of dry salts in 1 kg of seawater. In the oceans, salinity ranges from 33 to 37, on average it can be considered equal to 35. This means that seawater contains approximately 3.5% dissolved salts. The list of elements contained in seawater is very large, but the concentration of most of them is very low. Table 1 shows 11 ionic particles present in seawater at concentrations exceeding 0.001 g/kg, i.e. 1 millionth part (ppm) by mass. Among the substances contained in seawater in slightly lower concentrations (from 1 to 0.01 h/m), there are elements nitrogen, lithium, rubidium, phosphorus, iodine, iron, zinc and molybdenum. At least 50 other elements were found in seawater at even lower concentrations [2-6].

Since people began to monitor the composition of ocean water, it remains unchanged. The constancy of the composition of water in the oceans indicates a balanced process of water intake and removal. River water constantly flows into the oceans, which have a completely different mineral composition than ocean water. For example, weathering of rocks leads to the appearance of aluminum, silicon, iron or calcium in river water. In sea water, these elements are gradually included in the biological cycle or removed from it as a result of sedimentation. Therefore, the average content of many elements in ocean water is established as a result of the equilibrium between the rate of processes of these elements entering the sea water and their removal from it. This explains the more or less constant composition of ocean water [7, 8].

Table 1 – Ionic substances contained in seawater in concentrations above 0.001 g/kg (1 ppm) by weight [9]

Ionic substance	Content, g/kg	Concentration, mol/l
Chloride ion	19.35	0.55
Sodium ion	10.76	0.47
Sulfate ion	2.71	0.028
Magnesium ion	1.29	0.054
Calcium ion	0.412	0.010
Potassium ion	0.40	0.010
Carbon dioxide	0.106	$2.3 \cdot 10^{-3}$
Bromide ion	0.067	$8.3 \cdot 10^{-4}$
Boric acid	0.027	$4.3 \cdot 10^{-4}$
Strontium ion	0.0079	$9.1 \cdot 10^{-5}$
Fluoride ion	0.001	$7 \cdot 10^{-5}$

The composition of seawaters has a significant impact on the plants and animals that exist in it. The simplest link in the food chain are the smallest phytoplankton plants, in which CO_2, water and other nutrients are converted into organic matter through photosynthesis. Analysis of the composition of phytoplankton shows that it contains carbon, nitrogen and phosphorus in an atomic ratio of 108:16:1. Thus, on the basis of one phosphorus atom (usually present in the form of hydrophosphate ion HRO_4-and 16 nitrogen atoms (in the form of nitrate ion), 108 CO_2 molecules are required. Due to its high solubility in seawater, CO_2 is always in excess, so the concentration of nitrogen or phosphorus has a limiting effect on the rate of formation of organic matter in the process of photosynthesis [10].

Concentrations of nitrate and hydrophosphate ions are in a complex relationship with ocean currents and many other factors, the most important of which are vertical mixing of water. The latter is explained by the fact that the deep ocean waters are richer in phosphorus and nitrogen compared to surface water. Photosynthesis occurs near the surface, in the photosynthesis zone, where the sun's rays penetrate quite intensively. As a result of photosynthesis, the concentration of phosphate and nitrate ions decreases in the upper layer of seawater with a depth of about 150 m. In deeper layers, the concentration level of these ions is restored due to the decomposition of dead plants and animals. Since oxygen is released during photosynthesis, its concentration in the photosynthesis zone is high. At great depths, the oxygen concentration decreases sharply, since it is spent on the oxidation of dead plant and animal organisms. The oxygen concentration is minimal at a depth of about 1 km, in the same area where the phosphorus concentration is restored to the maximum level [11].

1.2 Desalination – past, present, future

Desalination is a process that takes away mineral components from saline water. More generally, desalination refers to the removal of salts and minerals from a target substance [12], as in soil desalination, which is an issue for agriculture [13, 14].

Desalination has been known in history for millennia as both a concept and a subsequent practice, albeit in a limited form. The ancient Greek philosopher Aristotle observed in his work Meteorology that "salt water, when it turns into steam, becomes sweet, and steam does not form salt water when it condenses", and also observed that a thin wax vessel would have drinking water after being immersed in seawater long enough, acting as a membrane to filter the salt [15]. There are many other examples of desalination experiments in antiquity and the middle ages [16], but desalination was never possible on a large scale until the modern era [17].

Before the industrial revolution, desalination was primarily concerned with ocean vessels, which otherwise would have to have fresh water on board. When the “tread” (frigate of 1779) was sold to Denmark in the 1780s (as the Hussaren ship), the desalination plant was studied and recorded in great detail. In the newly formed United States, Thomas Jefferson cataloged thermal methods dating back to the 1500s and made practical recommendations that were published for all US vessels based on sailing permits. Significant research on improving desalination techniques has been conducted in the United States after World War II. The Saltwater Office was created at the United States Department of the Interior under the Saltwater Transformation Act of 1952. It has been integrated into the Office of Water Research. Research has also been done at California state universities, and then at the Dow Chemical Company and DuPont. Many studies are devoted to methods for optimizing desalination methods [18]. Desalination technologies have been commercially available since 1960, and most of them were based on thermal processes. Later, multi-stage flash distillation processes (MSF) became popular, and the Arabian Gulf became the main area for the establishment of many commercial plants [19]. In the late 1960s, membranes entered the desalination market and were originally used to purify brackish water. Desalination became a fully commercial enterprise and the development of both thermal and membrane technology by the 1980s, which led to an exponential increase in world desalination capacities. The distribution of desalination capacities around the world is given in the table [20].

Table 2 – Top 10 countries employing desalination technologies [20].

No.	Country total	Capacity (million m^3/d)	Market share (%)
1	Saudi Arabia	9.9	16.5
2	USA	8.4	14.0
3	UAE	7.5	12.5
4	Spain	5.3	8.9
5	Kuwait	2.5	4.2
6	China	2.4	4.0
7	Japan	1.6	2.6
8	Australia	1.2	2.0

Desalination has become a suitable technology for drinking water in many other countries of the world, but in no other region of the world has desalination been as widespread as in the Middle East. In Europe, Spain and Italy use the main percentage

of desalination capacity [21].

Spain has used desalination since 1964 to provide drinking water to the Canary Islands, the Balearic Islands, and along the southern and Eastern coasts [22-24].

Currently, the world desalination market is dominated by reverse osmosis of seawater (SWRO) [25], based on installed capacity, surpassing thermal technologies (MSF and MED), which are common in the regions of the Gulf Cooperation Council (GCC) and the Middle East and North Africa (MENA); Of the installed desalination capacity in 2015, 86.5 mm^3/day, the share of RO (compared to other processes) and the use of sea water (compared to other sources) are 65% and 59%, respectively. While the annual installed capacity of the SWRO currently dominates thermal technology worldwide, its appearance in the GCC-MENA region, especially in the Arabian Gulf, has been slow due to the higher salinity of the nutrient waters, which are affected by hydrocarbons and red events tides. With the integration of energy recovery devices (ERD) in SWRO in the early 1990s, which were considered destructive technology at the time, the specific energy consumption was significantly reduced from 5 to 10 $kW \cdot h/m^3$ to its current 3-4 $kW \cdot h/m^3$ with the most effective ERD systems [26]; most of this energy (about 85%) is associated with the SWRO process itself, with lower energy requirements (about 15%) for other components of the SWRO system (i.e., input, pre-processing, and post-processing). While opportunities exist to reduce the energy consumption of pre-processing, our discussion of energy will focus on the most energy-intensive component of the system, the RO process itself. Double media filtration (DMF) remains the traditional pretreatment process, however, integrated membrane systems (IMS) with ultrafiltration pretreatment (UF), UF-SWRO, are becoming more common [27], especially for hard-to-handle waters. Both UF and dissolved air flotation (DAF) are receiving increasing attention for their potential stability during red tide events (harmful algal blooms (HABs)) (for example, tested in the Arabian Gulf) [28]. It has recently been shown that subsurface fences provide a significant degree of pretreatment as a biological filter to remove biodegradable organic carbon and reduce the associated biofouling of the RO membrane [29]. Effective pre-treatment can affect the energy of the RO stage by reducing fouling. Given the almost endless supply of seawater, SWRO installations usually operate as single-pass systems with a recovery of 35-60%; some installations include a second (split stream) passage to remove boron [30]. The addition of acid and / or anti-scalant is continued to be worked out to control scaling of both chlorine and sodium bisulfite for fouling control, although interest in alternative pre-disinfectants is increased: chloramines (transferred through the Ro membrane according to the residual principle) or chlorine dioxide (followed by sodium bisulfate prior to the membrane), as practiced in the Tampa Bay desalination plant. SWRO trends include higher power objects (e.g. Sorek facility in Israel, 624 MLD (2013)), larger elements (16-in.), Vertical orientation for RO membrane modules and pressure vessels (allow air to be scraped off), and improved operations (dirty control and sensors). While current SWRO practices serve the desalination industry well, it remains an energy-intensive technology with significant environmental impacts.

Advances in desalination technology are closest in dynamics to computer technology, and like computers, SWRO membranes are many times smaller, more productive and cheaper today than the first working prototypes. Traditional technologies, such as deposition and filtration, have made modest progress since their initial use for water purification several centuries ago; but every few years, new, more efficient desalination membranes, innovative thermal membranes or hybrid desalination technologies, as well as equipment improvements, are produced. No major technological advances are expected to significantly reduce the cost of seawater desalination in the next few years. However, it is expected that the continued reduction of production costs in combination with rising costs for water treatment due to more stringent regulatory requirements will accelerate the current trend towards an increasing reliance on the ocean as a water source. It will also make the desalination of water in the ocean is a credible alternative to drought for many coastal communities around the world. It is expected that technological advances will reduce the cost of desalinated water by 20% over the next five years and up to 60% over the next 20 years, making it a viable and cost-effective competitor in the production of drinking water [31].

1.3 Desalination methods and technology

In recent years, new alternative methods have been proposed for desalination of sea water due to exposure to ultrasound, acoustic, shock waves, electromagnetic fields, etc. [32]. The variety of existing methods for producing fresh water is explained by the fact that none of them can be considered universal, acceptable for these specific conditions. All methods of obtaining fresh water from the sea can be divided into two main areas:

1. Methods in which there is no change in the state of aggregation: chemical desalination, ion exchange, electrodialysis, direct osmosis and reverse osmosis.

2. Methods associated with a change in the state of aggregation of a substance: distillation and freezing.

1. Chemical desalination. In the chemical method of desalination, special precipitating agents are introduced into sea water, which, when interacting with salt ions dissolved in it (chlorides, sulfates), form insoluble compounds that precipitate. Due to the fact that sea water contains a large amount of dissolved substances, the consumption of reagents is very significant and amounts to about 3-5% of the amount of desalinated water. Substances capable of forming insoluble compounds with sodium ions (Na^+) and chlorine (Cl^-) include silver (Ag^+) and barium (Ba^{2+}) salts, which form silver chloride (AgCl) and barium sulfate precipitating during the treatment of salt water ($BaSO_4$). These reagents are expensive, the precipitation reaction with barium salts proceeds slowly, and barium salts are toxic. Therefore, chemical deposition during desalination is very rarely used.

1. Chemical desalination. In the chemical method of desalination of water, special precipitating agents are introduced into seawater, which in interaction with dissolved salt ions (chlorides, sulfates) forms insoluble compounds that precipitate. Due to the fact that sea water contains a large amount of dissolved substances, the consumption

of reagents is very significant and is about 3-5% of the amount of desalinated water. Substances capable of forming insoluble compounds with sodium (Na^+) and chlorine (Cl^-) ions include silver (Ag^+) and barium (Ba^{2+}) salts, which form silver chloride (AgCl) and barium sulfate precipitated during salt water treatment ($BaSO_4$), these reagents are expensive, the barium salt precipitation reaction is slow, and barium salts are toxic. Therefore, chemical deposition during desalination is used very rarely.

2. Distillation. Water distillation is based on a difference in the composition of water and the vapor generated from it [33]. The process is carried out in special distillation plants-desalination plants by partial evaporation of water and subsequent condensation of steam. During the distillation process, a more volatile component (low boiling point) passes into the vapor phase in greater quantity than a less volatile component (high boiling point). Therefore, upon condensation of the resulting vapors, low-boiling compounds pass into the distillate, and high-boiling components into a fixed residue. If not one fraction, but several is distilled off from the initial mixture, then distillation is called fractional. Simple and molecular distillation are distinguished depending on the process conditions [34].

Distillation desalination plant consists of an evaporator equipped with a heat exchanger for supplying the necessary amount of heat to water; a heating element for partial condensation of steam leaving the evaporator (during fractional distillation); a condenser for condensing the exhaust steam; a pump; distillate and bottom collectors [35].

Modern distillation desalination plants are divided into single-stage, multi-stage with tubular heating elements or evaporators, multi-stage with instantaneous boiling and vapor compression.

The main advantage of multi-stage distillation desalination plants is that a much larger amount of demineralized water can be produced per unit of primary steam. Therefore, at one-stage evaporation on 1 ton of primary steam about 0,9 tons of desalinated water turn out, and in installations with 50-60 stages 15-20 tons of desalinated water turn out. Specific power consumption at distillation plants is 3.5-4.5 kWh/m^3 of distillate.

The costs associated with the implementation of any version of the distillation process are associated with high costs of thermal energy, amounting to 40% of the cost of the resulting water (if the distillation is carried out in a vacuum, the boiling point of the water falls to 60°C and distillation requires less heat). Nuclear and thermal power plants are used as sources of thermal energy. The combination of a distillation plant with a thermal power plant using mineral or nuclear fuel, the so-called multi-purpose power plant, allows the industrial zone to provide all kinds of energy services with the lowest cost and the most efficient use of fuel. Solar desalination plants are used in the desert southern areas and on the waterless Islands; they produce in the summer months about 4 liters of water per day from 1 m^2 of the surface, which receives solar radiation.

The efficiency of distillation evaporators is limited by the formation of scale in the hot brine circulation system. When seawater evaporates from the distillation desalination plant, the salt solution becomes more concentrated and eventually precipitates on the walls of the apparatus in the form of hardness salts consisting mainly

of chlorides and carbonates of calcium ($CaCO_3$, $CaCl_2$) and magnesium ($MgCO_3$ $MgCl_2$) [36], which degrades the thermal conductivity of the walls of the heat exchanger, leading to the destruction of pipes and heat exchange equipment. For this purpose it is necessary to use special anti-pressure additives, which significantly increases the energy consumption for distillation up to 10 kWh/m^3 of demineralized water. Therefore, in recent years, other methods of desalination of seawater that are not associated with the need for evaporation and condensation have been proposed.

3. Ion exchange. The method is based on the property of solid polymer resins of different degree of crosslinking, covalently bound to ion groups (ion exchangers), reversibly exchanging ions of salts dissolved in water [37]. Depending on the charge, the ion exchangers are divided into positively charged cation exchange resin (H^+) and negatively charged anion (OH^-). In cationites, substances similar to acids, anions are represented as water-insoluble polymers, and cations (Na^+) are mobile and exchange with solution cations. Unlike cation exchangers, anion exchangers are based on the chemical structure of a base whose cations form an insoluble structure. Their anions (usually OH-hydroxyl groups) are able to exchange with solutions of anions.

The process of ion exchange desalination of water consists in the sequential passage of water through a fixed layer of the ion exchanger in a periodic process or counter-flow movement of water and the ion exchanger in a continuous process. In this process, the cations and anions of the purified water salts sequentially bind to the ion exchangers, and as a result, it is desalted. The ratio of ion exchanger, anionite and cationite is usually from 1:1 to 1.5:1.0 by weight [38].

The kinetics of ion exchange includes three successive stages: the movement of adsorbed Ion to the surface of the ion exchanger globule, ion exchange, the displacement of the displaced Ion into the ion exchanger globule and from its surface into the solution [39].

Ion exchange is used to produce desalinated and softened water in thermal and nuclear energy and in industry; in non-ferrous metallurgy during complex hydrometallurgical processing of ores, in the food industry, in the medical industry for the production of antibiotics and other medicines, as well as for wastewater treatment with the aim of organizing recycled water supply. At present, ion-exchange methods for the integrated extraction of valuable minerals from ocean water are also being developed [40].

Industrial devices for ion exchange are divided into three groups: installations, such as mixers, settling tanks, installations with fixed and moving layers of ion exchangers. The first type of apparatus is most often used in hydrometallurgy. In devices with a fixed ion exchanger layer, the initial and desalted solutions are fed in one direction (flow schemes) or in the opposite direction (counter-flow schemes). Such devices are used for ion exchange cleaning solutions, softening and desalination of sea water. In a countercurrent of continuous action, the movable ion exchanger moves from top to bottom under the action of gravity. Structurally, countercurrent devices are divided into three groups: with a suspended or boiling ionite layer, with a continuously moving ionite layer and with a moving solution through an ion exchanger. Depending on the desired degree of desalination of water, one -, two - and three-stage ion exchange

plants are designed. Residual salinity in single-stage ion exchange desalination is 20 mg/l. Plants with two-stage ionization scheme H^+ and OH^- are used to obtain water with mineralization up to 0.5 mg/l. Ion exchange method of desalination has several advantages: simplicity of equipment, low consumption of source water for own needs (15-20% of plant capacity), low power consumption, small volume of waste water.

The disadvantage of the ion exchange method is the relatively high consumption of reagents, the technological complexity of the process, which is limited by the initial salt content in the treated water, which is determined by economic costs. The profitability of ion exchange during desalination is usually limited by the initial content of dissolved salts of 1.5-2.5 g/l. However, if necessary, when the cost of water does not play a significant role, this method can be used to desalinate water with a sufficiently high salinity.

4. Electrodialysis. Electrodialysis is a membrane separation process in which ions of a solute are transferred across a membrane by an electric field. Thus, the driving force of this process is the gradient of the electric potential. Under the influence of an electric field, positively charged ions (cations) move to a negative electrode (cathode). Negative ions (anions) move to a positively charged electrode (anode). The electric field does not affect uncharged molecules. By using ion-permeable non-selective membranes, electrolytes and non-electrolytes can be separated. When using membranes that are more permeable to cations or, conversely, to anions, electrodialysis can increase or decrease the concentration of the electrolyte solution [41]. For this purpose, ion-exchange membranes are used: anion-exchange and cation-exchange. The matrix of the anion exchange membrane contains fixed cationic groups. The charge of fixed cations is neutralized by the charge of mobile anions located in the pores of the membrane. Anions of the electrolyte solution can be introduced into the membrane matrix and replace the anions initially present in it. Penetration of cations into the membrane is prevented by their repulsion forces by cations fixed in the membrane matrix. Cation-exchange membranes containing fixed anionic groups, act in a similar way. A multi-chamber electrodialyzer alternates a large number (usually several hundred) of cation-exchange and anion-exchange membranes located between two electrodes. An electric current transfers cations from the initial solution to the concentrate stream through a cation exchange membrane located on the cathode side. The cations are captured in this flow by the anion exchange membrane on the cathode side. The direction of motion of anions is opposite. They are transferred to the concentrate stream through the anion exchange membrane. On the anode side, the anions are captured in the concentrate stream by a cation exchange membrane. Thus, the overall result of the process is to increase the concentration of ions in alternating chambers while decreasing their concentration in other chambers. The electrolysis process takes place at the electrodes. In a multi-chamber device, the unavoidable overhead of electricity due to this process is distributed to a large number of chambers. Therefore, per unit of production, these costs are minimized.

The electrodialysis process is less used in industry than reverse osmosis and ultrafiltration processes. This is due to the fact that when using electrodialysis, only ions can be removed from the solution. The most widely used electrodialysis process

is the desalination of brackish water to produce drinking or industrial water. There are electrodialysis plants for drinking water from the sea. However, more often this process is used for water purification, the content of dissolved salts in which is approximately 10000 mg/l. In this case, the electrodialysis process is more economical than reverse osmosis or evaporation. Using electrodialysis, it is possible to obtain salt solutions with a relatively high concentration. Due to this feature of the process in question, electrodialysis is also used in the production of table salt and other salts from seawater. Electrodialysis is also used for pretreatment of water for thermal power plants. Another important area of use of electrodialysis is the treatment of wastewater. Electrodialysis is used for demineralization of waste water of galvanic and pickling plants, production of ammonium nitrate and for treatment of radioactive waste water. This process is used to concentrate wastewater containing valuable components (such as rare and precious metals) before further extraction of these components. Compared with reverse osmosis, electrodialysis has the advantage that it allows the use of thermally and chemically more stable membranes, so the electrodialysis process can be carried out at elevated temperatures, as well as at very low or Vice versa high pH values of the solution. In addition, as mentioned above, using electrodialysis, it is possible to obtain solutions with significantly higher concentrations than using reverse osmosis. The disadvantage of electrodialysis is the inability to remove uncharged components that may also be present in wastewater. Electrodialysis is also used in the food and pharmaceutical industries. For example, electrodialysis is used to remove salts from solutions and aqueous mixtures of organic substances: serums, vaccines, vitamins, amino acids, milk, juices, etc. Electrodialysis is also used for fractionation of substances, for example, separation of polyvalent cations from monovalent ones. More detailed information about electromembrane processes can be found in [42, 43].

5. Reverse osmosis. In reverse osmosis desalination, seawater is passed through semipermeable membranes under the influence of a pressure significantly exceeding the osmotic pressure difference between fresh and seawater (for seawater 25-50 ATM.). Such membranes are manufactured by the domestic industry from polyamide or cellulose acetate and are available in the form of hollow fibers or rolls. Small water molecules can freely penetrate the micropores of these membranes, while larger salt ions and other impurities are retained by the membrane [44].

Since the early 1970s, reverse osmosis has been used in our country in various technologies of water purification from impurities,including desalination. Modern industrial reverse osmosis plants include a fine water filter, reagent preparation system, high pressure pump, filter module and chemical washing plant.

In reverse osmosis desalination plants, the pipes are made of a porous material coated on the inside with a cellulose acetate film that acts as a semi-permeable membrane. The desalination plant consists of many similar pipes laid parallel to each other, through which a high-pressure pump (5-10 Mn/m^2 or 50-100 bar) is continuously pumped with seawater, and two streams, demineralized, penetrate and water with concentrated salts-concentrate, which is drained into the sewer. The flow of fresh water through the membrane is proportional to the applied external pressure. The maximum pressure is determined by the characteristics of the reverse osmosis membrane. If the

pressure is too high, the membrane can explode, clog with impurities present in the water, or miss too many dissolved salts. If the pressure is too low, the process slows down [45].

Reverse osmosis has significant advantages over other desalination methods: energy costs are relatively low, the plants are structurally simple and compact, their operation can be easily automated. The reverse osmosis system is operated in semi-automatic and automatic mode. Precipitation inhibitors are used to reduce the formation of unwanted salt deposits in pipe cavities. The chemical washing system is used to remove salt deposits from the membrane surface. For quality control of water treatment and pH values - flowmeters for salinity and pH meters. Permeate and concentrate flow is controlled by flow meters.

The degree of desalination of water and the performance of the membrane in desalinated water depends on various factors, primarily the total salt content in the source water, as well as the salt composition, pressure and temperature. Therefore, by desalting salt water from a well containing 0.5% dissolved salts at a pressure of 50 ATM during the day, approximately 700 liters of fresh water can be obtained from 1 m^2 of the membrane. Because many thin tubes are required to produce a large surface area, the reverse osmosis process is not widely used to produce large quantities of fresh water. However, this process seems very promising if improved, highly selective, energy-efficient low-pressure membranes are developed in the future, especially for desalination of salt water from wells. This water has a lower concentration of dissolved salts compared to seawater, which allows desalination at lower pressures [46].

6. The forward osmosis (FO) is an osmotic process that, like RO, uses a semipermeable membrane to separate water from dissolved solutes. The driving force behind this separation is the osmotic pressure gradient, so that a" pull" solution of high concentration (compared to the original solution) is used to create a flow of pure water through the membrane into the waste solution, thus effectively separating the supply of water from its solutes. In contrast, the reverse osmosis process uses hydraulic pressure as the driving force for separation, which serves to counteract the osmotic pressure gradient that would otherwise facilitate the flow of water from the permeate into the feed. Therefore, reverse osmosis requires significantly more energy than direct osmosis.

The simplest equation describing the relationship between osmotic and hydrostatic pressures and water flow (solvent):

$$J_w = A(\Delta\pi - \Delta P) \quad (1)$$

where J_w is water flux, A is the hydraulic permeability of the membrane, $\Delta\pi$ is the difference in osmotic pressures on the two sides of the membrane, and ΔP is the difference in hydrostatic pressure (negative values of J_w indicating reverse osmotic flow). The modeling of these relationships is in practice more complex than this equation indicates, with flux depending on the membrane, feed, and draw solution characteristics, as well as the fluid dynamics within the process itself.

The solute flux (J_s) for each individual solute can be modelled by Fick's Law:

$$J_s = B\Delta c \quad (2)$$

where B is the permeability coefficient of the solute and Δc is the difference in the membrane concentration of the solute. From this defining equation, it is clear that the solute will diffuse from the high-concentration region to the low-concentration region. This is well known in reverse osmosis, when solutes from feed water diffuse into food water, but in the case of direct osmosis, the situation can be much more complex.

In FO processes, diffusion of the solute in both directions can be observed, depending on the composition of the waste solution and the supplied water. This does two things; waste solution solutions can diffuse into the source solution, and the source solution solution can diffuse into the waste solution. It is obvious that these phenomena have importance from the point of view of the choice solutions for the extraction for any specific process FO. For example, the loss of the pulling solution may affect the supply of the solution, possibly due to environmental problems or contamination of the feed stream, for example in osmotic membrane bioreactors.

An additional difference between reverse osmosis and direct osmosis is that permeate water produced in the reverse osmosis process is in most cases fresh water ready for use. In the FO process, this is not the case. The membrane separation of the FO process actually results in an "exchange" between the solutes of the starting solution and the spent solution. Depending on the solute concentration in the raw material (which dictates the required solute concentration in the process) and the intended use of the FO process product, this step may be all that is required [47].

7. Freezing. This method is based on the fact that under natural conditions, ice formed from sea water is fresh, since the formation of ice crystals at temperatures below zero occurs only from water molecules (the phenomenon of cryoscopy). During artificial slow freezing of salty sea water around the crystallization centers, fresh ice of a hexagonal needle-like structure with an average density of 930 kg/m^3 is formed. At the same time, in the channels of the inner needle, the concentration of the solution and its density increase, and it, as a heavier one, settles as it freezes. Subsequent separation, washing, and melting of crystalline ice produces fresh water with a salt content of 500-1000 mg/L NaCl [48].

Freezing of sea water is carried out in crystallizers (contact, vacuum, with heat transfer through the walls) with direct contact of the cooled solution with the refrigerant - gaseous or liquid.

For better desalination of sea ice, fractional melting at a temperature of 20°C is used with washing and separation of ice crystals from the mother liquor by filtration, hydraulic pressing and centrifugation.

This method is used for concentration of non-food products, for desalination of seawater, concentration and separation of chemical solutions, etc. It is quite simple and economical, but requires complex equipment and energy consumption. Therefore, in practice, it is rarely used.

With all the advantages of contact freezing, the gas hydrate method compares favorably with the higher process temperature, which reduces energy costs and cold losses to the environment.

A variation of this method is the desalination of seawater using associated gas from a mixture of butane and propane. Frozen seawater is treated with associated gas;

Hydrocarbon-containing crystalline hydrates form a solid crystalline phase (one molecule of propane attaches 17 molecules of water). The solidified crystalline mass is then separated. To do this, it is enough to lower the pressure and slightly increase the temperature: hydrocarbons evaporate, fresh water remains. After capture and liquefaction, the hydrocarbons return to the cycle.

It should be emphasized that when choosing a desalination method, attention should be paid to the presence of deuterium in the form of heavy water D_2O in seawater. The ratio between heavy and ordinary water in natural waters is 1:5500. Different natural waters contain different deuterium content. Ordinary tap water contains about 100 g of deuterium per ton of water, and seawater contains between 130 and 150 g of deuterium per ton of water.

The physicochemical properties of heavy water differ from those for ordinary water. The molecular weight of D_2O is 10% higher than the mass of H_2O. Such a difference leads to significant differences in the physical, chemical and biological properties of heavy water. Heavy water boils at 101.44°C, freezes at 3.82°C, has a density at 20°C of 1.105 g/cm^3, and the maximum density is not at 40C, like ordinary water, but at 11.2°C (1.106 g/cm^3). Greater D-O bond strength than H-O causes differences in the kinetics of reactions of heavy and ordinary water. The mobility of deuterium D^+ is less than the mobility of protium H^+, the ionization constant of heavy water is 5 times less than the ionization constant of ordinary water. Chemical reactions and biochemical processes in D_2O are significantly slowed down. In mixtures of heavy water with ordinary water, an isotopic exchange occurs at high speed: $H_2O + D_2O = 2HDO$.

Heavy water in high concentrations is toxic to the body. For animal cells, the maximum concentration of H2O is 25 vol.% , For plant cells - 50 vol.% , For ordinary-70-80%. Therefore, it is advisable to carefully monitor the isotopic composition of the resulting fresh water.

Thus, the choice of method and technology of desalination depends on the requirements for water quality and salinity, as well as on technical and economic indicators. Depending on the water desalination method used, different types of desalination plants are used. Distillation desalination plants (single - hull and multi-hull, by the method of desalination-steam compression and solar) are used for desalination of sea water and salt water with high mineralization up to 35 g/l. Desalination of seawater by electrodialysis and hyperfiltration (reverse osmosis) is economical with a salt content of 25 g/l, ion exchange-less than 25 g/l. of the total volume of desalinated water obtained in the world, 96% are distillation desalination plants, 2.9% are electrodialysis plants, 1% are reverse osmosis plants and 0.1% are freezing and ion exchange desalination plants.

The main task of desalination is to carry out the process with minimal energy costs and minimal equipment costs. This requirement is important because a country that has to rely more on desalinated water must be able to withstand economic competition from other countries with more extensive and cheaper sources of fresh water.

Design studies show that the transportation of fresh water from a natural source even over a distance of 400-500 km is cheaper than desalination of water only for small

water consumers. An assessment of the projected operational reserves of brackish and salty groundwater in arid regions, taking into account the remoteness of most of them from natural sources of fresh water, leads to the conclusion that desalination is the only possible and economically viable method of water supply for them.

The methods used in the salt water desalination method can be effectively used to restore the character of the used water, which does not degrade the condition of fresh water bodies.

1.4 Alternative technologies of desalination

In addition to commercially available desalination technologies, a number of other seawater desalination processes have been developed. These processes may not reach the level of commercial success of MSF, MED and RO, but they can become valuable in special circumstances or with further development. These important processes include solar hydration and membrane distillation.

Solar humidification is a method of thermal desalination of water. It is based on the evaporation of seawater or brackish water and the subsequent condensation of the resulting moist air, mainly at atmospheric pressure. This process mimics the natural circulation of water, but for a much shorter period of time. Through the transparent glass, solar energy enters the device and produces heat that evaporates the water inside it. The seawater pool is usually black in color to improve the absorption efficiency of solar energy. The evaporated water is then condensed on the glass panels of the refrigerator, and the condensed drop flows down the panels and is collected for use.

The advantages of the solar humidification process are its relative ease of use and maintenance and obviously its ability to use solar or other renewable energy as an energy source, so the operating costs are very low. However, the efficiency of this type of plants is less than 50%, which makes them unviable for use [49]. The General rule is that about 1 m^2 of land will produce only 4 liters of fresh water per day. Accordingly, in order to obtain a large amount of fresh water, it is important to use very inexpensive building materials to minimize capital costs, since a huge area is required. However, the cost of installing solar distillation cubes is usually much higher than other methods [50]. In addition, the frames are vulnerable to weather damage.

Membrane distillation (MD) is a thermal separation program in which separation is carried out through a phase transition and becomes a new technology [51]. In the prior art, the MD process that separates mass flows through a membrane mainly uses a static pressure difference as the driving force between two limiting surfaces, a concentration difference (dialysis) or an electric field (ED). The selectivity of a membrane is determined by the size of its pores in relation to the size of the substance held, its diffusion coefficient or electrical polarity. However, the selectivity of membranes used for membrane distillation (MD) is based on the retention of liquid water with simultaneous permeability to free water molecules and therefore to water vapor. These membranes are made of a hydrophobic synthetic material (e.g. PTFE, PVDF or PP) and have pores with a standard diameter of 0.1 to 0.5 microns.

The use of MD is advantageous in comparison with some other separation processes, since it requires lower operating temperatures and pressures than

conventional distillation, a decrease in the chemical interaction between the membrane and technological solutions, and a decrease in the vapor space compared to traditional distillation processes. The main limitation is associated with the determining phenomenon itself: technological solutions must be aqueous and sufficiently diluted to prevent wetting of the hydrophobic microporous membrane. This limits the use of MD for desalination [52].

1.5 Modern achievements in the desalination industry

In recent years, research in membrane technology has advanced significantly. Advances in membrane production include nanocomposite membranes, carbon nanotubes, and graphene-based membranes.

Nanocomposite membranes are membranes based on polymeric material within which inorganic nanoparticles are scattered. These particles create preferred pathways for the penetration of water molecules, while being a barrier to undesirable components. Oxides of various metals, such as TiO_2, Al_2O_3, SiO_2, MgO, AgO, etc., pure materials (nanosilver), zeolites, carbon nanoparticles, and mineral clays can serve as inorganic materials used for nanocomposite membranes [53].

As you know, titanium oxide is a photocatalytic material widely used for disinfection and decomposition of organic substances. Due to these properties, the use of TiO_2 as a filler contributes to the resistance of membranes to biofouling, being a coating that prevents contamination.

Recent studies have demonstrated the use of Boehmite particles (aluminum hydroxide) as a material for the manufacture of membranes [54]. Another new material used as a filler is quartz. It was proved that quartz significantly improves the productivity of membranes, such qualities as filtration ability, roughness, and electrokinetic potential (ζ potential) [54]. In addition, there are various combinations between nanoparticles, which also lead to a significant improvement in membranes. For example, a new nanocomposite membrane was invented using polyaniline oxide and iron [54].

Graphene-based membranes. Graphene is a relatively new material that has been synthesized since 2004 [55]. Graphene has a honeycomb lattice structure. The unique property of graphene is the monatomic film, it is a two-dimensional material that has high thermal conductivity and electrical conductivity; in addition, it has the fastest electronic mobility, making it much heavier than diamond and heavier than steel. Graphene-based membranes are gaining popularity. Recently, the method of desalination of marine water through nanoporous graphene membranes has been actively developed. The desalting process is shown in Figure 1 [56].

Carbon nanotubes, discovered in 1991, have aroused great interest due to their unique mechanical, optical and electrical properties. They are cylindrical graphite sheets (allotropic carbon form).

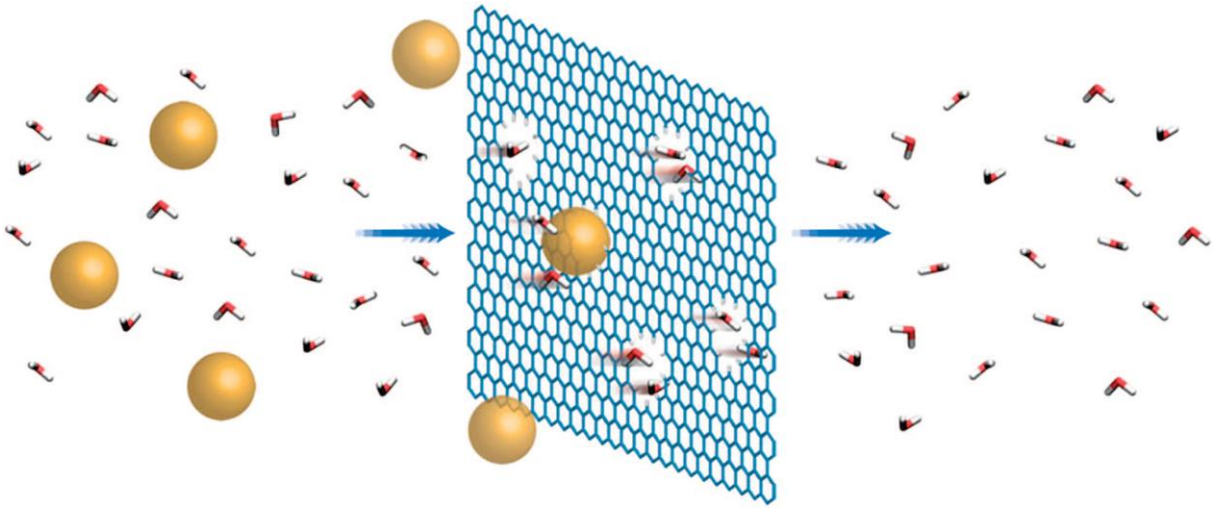

Figure 1 – A graphene membrane with subnanometer pores as an RO membrane. In this process, the salt water (left), subjected to a high pressure, is divided into two parts: water molecules (red and white) passing through the membrane (right) and salt ions (golden spheres) that are blocked. (Reprinted with permission from Wang and Karnik [57]. Copyright 2016 Nature Publishing Group.)

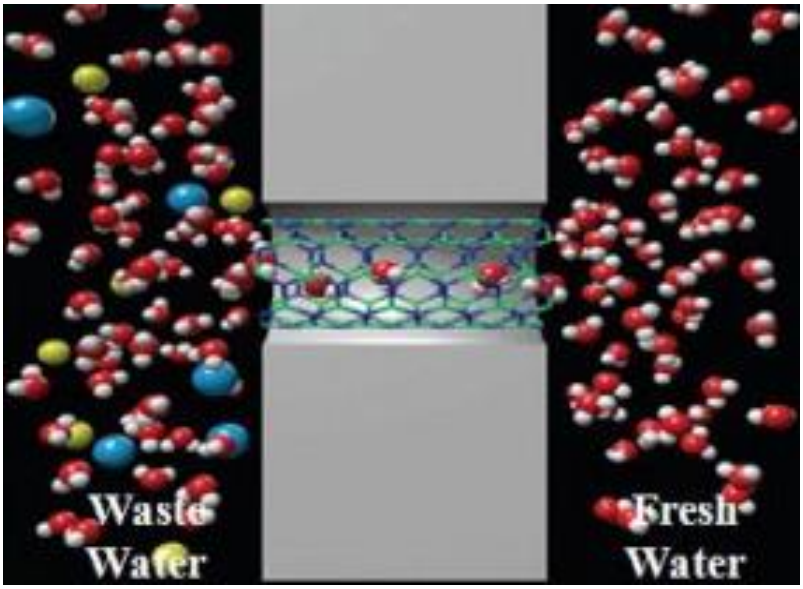

Figure 2 – Scheme of movement of water molecules through a carbon nanotube [55]

With the development of production technologies, single-walled, double or multi-walled carbon tubes of various sizes began to be built into the filtration membranes. Experimental studies have already shown that water can penetrate through relatively narrow carbon tubes at a fairly high speed. These membranes are of great interest in connection with low energy consumption, as well as high filtering ability. The membrane structure is shown in Figure 2 [58].

1.6 World experience and development trends of membrane technologies

Water shortages are currently experienced by the Southwestern United States (which includes California, Arizona, New Mexico and Texas), Mexico, Middle East and North African countries, as well as India, Pakistan, Mongolia, Afghanistan, Kazakhstan, Turkmenistan, Uzbekistan, Western Australia, Central America and parts of China. Although the cost of desalination has declined significantly in recent years and seems reasonable, many countries in the world cannot afford them.

The leading countries for desalination at the moment are: Saudi Arabia, USA, Australia, Israel, Kuwait, Libya, UAE, China, India, Czech Republic, Caribbean Islands, Morocco, Spain, Oman, Iran, Egypt, Bahrain, Turkey, Jordan [59].

Desalination in Saudi Arabia is a strategic direction in the country's development plans, where the problem of water supply is aggravated by the fact that there are practically no natural sources of drinking water on the continent. Saudi Arabia has the world's largest desalination corporation in the world, which can produce up to 0.728×106 m^3/day (2014) [60]. The hybrid desalination plant, which is located in the industrial city of Al Haier, consists of 8 MSF units (multi-stage flash evaporation) and 17 RO units (reverse osmosis). MSF-plant produces 0.606 106 m^3/day, and RO - 0.257 m^3/day of fresh drinking water. The scheme of the desalination plant is shown in figure 3.

Figure 3 – Scheme of desalination plant in the city of Ras Al-Khair [60]

This is the largest desalination plant of its kind in the world, which is capable of providing approximately 33 million people with drinking water. The project also

includes a 2650 MW power plant building. The entire desalination process is initially pretreated using methods such as coagulation, fluctuation, or micro-ultrafiltration. Energy recovery devices or turbocompressors carry out the final stage, or post-processing stage. This includes the processes of water stabilization by removing gases from it, such as hydrogen sulfide, measuring the acidity and alkalinity of water and preparing it for distribution. Currently, Saudi Arabia is interested in the efficient use of solar and atomic energy for desalination [59].

Australia is the driest inhabited continent in the world, whose water supplies are constantly at risk due to climate change, droughts, accompanied by forest fires and floods. Australia's main desalination plant was commissioned in 2006. It produces 45 million m^3 per year [61]. Another desalination plant produces approximately 50 million m^3 per year; it is planned to expand it to increase productivity [59]. But the most expensive and controversial plant was built in Melbourne with a capacity of 150 million m^3/day [59]. However, during periods of improvement in the drought situation and during excessive rainfall, some plants do not work for hours or even for a longer time. Many plants have used renewable energy sources such as wind farms. Australia's annual investment in water supplies is approximately $ 2 billion per year.

Sydney desalination plant is a large-scale reverse osmosis plant. It occupies 45 hectares and is located 25 km from Sydney on the coast of Kernel. Water enters the plant from the Tasman Sea through an underground and underwater tunnel, and then it is fed to filters to remove large contaminants (algae, sand). Then the water is pumped into the RO structure, where it passes under high pressure through membranes that remove both salts and nutrients. Next, beneficial salts are added to completely desalinated water, bringing the properties to the level of drinking quality. After that, re-mineralized water is disinfected and goes to water storage tanks. Drinking water is supplied to the water supply network in Erskine Ville through an 18-kilometer pipeline, and the seawater concentrate is returned to the sea [61].

The USA is a country with very uneven water resources. Moreover, although it is quite rich in water terms, there are still problems. For example, the southwestern part of the country is arid, while in the regions of the Northeast, Midwest there is a lot of rainfall, and there is access to the lakes. The leader in the United States for the use of desalination technology is Florida. Some of its installations are used for desalination of coastal seawaters, but most sources are brackish groundwater or surface water.

The Tampa Bay desalination plant is an alternative water supply that provides regions with up to 25 million gallons of drinking water per day. The principle of its operation is based on reverse osmosis (Figure 4) [62].

Although desalination is a promising alternative for drinking water, a significant drawback of many technologies is the high energy consumption, which, in turn, leads to environmental pollution (greenhouse gas emissions, seawater concentrate). International desalination is increasing at a steady pace along with increased consumption of fossil fuels.

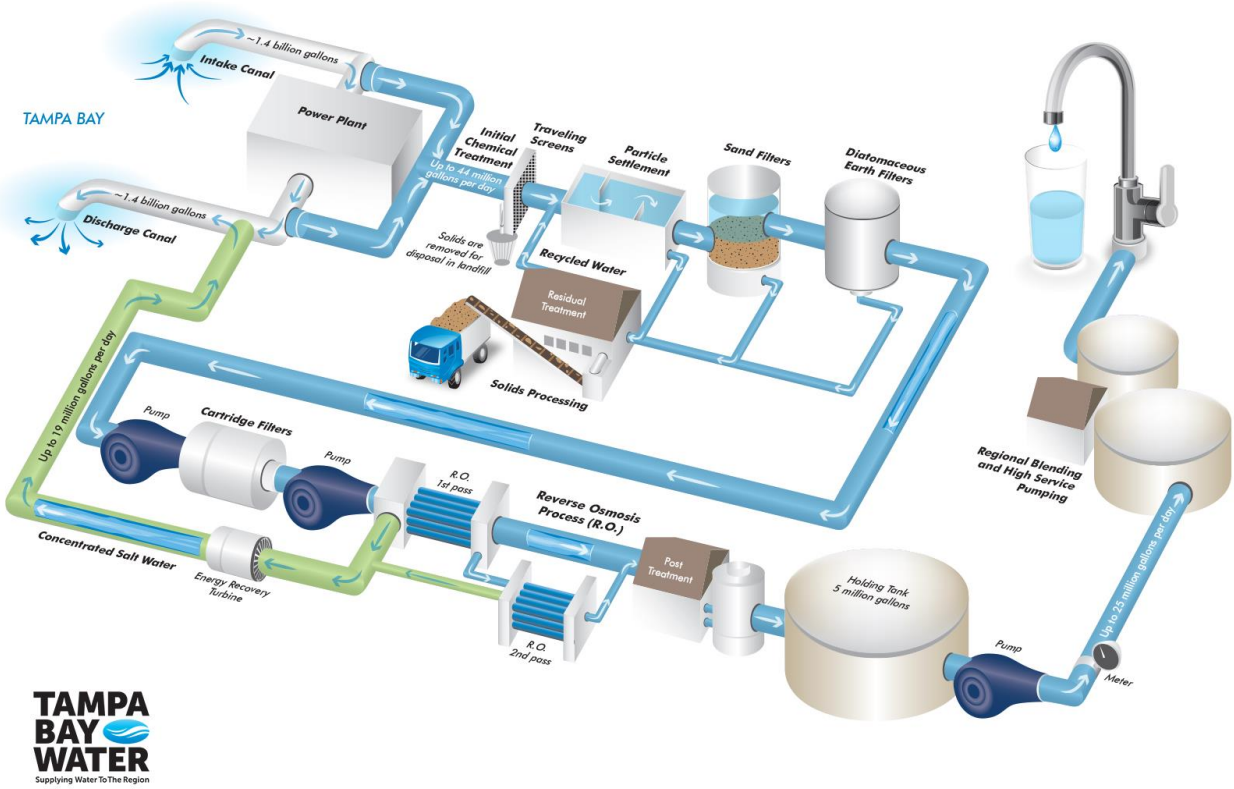

Figure 4 – Process diagram of Tampa Bay seawater desalination plant [62]

The production of 1000 tons (m^3) of fresh water per day using desalination technology requires 10,000 tons of oil per year, which also leads to environmental degradation [63]. In this regard, the use of renewable energy sources, such as the energy of the sun, wind, waves, is promising for the sustainability of desalination technologies.

1.7 Water desalination cost

In the scientific literature, the calculation of the desalination cost is based on different assumptions, by different authors. There is for example significant variation in interest rates and life expectancy of the equipment. In some cases the estimation of freshwater cost does not include the investment cost and in some others the required labour, or other operation costs. However, the taxonomy of all these cases can facilitate the derivation of useful conclusions.

Out of a very large number of publications on the subject, this is an attempt to present the most recent, which are closer to today's situation and can provide more accurate data for the cost of desalination.

Thermal methods seem to be more effective than membrane methods in terms of efficiency in the desalination of very salty seawaters. In the year 2000, the cost of RO units, was estimated between 189.2 tenge/m^3 (0.55 \$/m^3) and 860 tenge/m^3 (2.50 \$/m^3) when plant capacity was in the range of 1000-100,000 m^3/day.

With regard to thermal methods (namely MSF), the cost varies from 240.8 tenge/m^3 (0.70 \$/m^3) to 860 tenge/m^3 (2.50 \$/m^3) in the range of capacity 10,000-100,000 m^3/day (estimations in year 2000) [64].

Fiorenza et al. [65] claim that the typical average capacity and corresponding cost for desalination technologies in the world was

- MSF: 25,000 m^3/day and 378.4 tenge/m^3 (1.10 \$/m^3)
- MED: 10,000 m^3/day and 275.2 tenge/m^3 (0.80 \$/m^3)
- VC: 3000 m^3/day and 240.8 tenge/m^3 (0.70 \$/m^3)
- RO: 6000 m^3/day and 240.8 tenge/m^3 (0.70 \$/m^3)

Thermal methods are more expensive because of the large quantities of fuel required to vaporize salt water. Membrane methods, mainly RO, which can desalt brackish water somewhat more economically, have replaced thermal methods for the desalination of brackish water. However, because of the high cost of membrane replacement, membrane methods are less suitable for desalinating seawater. Technological advancement has also allowed some reduction in the total desalination cost, by improving energy efficiency (multiflash distillation or hybrid systems), by facilitating transfer processes or by energy recycling (process of cogeneration) [66].

Systems that use thermal methods have usually large production capacity. In the case of MED, the cost for large systems with a daily production from 91,000 m^3 to 320,000 m^3 ranges between 180.6 tenge/m^3 (0.52 \$/m^3) and 348.3 tenge/m^3 (1.01 \$/m^3). These costs refer to cases between 1999 and 2006 the most recent cases having lower cost, while the older installations are the most expensive. For medium size systems, with a daily production from 12,000 m^3 to 55,000 m^3, the cost ranges between 326.8 tenge/m^3 (0.95 \$/m^3) and 516 tenge/m^3 (1.5 \$/m^3). For small systems with a daily capacity around 100 m^3, the cost varies between 860 and 3440 tenge/m^3.

For the MSF method, the cost can vary between 180.6 tenge/m^3 (0.52 \$/m^3) and 602 tenge/m^3 (1.75 \$/m^3) and refers to systems with daily production from 23,000 m^3 to 528,000 m^3.

VC is used mainly for small systems with production around 1000 m^3/day, at a cost that ranges between 692.3 tenge/m^3 and 915.9 tenge/m^3 (table 3) [67, 68].

Table 3 – Thermal methods and cost of water produced (per m^3)

Desalination method	Size of plant (m^3/day)	Cost (per/m^3)
MED	<100	860-3440 tenge
	12 000-55 000	326.8-670.8 tenge (0.95\$-1.95\$)
	>91 000	180-348.3 tenge (0.52\$-1.01\$)
MSF	23 000-528 000	180.6-602 tenge (0.52\$–1.75\$)
VC	1000-1200	692.3-915.9 tenge

In the past RO was used mainly for the desalination of brackish water, but more recently it is the predominant method for many types of desalination, due to its lower energy requirements. Hence the application of the method has been extended to larger units that can reach a daily production of 320,000 m^3. The cost of brackish water ranges between 90.3 tenge/m^3 (0.26 \$/m^3) and 144.9 tenge/m^3 (0.54 \$/m^3) for systems with

daily capacity around 40,000 m^3. For smaller systems (20–1200 m^3 daily production) the cost ranges between 266.6 (0.78 \$/m^3) and 455.8 (1.33 \$/m^3). For very small systems that produce a few cubic metres per day the cost varies between 1935 tenge/m^3 and 4437.6 tenge/m^3.

Table 4 – Membrane methods and cost of water desalination (per m^3)

Type of feed water	Size of plant (m^3/day)	Cost (per/m^3)
Brackish	<20	1935-4437.6 tenge
	20-1200	266.6-455.8 tenge (0.78\$-1.33\$)
	40 000-46 000	90.3-184.9 (0.26\$-0.54\$)
Seawater	<100	516-6450 tenge
	250-1000	430-1350 tenge
	1000-4800	240.8-593.4 tenge (0.70\$-1.72\$)
	15 000-60 000	163.4-559 tenge (0.48\$-1. 62\$)
	100 000-320 000	154.8-227.9 tenge (0.45\$-0.66\$)

RO has begun to compete in seawater desalination. During the last few years it is used for even larger systems. In these cases (daily production of 100,000–320,000 m^3) the cost ranges between 154.8 tenge/m^3 (0.45 \$/m^3) and 227.9 tenge/m^3 (0.66 \$/m^3). Medium size systems, with a daily capacity of 15,000–60,000 m^3 produce water between 167.7 tenge/m^3 (0.48 \$/m^3) and 559 tenge/m^3 (1.62 \$/m^3). Small size systems, with a capacity of 1000-4800 m^3 per day, produce water at a cost between 240.8 tenge/m^3 (0.7 \$/m^3) and 593.4 tenge/m^3 (1.72 \$/m^3). Even smaller systems than the above, (with daily capacity of 250-1000 m^3), produce water at a cost ranging from 430 tenge/m^3 to 1350.2 tenge/m^3. The majority of these cases is powered by renewable energy, causing the higher cost. Finally, very small units, (2-24 m^3 daily production) using renewable energy sources alone, have a cost that varies between 516 tenge/m^3 and 6450 tenge/m^3. Table 4 summarise the above comments.

1.8 Environmental risks, health effects and the development of the desalination process

Environmentalists continue to speak out against the process of desalination, claiming that it harms the environment. Removal of salt from sea water leads to the formation of a concentrated sludge. Brine, which is twice as heavy as salty sea water and contains impurities that can affect marine life when discharged back into the sea. In case of brine removal on land, it can seep through the soil, penetrating into groundwater. The United States Environmental Protection Agency found that a huge number of constructed desalination plants for processing sea water during the year damaged about 3.4 billion fish and other representatives of the marine fauna and caused losses for the country's fishing industry in the amount of \$212.5 million. Desalination plants can also destroy about 90% of plankton. In addition, desalination plants emit a huge amount of carbon dioxide emissions, because they work on fossil fuels. The San Diego Coast Guard Research Organization estimates that a plant that produces about 53 million gallons of water per day will consume

twice as much water for recycling and reuse. The situation seems quite ironic, since the creation of similar plants for the desalination of sea water would seem to be a solution to the problem of lack of drinking water and a way out of the current crisis situation, but experts argue that this can create only a more serious environmental problem, such as climate change on the planet.

The use of desalinated water also raises some conflicting opinions regarding the effect of the desalination process on health. According to Peter Gleick, chairman of the Institute for Research in the Development and Safety of the Environment of the Pacific Region, reverse osmosis membranes are able to remove only 50% of boron, which is part of the chemical composition of sea water. Excess boron can cause problems in the reproductive system, both people and animals, as well as lead to disruption of the gastrointestinal tract.

To solve the problems associated with an increase in carbon dioxide emissions into the atmosphere, which leads to the greenhouse effect, leading research universities and water development companies have begun developing future carbon neutral desalination plants using renewable energy sources. One example of such facilities is a project of a desalination plant in Saudi Arabia, which will be solar-powered, jointly developed by IBM and the Center for Science and Technology named after King of Saudi Arabia Abdel Aziz. Meanwhile, researchers from the Massachusetts Institute of Technology and the South Korean University of Science and Technology have developed a microchip that can reflect salts from the reverse osmosis membrane. The device is equipped with a special technology capable of producing about 15 liters of water per hour, which can provide drinking water to a small village. Experts express their opinion that politicians do not provide an accurate assessment of the most economically viable and safe options and proposals for the desalination of seawater. In any case, the solution of issues related to the lack of fresh water, which causes serious problems in the arid regions of many countries, is timely and correct. The World Health Organization predicts that by 2050, almost two-thirds of the world's population will face an acute shortage of fresh water. However, the problem of a shortage of fresh water can be solved by other means, and not by desalination. According to the National Research Management, redistribution of water can be more efficient and cheaper than desalination. Numerous studies support the report of the National Research Management, providing data on the effectiveness of programs that offer ample opportunities to solve water supply problems at a lower price, while being more secure than large-scale desalination plants. According to Buki Oren, chairman of Watec Israel, the preservation of existing water resources, rather than the development of new sources, is the most promising direction, both from an environmental and economic point of view. Desalination should not be taken as a panacea for the conservation of water resources. Each person is able to contribute to the conservation of water resources by simply saving water every day, using it for its intended purpose. Responsibility and commitment on the part of mankind can solve the problem of "thirst" on a planetary scale [69].

Resolution of the research task. From the presented literature review, the current state of the presented research is determined and the following tasks are set:

1. To develop a method for producing multilayer graphene materials and to identify them using Raman spectra.

2. To determine of morphology, elemental composition and surface area of obtained graphene materials from rice husk.

3. To develop methods for producing graphene membranes and determine the permeability characteristics for the resulting membranes.

4. To analyze the possibility of graphene based membranes to transform salted water into clean water with the help of a suitable membrane technology.

2 EXPERIMENTAL METHODS

2.1 Chemicals, raw and commercial materials

The separation characteristics such as water flux and salt rejection of membrane mainly depends on the intrinsic properties of the material, also including chemical and mechanical stability, resistance to fouling, and cost. Therefore, a number of materials such as rice husk, graphite, graphene, carbon nanotubes, cellulose acetates, polyethylamides and polyvinylpyrrolidone have been used to make membranes. In addition, the following reagents were used: the commercial GO powder was purchased from XFNANO (Nanjing XFNANO Materials Tech Co., Ltd., China). As denoted by the manufacturer, the GO powder has a lateral size of 1 μm with a thickness of 0.8-1.2 nm, and the purity is higher than 99%. Potassium hydroxide and sodium hydroxide were purchased from "LABHIMPROM" (Chemical Analytical Trading Company, Almaty, Kazakhstan) (TU 24363-80). Graphite was delivered from Russia. Hydrogen peroxide (37%) was purchased from "LABOR PHARMA" (Trade and Production Company, Almaty, Kazakhstan) (OST 301-02-206-99). Sodium nitrate (pure) was purchased from FIRMA SCAT (produced by Open Joint Stock Company "Reactiv", Russia) (GOST 4168-79). H_2SO_4 (98 wt.%), Polyvinylpyrrolidone (PVP) average Mw ~1.300.000 Da and N-methyl pyrrolidone (NMP) were purchased from Sigma Aldrich and used as received. Polyetherimide (PEI) 1000 was procured from Ultem. Carbon black (N110 type) by Sid Richardson Carbon & Energy was used as reference material. Vladipor membrane type MFAS – SPA was purchased from "LABOR PHARMA" (Trade and Production Company, Almaty, Kazakhstan). It is a microporous film material (d=47 mm) made on the basis of a mixture of acetates with a pore size of 1.5-3 microns and a total porosity of 80-85%. Productivity for distilled water at P = 0.05 MPa around 150-300 ml/(cm^2min). Minimum pressure of a bubble breakthrough through a membrane moistened with water is 0.05 MPa (TU 6-55-221-1518-2003). Sodium chloride (chemical pure) was purchased from REACHEM (Chemical Reagents Company, Moscow, Russia) (TU 6-09-5417-88) and from "LABOR PHARMA" (Trade and Production Company, Almaty, Kazakhstan) (GOST 4233-77). Graphene oxide was obtained by two methods from rice husk and graphite. Rice husk was delivered from Bakanas village, district center of Balkhash, Almaty region, Kazakhstan.

2.2 Methods

2.2.1 Obtaining graphene oxide from rice husk

The graphene layers was obtained in four successive stages: pre-carbonization, desilication, activation and exfoliation of the carbonized rice husk (CRH). This method was developed starting from the method for the production of graphene oxide from rice husk.

Firstly, the rice husk (RH) was washed several times with distilled water to remove impurities, and then dried at 383 K for 1 hour. The pre-carbonization of RH was carried out in a reactor at a temperature of 523-573 K. The pre-carbonization time was 45 minutes. The resulting samples of pre-carbonization step (CRH) were

desilicated in 3 liters of 1M NaOH solution and heated at 353 K for 3 hours to remove SiO_2, then let stay to sediment. The solution was decanted to remove the surfactant containing sodium silicate. After that the solid was washed 5-7 times with distilled water (through boiling-sedimentation-decantation) to reach approximately a netrual pH, and dried in hot air oven for at least 2 h at 383 K [70-77]. A series of 5 desilicated samples was mixed with crushed KOH at different temperatures and ratios. The mixtures were compacted in an iron crucible and annealed at 1123 K for 2 h. To protect from oxidation, Argon was supplied at a rate of 5 sccm (standard cubic centimeter per minute). In one case (sample $Gr(1/4)_1$) activation was performed in air. After activation treatment, the resulting samples were washed with distilled water several times to reach the equilibrium of pH~7 and the filtered samples were dried at 373 K for 24 h.

The exfoliation process of the GO was carried out on sample $Gr(1/4)_3$ by using a hydrogen peroxide solution (H_2O_2, 37%) for 48 h, to remove amorphous carbon from the samples. After exfoliation process, the resulting samples were washed and dried following the same procedure described above.

2.2.2 Obtaining graphene oxide from graphite

Synthesis of graphene oxide from graphite was developed using Robert Murray Smith method. Firstly, 5 g graphite powder, 2.5 g $NaNO_3$ and 115 mL H_2SO_4 were added in a round-bottom flask by stirring for 30 min to get homogeneous solution. Then the mixture was putted in ice bath and 15 g $KMnO_4$ slowly added. After that 230 mL deionized water was added in this mixture by stirring for 15 min with magnetic stirrer. Then 400 mL H_2O and 50 mL H_2O_2 (37%) were added in this solution and heated around 98°C by sonicating for 1 h. Then resulting solution was filtered through membrane (type MFAS – SPA) and washed several times with deionized water up to reach neutral pH. The final product weight 5 g.

2.3 Material purification

Purification of the samples was performed at IRC-CNR, Naples. To purify the samples from inorganics (Fe, Si, K) a water washing was performed. 0.5 g of each sample was dispersed in 100 mL of bidistillated water, then the mixture was sonicated for 30 min by using an ultrasound bath at 65 kHz. After that, the mixture was filtrated under vacuum (50 mbar) on a PVDF membrane. The solid was dried at 105°C for 12 h and the eluate was analyzed by ICP-MS to check the composition of the components removed from the samples.

2.4 Material functionalization

In order to activate the materials toward desalination, a functionalization aimed to add sulfonic groups was performed (at the IRC-CNR, Naples). To functionalize the samples, 0,3 g of each selected sample and 10 mL of 15M H_2SO_4 were added in a round-bottom flask. The temperature was controlled at 80ºC. After stirring for 60 min or 24 hours, the mixture was centrifuged for 10 min (4000 t/min), then the recovered solid was washed with bidistilled water many times up to reach pH=7 and filtrated with PVDF membrane. The resulted sample was dried at 105°C for 12 h.

2.5 Membrane preparation

So far, two different techniques have been adopted for the development of graphene based membranes, namely (I) the vacuum filtration and (II) the phase inversion method [78]. Vacuum filtration has been employed to prepare a thin layer of cross-linked graphene depositing on a substrate ultrafiltration membrane. Phase inversion is a process in which a polymer in solution is converted to a solid in a controlled manner. The change in phase can be initiated in a number of ways, such as solvent evaporation, thermal precipitation, immersion precipitation and vapor precipitation [79]. In the first method, the GO powder was dispersed in deionized (DI) water and sonicated for 2 h. Unless otherwise specified, 40 mL of the GO suspension (0.01 mg/mL) was filtered through the membrane (filtration area 38 mm^2) under -0.8 bar at room temperature, forming the GO membrane composed of a thin GO layer on the membrane support. The resultant GO membrane was vacuum-dried (-0.95 bar) at 40°C for 40 h. In the second method, firstly, 0,41 g of PEI and 1,95 ml of N-Methyl-2-pyrrolidone (NMP) were added in heat-resistant glass and heated around 50°C by stirring for 18 h to get homogeneous polymer solution. Then the 0.1 g of carbon sample was dispersed in a little amount of NMP (1 mL) and it was sonicated for 30 min to obtain a uniform dispersion and added to PEI suspension. After that, 0.1 g of polyvinylpyrrolidone (PVP) was added to the dispersed suspension of PEI/GO and gently stirred for 1 h to get homogeneous suspension. The resulting suspension was degasified by sonication to eradicate trapped air bubbles. The homogeneous casting solution was cast over a glass plate (adjuting the thickness at 400 microns) and immersed in the coagulation bath containing water as non-solvent. The resulting membrane was kept in coagulation bath for 24 h to ensure the complete phase inversion.

2.6 Membrane testing

The membrane performance was evaluated by measuring the flux of DI water and 100 ppm salt water using a laboratory vacuum filtration apparatus at a trans-membrane pressure of -0.8 bar. The water and salt water fluxes (J) in L m^{-2} h^{-1} (LMH) were calculated as follows:

$$J = \frac{V \times 60}{t \times A \times 1000} \tag{3}$$

where V is the volume of permeated water (mL), t is time (min), and A is the active membrane surface area (14.6 cm^2). The salt concentration of the feed, permeate and filtrate solution was measured using graphene based membranes for the salt water before and after permeation by the following equation:

$$R(\%) = \frac{(C_0 - C_p)}{C_0} \times 100 \tag{4}$$

where R is the salt filtration and C_0 and C_P are the feed and permeate concentrations (ppm).

2.7 Instrumental techniques

The following instruments and equipment were used in this work: scanning electron microscope (SEM), transmission electron microscope (TEM), elemental analyzer, Raman spectroscope, sorbtometr, fourier-transform infrared spectroscope (FTIR), thermogravimetric analyzer (TGA), X-ray diffractometer (XRD), inductively coupled plasma - mass spectrometer (ICP-MS), atomic absorption flame emission spectrophotometer. All of the above instruments and equipment were from: laboratories of KazNU named after Al-Farabi (Almaty, Kazakhstan), Center for Physico-Chemical Research and Analysis Methods (CPhCAM) (Almaty, Kazakhstan), Institute of Combustion Problems (Almaty, Kazakhstan), The Institute of Nuclear Physics (Ministry of Energy of the Republic of Kazakhstan), the "Analytical Chemistry for the Environment" laboratory of University of Naples Federico II (Naples, Italy) and Combustion Research Institute (IRC-CNR) (Naples, Italy).

2.8 Description of laboratory setups and auxiliary equipment for carbonization processes

As a main laboratory device was for developed and manufactured a self-built carbonization setup for carbonization and thermochemical activation (Fig. 5). The carbonization setup consists of a steel reactor with a height of 50 cm and a diameter of 89 mm, installed in a vertical position in a tubular electric furnace equipped with a thermostat, which allows the temperature to be raised with a step interval of 7.5°C/min to 1000°C and a digital gas flow regulator.

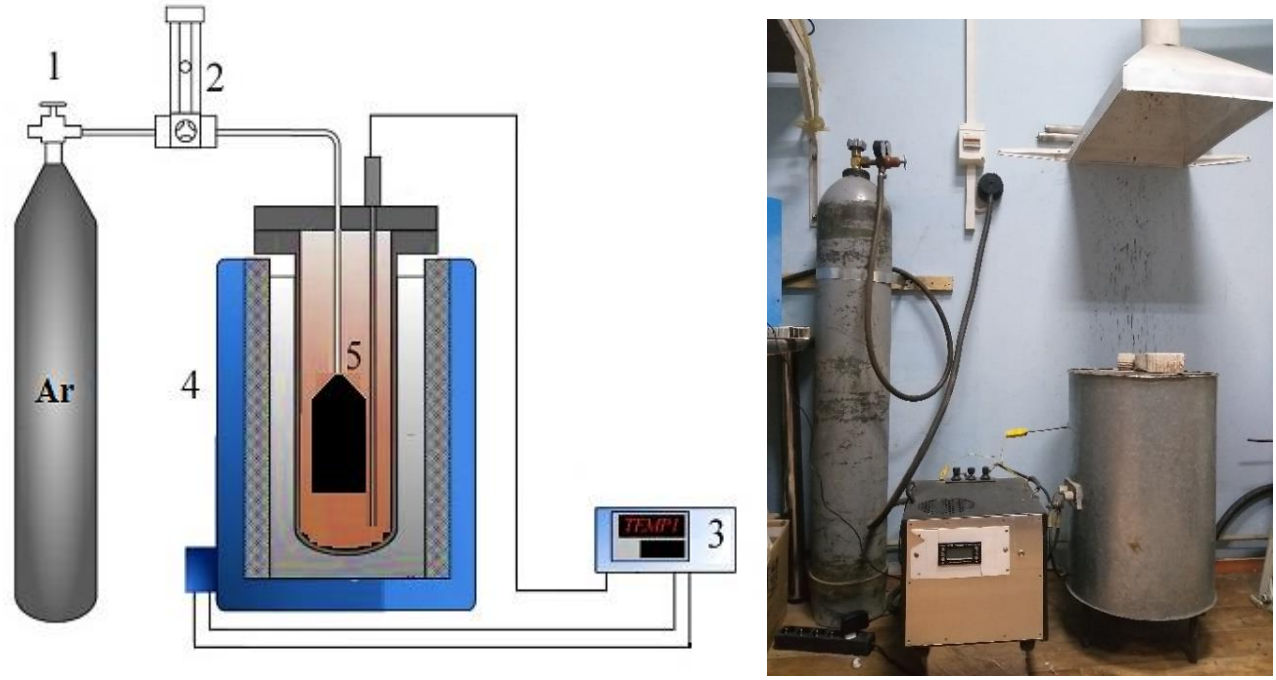

a b

1 – argon cylinder, 2 – gas flowmeter, 3 – temperature controller, 4 – carbonization reactor, 5 – iron crucible

Figure 5 – The schematic diagram (a) and image (b) of self-built carbonization setup

As an auxiliary equipment for providing experiments were used: laboratory glassware (plastic, glass, ceramics), pump, ultra-sonication bath, vacuum filter flask, scales, porcelain crucible, magnetic stirrer with heating, laboratory sieve (mesh sizes: 75 μm, 150 μm, 260 μm), Petri dish, pH meter, analytical balance Pioneer PA214C, Ohaus; pipettes Capp bravo; laboratory vacuum pump XP-125; drying cabinet SNOL 58/350; muffle furnace SNOL 4/1100; electric laboratory tile LOIP LH-302; mantle heater LH-150; Laboratory shaker LAB-PU-02; laboratory benchtop centrifuge OPN-3.02.

There are a number of regulations and documents that prescribe the rules of conduct in a chemical laboratory, especially the work with caustic and toxic substances. During the experiments, the following basic and most necessary precautions were observed:

1. Work in the laboratory in special clothing (lab coat), and when conducting experiments with highly hazardous substances, use safety glasses and gloves.

2. All experiments with toxic and odorous substances were carried out in a fume hood.

3. The work was pre-planned before experiments.

3 SYNTHESIS GRAPHENE MATERIALS

3.1 Rice husks as raw material for synthesis of graphene

Currently, plant biomass is increasingly becoming an object of research in relation to its use as a renewable raw material for the production of various products of the chemical industry – as an alternative to non-renewable sources of fossil carbon-containing raw materials (coal, natural gas, oil, etc.). The ways of obtaining biofuels and their precursors (bio-diesel, bio-ethanol, bio-oil), synthesis gas, methane, as well as various products of fine organic synthesis are intensively studied. At the same time, the use of biomass for the production of charcoal, as well as carbon materials with a developed porous structure – activated carbons, amorphous microporous carbon materials – is more traditional.

There is a special type of biomass that includes an abnormally high amount of the mineral component - high-ash biomass, which is most interesting for use as a raw material for the production of porous carbon materials, due to the fact that the porosity of the resulting materials can be controlled using the mineral component. The most common biomass with a high ash value is rice husk (RH), which contains 15-23% of amorphous silicon dioxide with impurities of alkaline-earth, alkaline, and transition metal oxides in an amount up to 4% of the total mineral content. At the same time, high-ash biomass can be successfully used to produce carbon-mineral composites (in this case, carbon-silica). On the other hand, due to the presence of a significant amount of silicon dioxide, RS is a rather attractive raw material for producing carbon-containing materials with developed porosity of carbon-silica composites and amorphous carbon materials with a high specific surface and pore volume [80].

Rice husk is a large-tonnage by-product of rice production. The global volume of education for schoolchildren is 150-180 million tons per year. Up to 50-60 thousand tons of RH are formed annually at rice processing factories of Kazakhstan alone, for the most part which is sent to dumps, creating significant environmental problems in these regions. Issues of utilization of RH, of which the annual annual renewability is of particular value as raw materials for chemical production, are very relevant today in almost all countries producing rice: Japan, China, India, the USA, Russia, and Uzbekistan. Disposal of RS is an urgent and difficult task, over which scientists of many countries have been working for a number of years [81].

Rice husk has a number of specific properties, which include: low bulk density; low calorific value, which substantially increases the cost of transporting RS during processing away from farms that cleanse grain; high abrasiveness, due to the high content of SiO_2, leading to rapid wear of equipment and lower feed quality. The physical and thermal properties of RH are also well studied. For most varieties, husk length is from 2 to 4 parts of rice length; specific gravity is approximately 0.1 g/cm^3. The calorific value ranges from 1000 - 3600 kcal/kg depending on the rice variety, and the hardness on the Mohs scale is 5.5 - 6.5 units [81, p. 43].

Among the inorganic components of ash, silicon oxide is in first place. The relatively wide fluctuations in the indices of inorganic components found in literary sources are explained by the unequal composition of plant materials, different purity

of ash samples, and different accuracy of analysis methods. In general, husk can be considered as silicon dioxide, containing a certain number of related impurities, the concentration of which depends on the plant variety and field soil composition [82, 83].

Figure 6 – The image of raw rice husk and carbonized rice husk

The nature of silicon in the husk of rice has been repeatedly studied by many scientists, most of whom believe that silicon in the plant is distributed in the form of monosilicic acid, which moves to the outer surfaces of plant tissues. Here, due to evaporation, it is concentrated and transformed due to polymerization into a cellulose-silica membrane.

The first publication on the study of RH appeared in Germany in 1871, then the next - after 2 years in the United States. Research on RH processing is still ongoing in all countries associated with rice cultivation. The results of studies showed that RH, subjected to heat treatment, can serve as the most valuable raw material for the production of various silicon compounds with unique properties [84-87].

3.2 Synthesis processes

In order to obtain graphene with a developed surface for membranes, the parameters of heat treatment of RH – carbonization (pyrolysis), which is a method of heat treatment of raw materials without air access in order to increase the carbon content in the final product, were optimized.

The process of pre-carbonization and carbonization were monitored through measurements of density, elemental composition, mechanical properties, and the stacking height of the carbon layer plane. Therefore, we pre-carbonized our RH before carbonization without air. The surface area of the resulting samples were investigated on the analyzer “Sorbtometr M” by low temperature nitrogen adsorption method (BET-method). The standard calculations of CRH shows that surface area of samples lies from 270 to 350 m^2/g.

In the case of silicon, containing carbon composites the use of alkaline agents such as NaOH or KOH is an extra way to obtain mesoporous materials due to washing out from the matrix the water-soluble Na or K silicates formed by the reaction:

$$2MeOH + SiO_2 \rightarrow Me_2SiO_3 + H_2O \quad (5)$$

where (Me = Na, K), and SiO_2 serves as a template for pore formation. Therefore, 1 M NaOH solution was used to obtain porous materials [88].

Potassium hydroxide is a known hydroscopic material letting the carbonization reactions to occur at substantially lower temperatures (its melting point is 380°C) compared to standard pyrolysis which, is governed mostly by radical processes leading in turn to disproportionation reactions yielding tar formation. The purpose of potassium hydroxide is therefore to provide both carbon retention (higher yields, e.g., less amount of volatiles are formed as hydrocarbon tar) and high surface area.

Although the KOH activation is a well-known method to generate the pore network in carbons, the activation mechanism has not been well understood because of the complexity due to the large number of variables in both the experimental parameters and the reactivity of different precursors used. In a general view, the interaction of carbon and KOH starts with solid–solid reactions and then proceeds via solid-liquid reactions including the reduction of potassium (K) compound to form metallic K, the oxidation of carbon to carbon oxide and carbonate, and other reactions among various active intermediates [89].

The real reaction processes and activation mechanisms are variable depending not only on the activation parameters (i.e. amount of KOH, activation temperature, etc.), but also on the reactivity of various carbon sources.

Table 5 – The general characteristics of raw materials and obtained samples

No	ID sample	Label	Conditions for obtaining samples
1	Raw rice husk	RH	Don’t treated
2	Precarbonized rice husk	CRH	Desilicated
3	Graphene (Rice Husk:KOH = 1:4)	$Gr(1/4)_1$	30 min desilicated, in air
4	Graphene (Rice Husk:KOH = 1:4)	$Gr(1/4)_2$	60 min desilicated, in argon gas,
5	Graphene (Rice Husk:KOH = 1:4)	$Gr(1/4)_3$	Don’t desilicated, exfoliated by H_2O_2,
6	Graphene (Rice Husk:KOH = 1:5)	$Gr(1/5)_1$	Desilicated (28.03.18)
7	Graphene (Rice Husk:KOH = 1:5)	$Gr(1/5)_2$	Desilicated (17.01.18)
8	Graphene oxide	GO	Oxidation graphite with H_2SO_4, by Robert Murray Smith method

According to the given method, 5 samples were synthesized with different KOH ratios. The main characteristics of samples are given in Table 5.

After synthesizing processes, samples were washed several times with bidistilled water up to reach neutral pH. The yields are given in Table 6.

Table 6 – The yields of samples

№	Before washing (g)	After washing (g)	%
CRH	0.504	0.428	84.92
$Gr(1/4)_1$	0.502	0.441	87.85
$Gr(1/4)_2$	0.507	0.439	86.59
$Gr(1/4)_3$	0.307	0.283	92.18
$Gr(1/5)_1$	0.502	0.450	89.64
$Gr(1/5)_2$	0.509	0.380	74.66

After washing processes, a functionalization was performed to activate the materials toward desalination. The yields of functionalized samples are given in Table 7.

Table 7 – The yields of samples

№	Before functionalization (g)	After functionalization (g)	%
CRH	0.309	0.289	93.53
$Gr(1/4)_3$	0.251	0.219	87.25
$Gr(1/5)_1$	0.308	0.243	78.89

After functionalization processes, samples were washed several times with bidistilled water up to reach neutral pH=7.

3.3 Material composition

3.3.1 Elemental analysis

The carbon, hydrogen and nitrogen contents of the samples were measured at the "ACE" laboratory of University of Naples Federico II by a PRIMACS100 analyzer and at IRC-CNR by a CHN 628 LECO elemental analyzer according to the ASTM E870 procedure using EDTA as standard. For each sample, two replicates were done and the average values are reported (maximum relative error around 0.7%) (Fig. 7).

As reported in Fig. 7, the sample $Gr(1/4)_3$ exhibits the highest amount of carbon (75%), while the raw rice husk exhibits the lowest amount ~36 %. We can generalized that the carbon contents increased by increasing the activation temperature of rice husk. Accordingly, the hydrogen contents of samples decreased by increasing the activation temperature. Different nitrogen contents were detected among of the samples. To ensure the reliability of the obtained data, the elemental composition of these samples was analyzed also at the University of Naples Federico II, a good accordance between the data collected at the University of Naples Federico II and those collected at the IRC-CNR is found.

The elemental composition of the samples was evaluated also after the washing and functionalization (with -SO_3H) processes. The average value of carbon content in samples are given in Fig. 8.

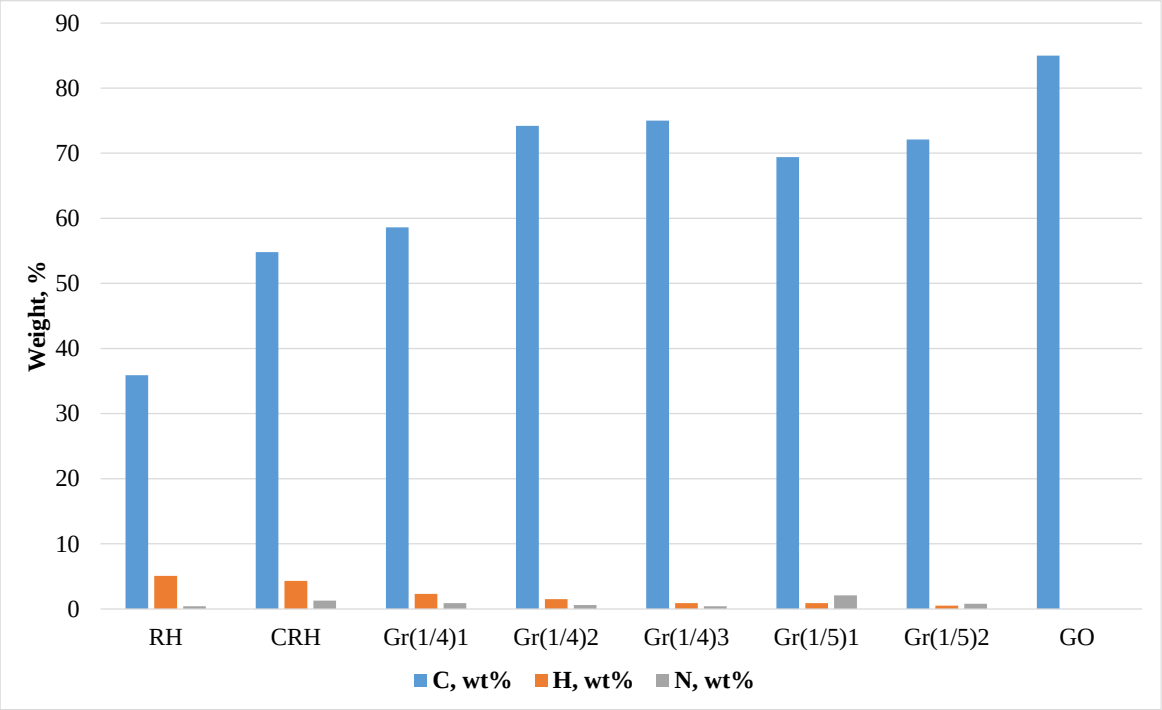

Figure 7 – Carbon, hydrogen and nitrogen contents of the samples (performed at the IRC-CNR)

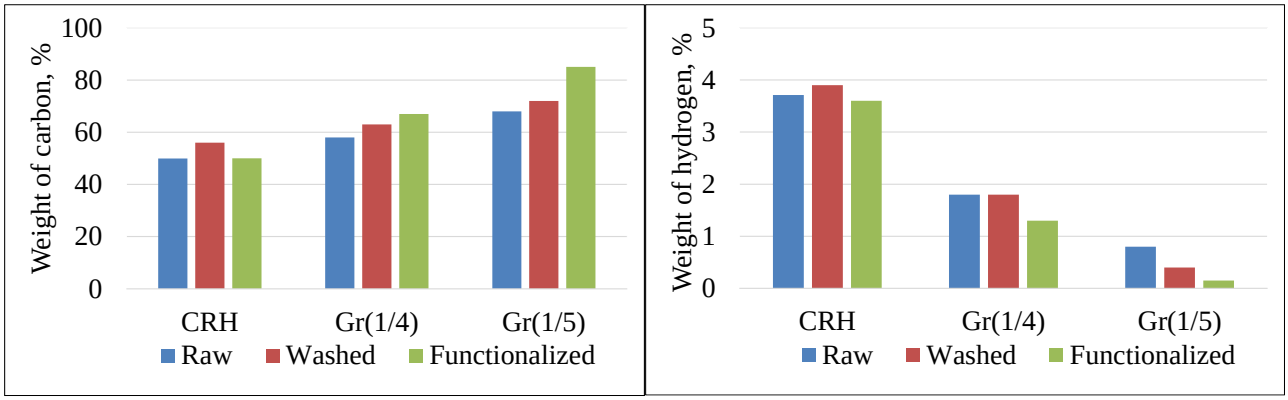

Figure 8 – Elemental composition of the samples after washing and functionalization processes

It can be clearly seen that the carbon content in all samples slightly increases and hydrogen content decreased after functionalization, while only for CRH it decreases after functionalization. The sample Gr(1/5) after functionalization exhibited the highest amount of carbon (85%).

3.3.2 Thermogravimetric analysis

Proximate analysis and ash content evaluation were performed at IRC-CNR, Naples, by using a thermogravimetric analyzer (TGA) 701 LECO. This measurement provided information about phase transitions, absorption and desorption; as well as chemical phenomena including chemisorptions, thermal decomposition, and solid-gas reactions (e.g., oxidation or reduction). The thermogravimetric analysis allowed for the estimation of the ash content of a selection of samples.

Even if the samples were burned at 800°C in pure oxygen, a little amount of carbon was still present Fig. 9(a-b). The thermogravimetric profile of raw RH is reported in Fig. 9c. The profile is characterized by a significant weight loss at a temperature below 400°C ascribable to volatiles relies, then the weight slowly decreases and keeps constant up to a final residue of 15,5 wt.%.

a

b

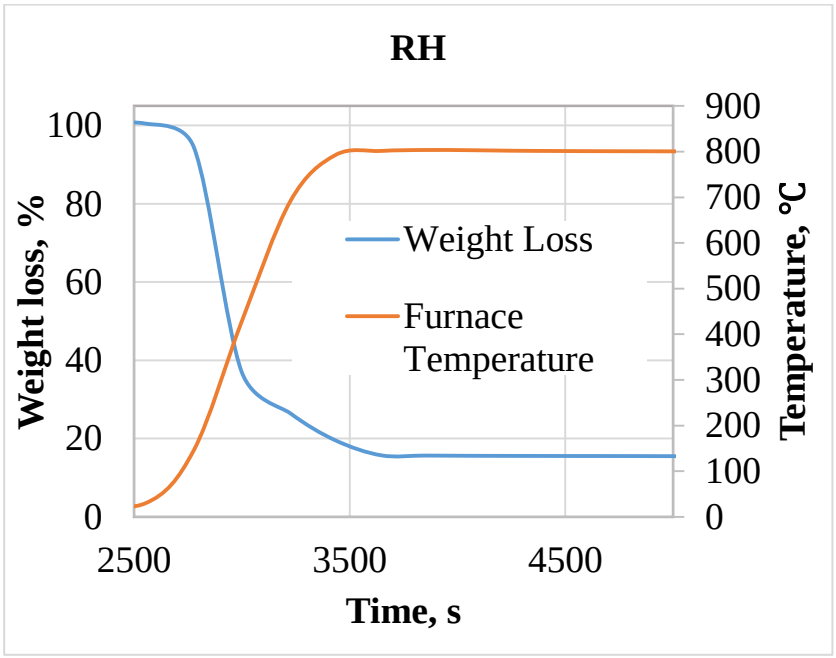

c

Figure 9 – The images of raw rice husk (a) and ash from rice husk (b) and TGA graph (c)

The thermogravimetric profile of raw CRH is reported in Fig. 10c and it is characterized by a weight loss at a temperature below 400°C ascribable to volatiles relies, then the weight slowly decreases and keeps constant up to a final residue of 15.53 wt.%. Amorphous carbon contains many impurities such as hydrocarbons and sulfur compounds. Graphene is one of the pure natural forms of carbon. Heating in a TGA instrument with give a significant difference between the amorphous carbon and graphene materials. Further, using an inert atmosphere, e.g. nitrogen, during the heating up gives another significant difference in comparison with air normal ambient air atmosphere.

For Gr(1/4), two stages of mass loss are shown, the first stage starts at 150°C is due to the loss of hydroxyl, epoxy functional groups and remaining water molecules

(Fig. 11c). The second stage lay between 500 and 650°C and involved the pyrolysis of the remaining oxygen-containing groups and cause formation of carbon ring.

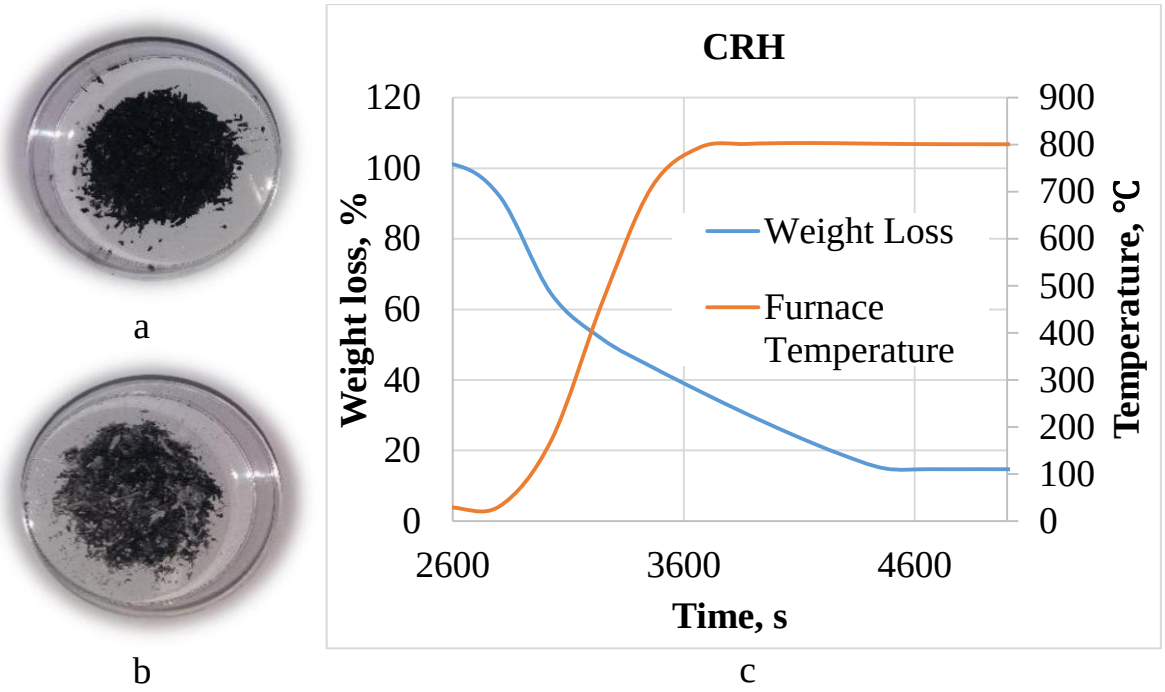

Figure 10 – The images of raw pre-carbonized rice husk and ash from pre-carbonized rice husk (CRH) and TGA graph (c)

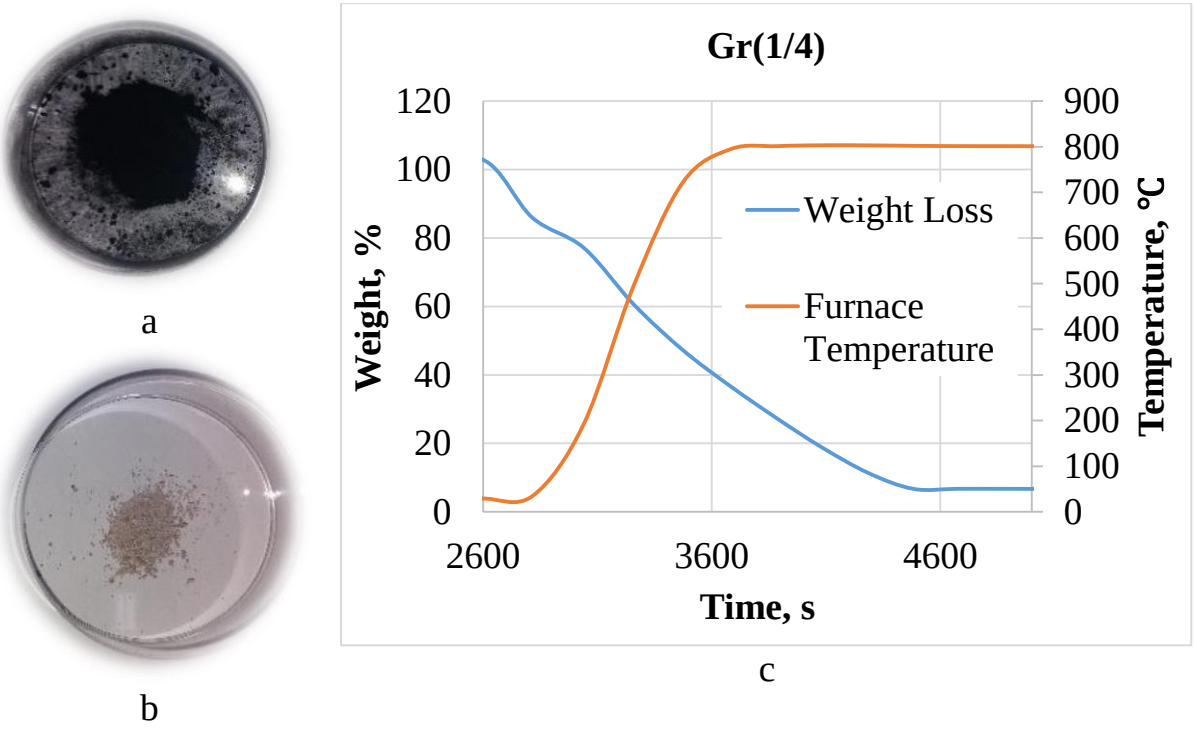

Figure 11 – The images of raw Gr(1/4) and ash from Gr(1/4) and TGA graph (c)

Also, the thermogravimetric profile of raw Gr(1/4) is characterized by a slowly weight decrease up to a final residue of 14.67 wt.%. The presence of a so low ash amount is indicative of a good purification process (Fig. 11b).

The thermogravimetric profile of raw Gr(1/5) is reported in Fig. 12c and it is characterized by a slowly weight decrease up to a final residue of 6.71 wt.%.

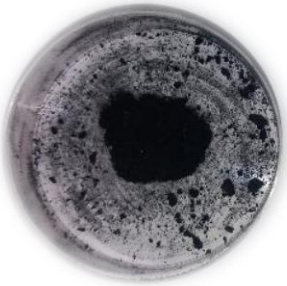

a

b

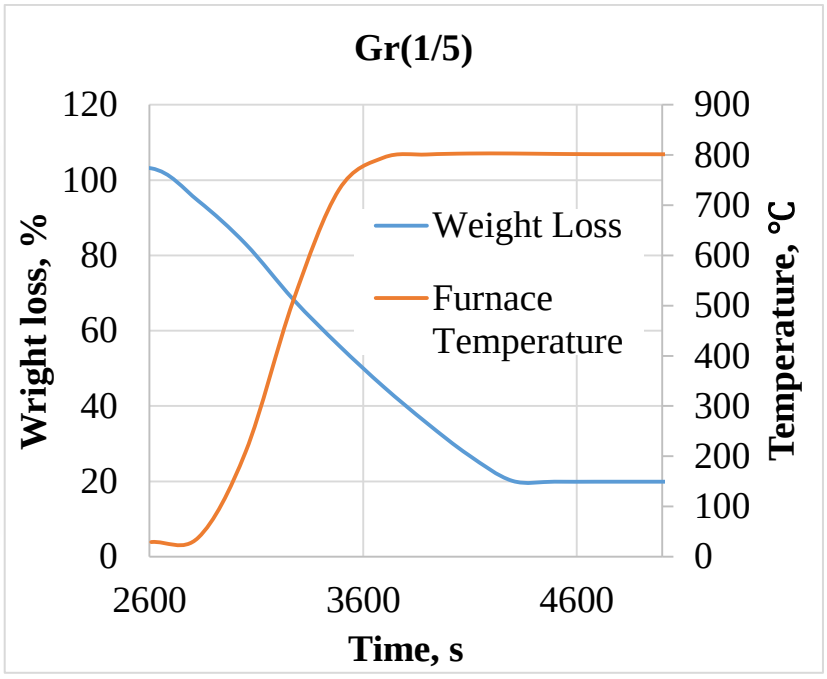

c

Figure 12 – The images of raw Gr(1/5) and ash from Gr(1/5) and TGA graph (c)

It is noteworthy the reddish color of the ashes (Fig. 12b). That color is indicative of the presence of some iron oxide that probably has been released by the overused crucible used for the synthetic procedure.

Thus, the thermogravimetric analysis results of Gr(1/4) and Gr(1/5) showed that the graphene sheets had good thermal stability below 100°C and up to 600°C. A slight weight loss appeared from 250 to 800°C is caused by the decomposition of the carbon skeleton.

3.3.3 Inductively coupled plasma mass spectrometry

The ICP-MS analysis of the liquids were performed at IRC-CNR, Naples on an Agilent ICP-MS 7500ce spectrometer. Each measurement was repeated twice. The quantitative determination of each metal was achieved extrapolating from a four points calibration curve. Some liquids collected after the washing process performed on the samples were analyzed by ICP-MS with the aim of achiving the quantitative determination of each metal. Figure 13 gives the ICP-MS results on the amount of various metals present in CRH, Gr(1/4) and Gr(1/5).

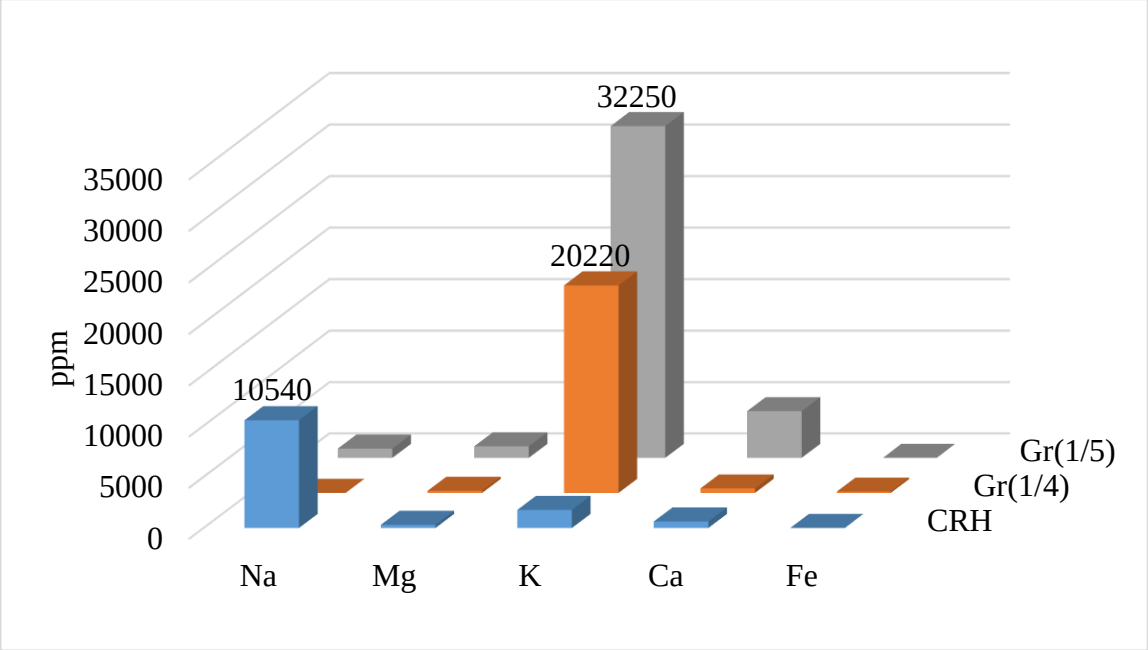

Figure 13 – Composition of metals in samples

As shown in the Figure 13, a large amount of sodium is present in the composition of the CRH, and this is explained by the fact that CRH is desilicated with 1M NaOH. Also, the presence of a large amount of potassium in Gr(1/4) and Gr(1/5) is explained by the activation with KOH of samples. The amount of potassium in Gr(1/4) is around 20220 ppm, while in Gr(1/4) is 32250 ppm. Therefore, these samples were washed several times with bidistilled water through boiling-sedimentation-decantation procedure. The yields are given in Table 5.

3.4 Morphology and surface chemistry

3.4.2 Scanning electron microscopy

The surface morphology of RH, CRH and graphene material, the elemental composition, including mapping, were performed by using three different scanning electron microscopes at the National Nanotechnological Laboratory of Open Type (Quanta 3D 200i Dual System, FEI.), at the "ACE" laboratory of University of Naples Federico II and at IRC-CNR (Nova NanoSem 450 FEI/Termofisher). The powders are deposed on an aluminium stub, Au, Pd coated and introduced into the specimen chamber of a field emission scanning electron microscope, at 3.00 kV in high vacuum mode, using an Everhart Thornley Detector and Through the Lens Detector for details micrographs and elemental microanalysis (EDX) at 15.00 kV. The main characteristics of samples are given in Table 8.

SEM images of raw rice husk at different magnifications are shown in figure 14 (a)-(d). Figure 14b shows the inner epidermis of rice husk, which has lamella structure. Figures 14c-d show the outer epidermis of rice husk, which is well organized and has a corrugated structure. The EDX analysis indicated that silica is mainly localized in the tough interlayer (epidermis) of the rice husk and also filling in the spaces between the epidermal cells. The concentration of silica was high on an external surfaces of the

husk (Fig. 14a) and much weaker on the internal face and practically non-existent within the rice husk (Fig. 14b).

Table 8 – The general characteristics of samples

ID sample	General characteristics	Size of samples by SEM analysis
RH	Intact and not friable sample	Millimetric size
CRH	Very friable sample	Millimetric size
$Gr(1/4)_1$	Particles of similar dimension and friable aggregates	Many (800-90) µm; some small (40-4) µm
$Gr(1/4)_2$	Very friable sample	Few 1 mm-300 µm; many (70-3) µm and also very small (<3) µm
$Gr(1/4)_3$	Particles as sheets very friable	Many (900-200) µm; some (100-20) µm; some very small (<10) µm
$Gr(1/5)_1$	Aggregates and very friable fragments	Some big 1,9 mm; many (500-80) µm; few very small (<10) µm
$Gr(1/5)_2$	Aggregates and very friable fragments	Many (400-100) µm; some (20-2) µm
GO	Friable fragments	100-50 (many) µm; 20-2 (some) µm

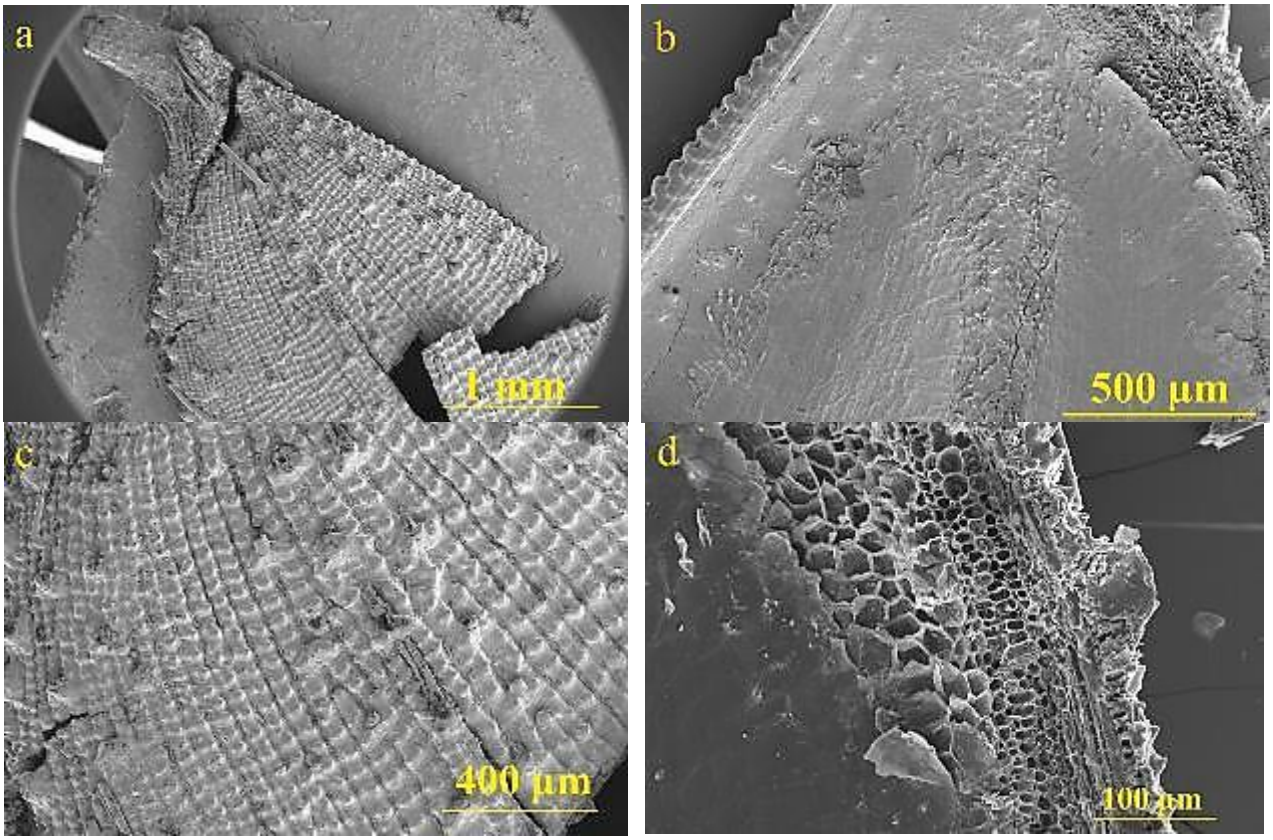

Figure 14 – SEM images of raw rice husk

To reach a good statistic of data, a first multi-element map to recognize the kind of element present in the sample and their distributions on the area considered was performed; then the multipoint analysis that consists to perform a single spectrum, point for point of area to examine was performed (Fig. 15).

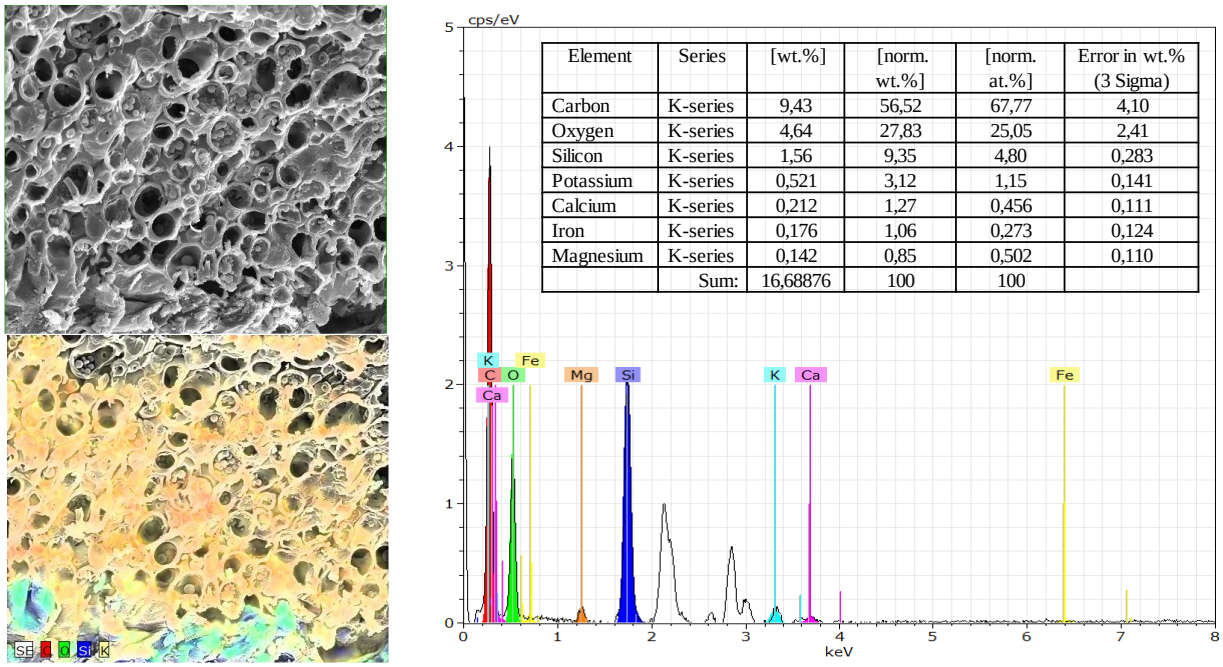

Element	Series	[wt.%]	[norm. wt.%]	[norm. at.%]	Error in wt.% (3 Sigma)
Carbon	K-series	9,43	56,52	67,77	4,10
Oxygen	K-series	4,64	27,83	25,05	2,41
Silicon	K-series	1,56	9,35	4,80	0,283
Potassium	K-series	0,521	3,12	1,15	0,141
Calcium	K-series	0,212	1,27	0,456	0,111
Iron	K-series	0,176	1,06	0,273	0,124
Magnesium	K-series	0,142	0,85	0,502	0,110
	Sum:	16,68876	100	100	

Figure 15 – EDX of raw rice husk

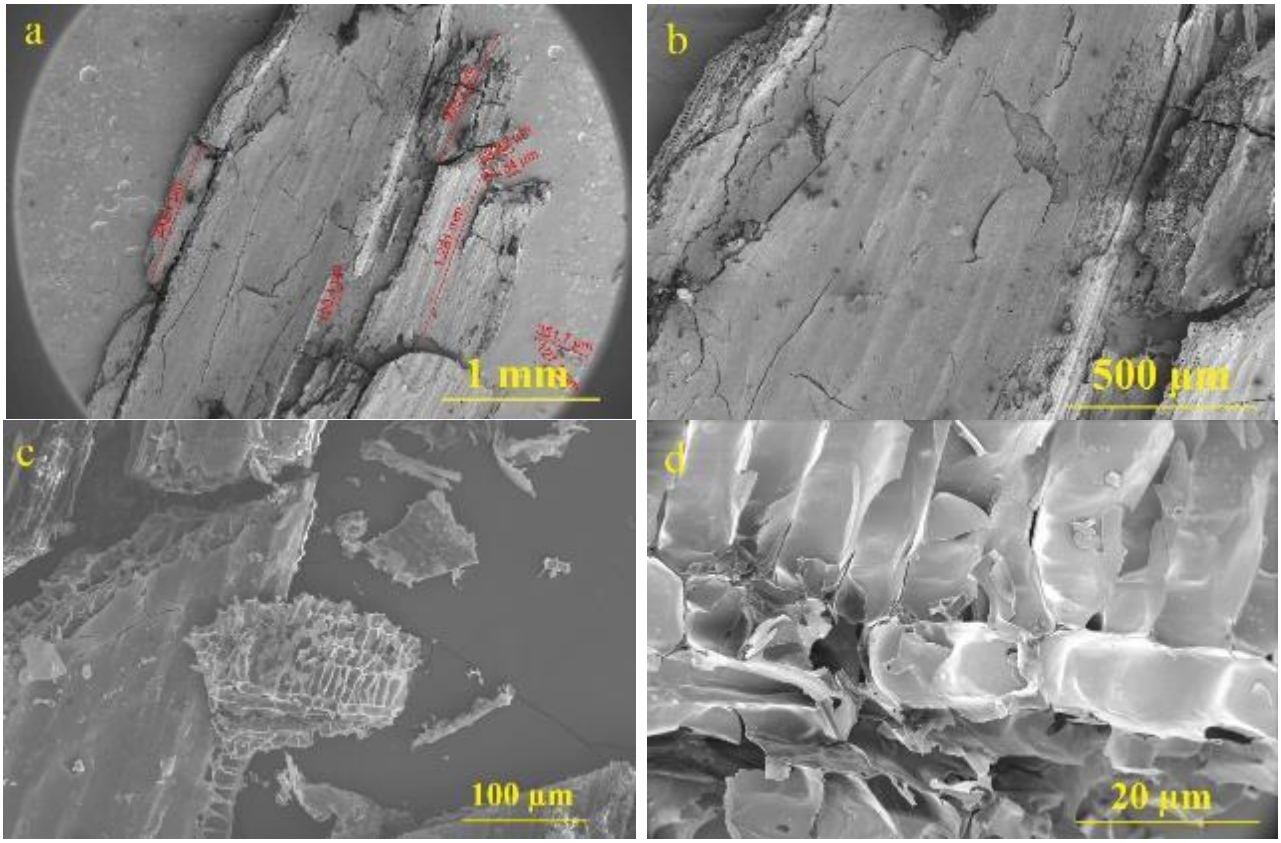

Figure 16 – SEM images of pre-carbonized rice husk

The rice husk have broken up during thermal decomposition of organic matter (Fig. 16a-b). Although the result data did not show much changes in its morphology compared to the initial rice husk, the SEM images show that the surface structure of the pre-carbonized rice husk changed significantly. The raw rice husk was intact and had a rather smooth surface, while the surface of CRH appeared to be uneven and had cracks.

Figure 17 shows the EDX results of pre-carbonized rice husk. The presence of elements: C, O, Si, K, Ca, Fe, Mg, Na and Al was confirmed by multipoint analysis of all the points analysed. The content of carbon equal to ~68 wt.%.

When CRH is activated with the chemical reagent KOH (1/4) at the temperature 850℃ for 2 h, there is the start of exfoliation in CRH and the structure becomes more defined and ordered (Fig. 18a-d): the annealed graphene sheets stack into a layer-by-layer structure throughout the transverse section, extending continuously along the longitudinal direction. However, microvoids are generated between graphene sheets during thermal annealing, resulting in a higher porosity.

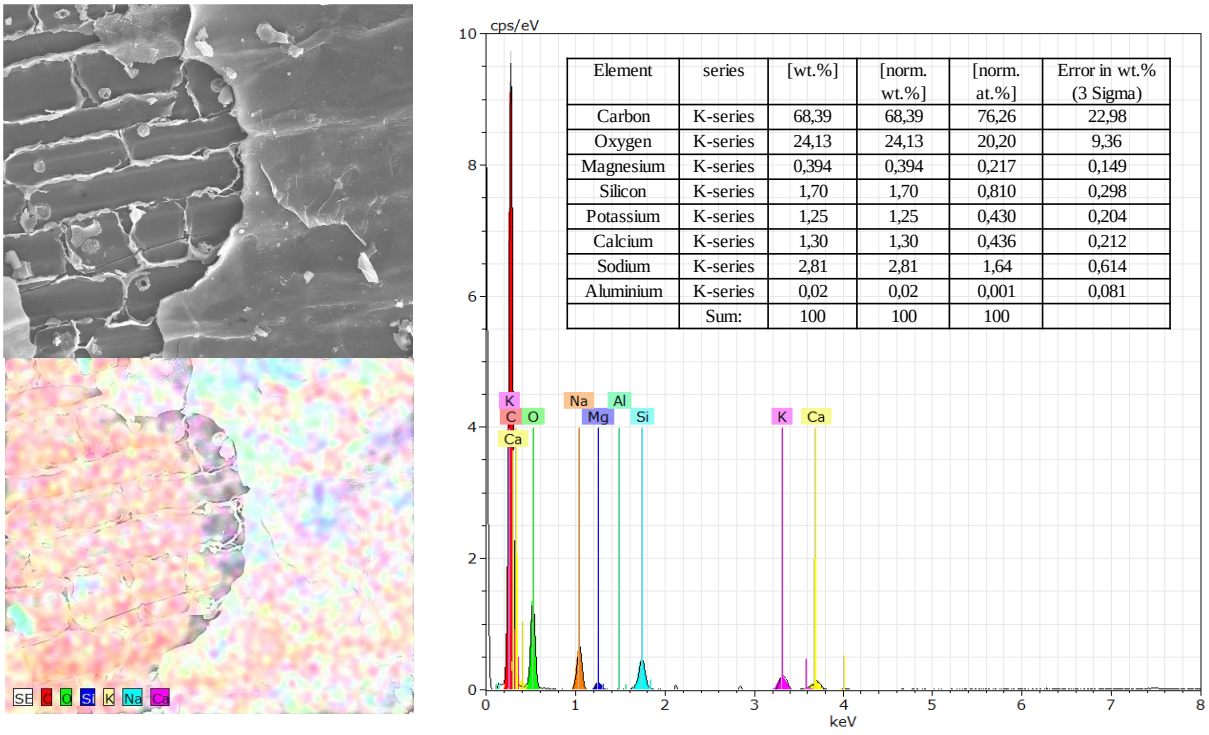

Element	series	[wt.%]	[norm. wt.%]	[norm. at.%]	Error in wt.% (3 Sigma)
Carbon	K-series	68,39	68,39	76,26	22,98
Oxygen	K-series	24,13	24,13	20,20	9,36
Magnesium	K-series	0,394	0,394	0,217	0,149
Silicon	K-series	1,70	1,70	0,810	0,298
Potassium	K-series	1,25	1,25	0,430	0,204
Calcium	K-series	1,30	1,30	0,436	0,212
Sodium	K-series	2,81	2,81	1,64	0,614
Aluminium	K-series	0,02	0,02	0,001	0,081
	Sum:	100	100	100	

Figure 17 – EDX images of pre-carbonized rice husk

The presence of elements: C, O, Si, K, and Fe is confirmed by multipoint analysis of all the points analyzed. The carbon content is ~88 wt.%, which is higher than carbon in pre-carbonized rice husk (Fig. 19).

The structure of sample activated in ratio of KOH 1/5 was found to be highly porous (Fig. 20a-d). A subsequent comparison of these samples with respect to the treatment ratio (activation at 850ºC and 2h and 1/5 of CRH/KOH) reflects a homogenous and uniform distribution of macropores and a greater size of pore. Probably, this effect obeys to the interconnection of pores and to the treatment ratio of KOH.

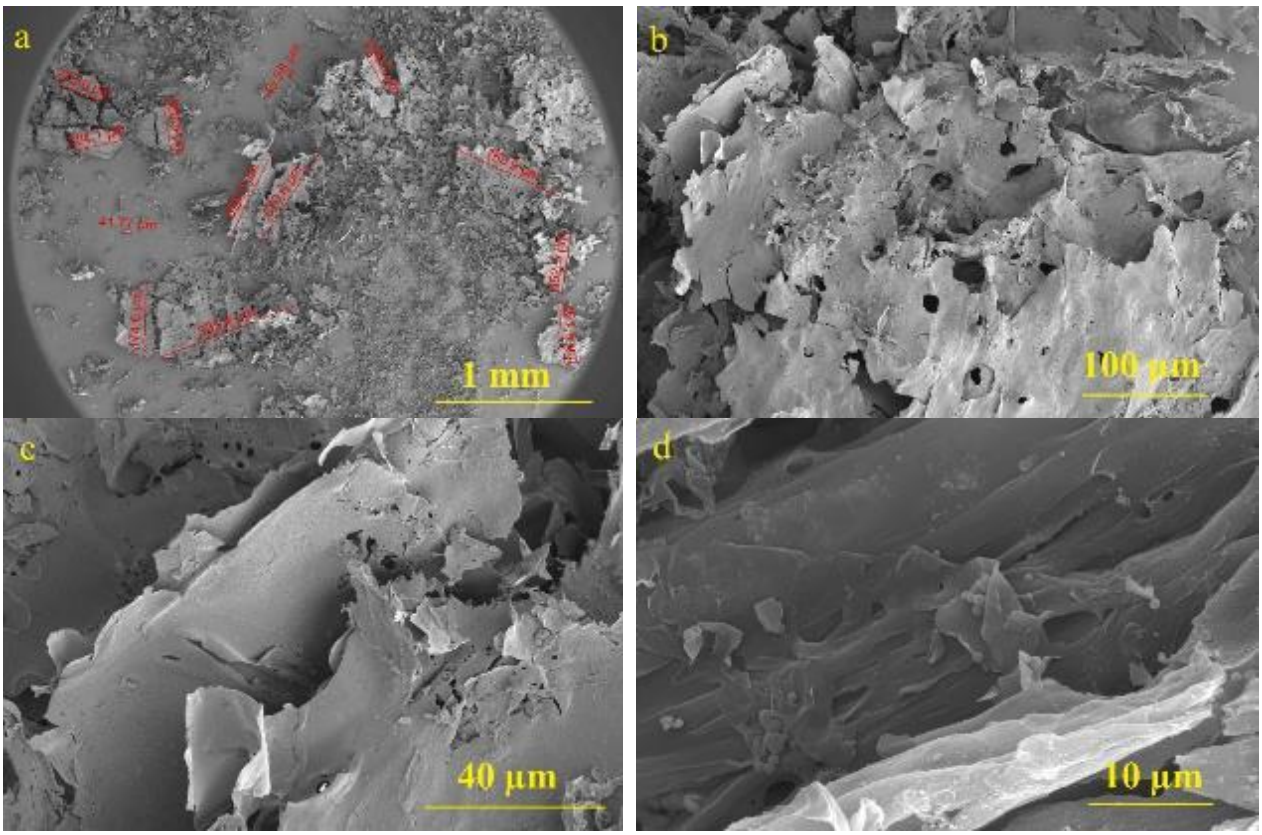

Figure 18 – SEM images of sample Gr(1/4)

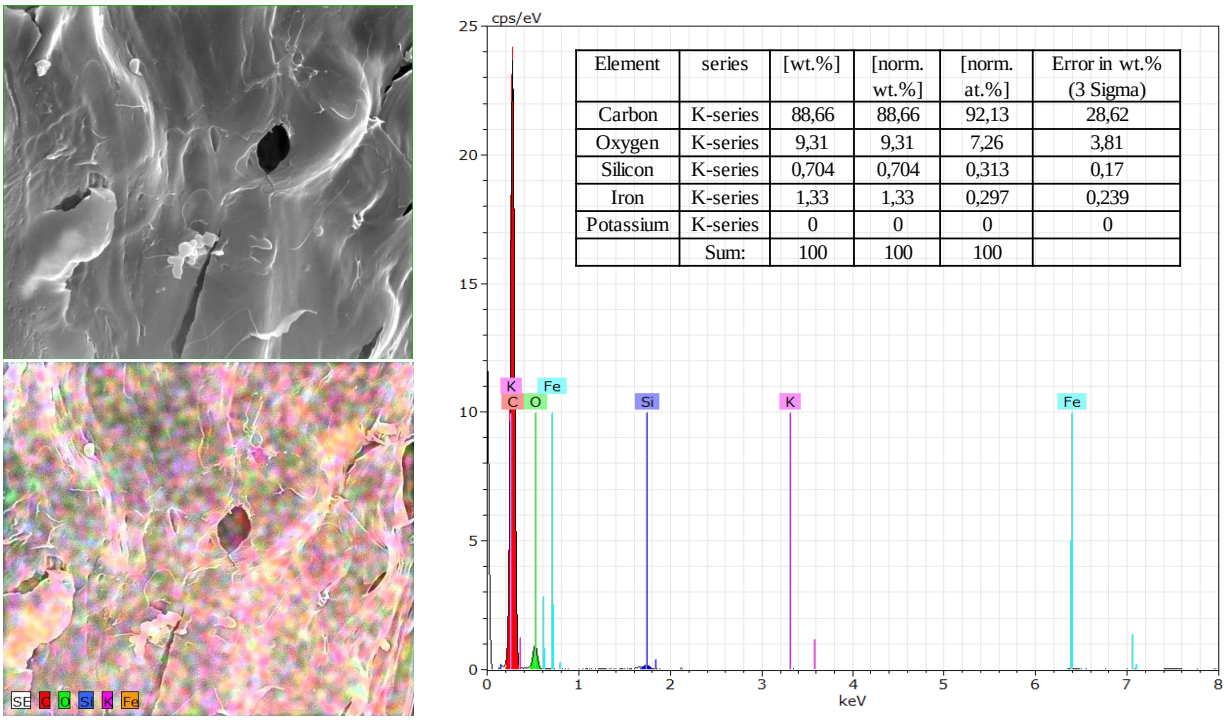

Element	series	[wt.%]	[norm. wt.%]	[norm. at.%]	Error in wt.% (3 Sigma)
Carbon	K-series	88,66	88,66	92,13	28,62
Oxygen	K-series	9,31	9,31	7,26	3,81
Silicon	K-series	0,704	0,704	0,313	0,17
Iron	K-series	1,33	1,33	0,297	0,239
Potassium	K-series	0	0	0	0
	Sum:	100	100	100	

Figure 19 – EDX images of sample Gr(1/4)

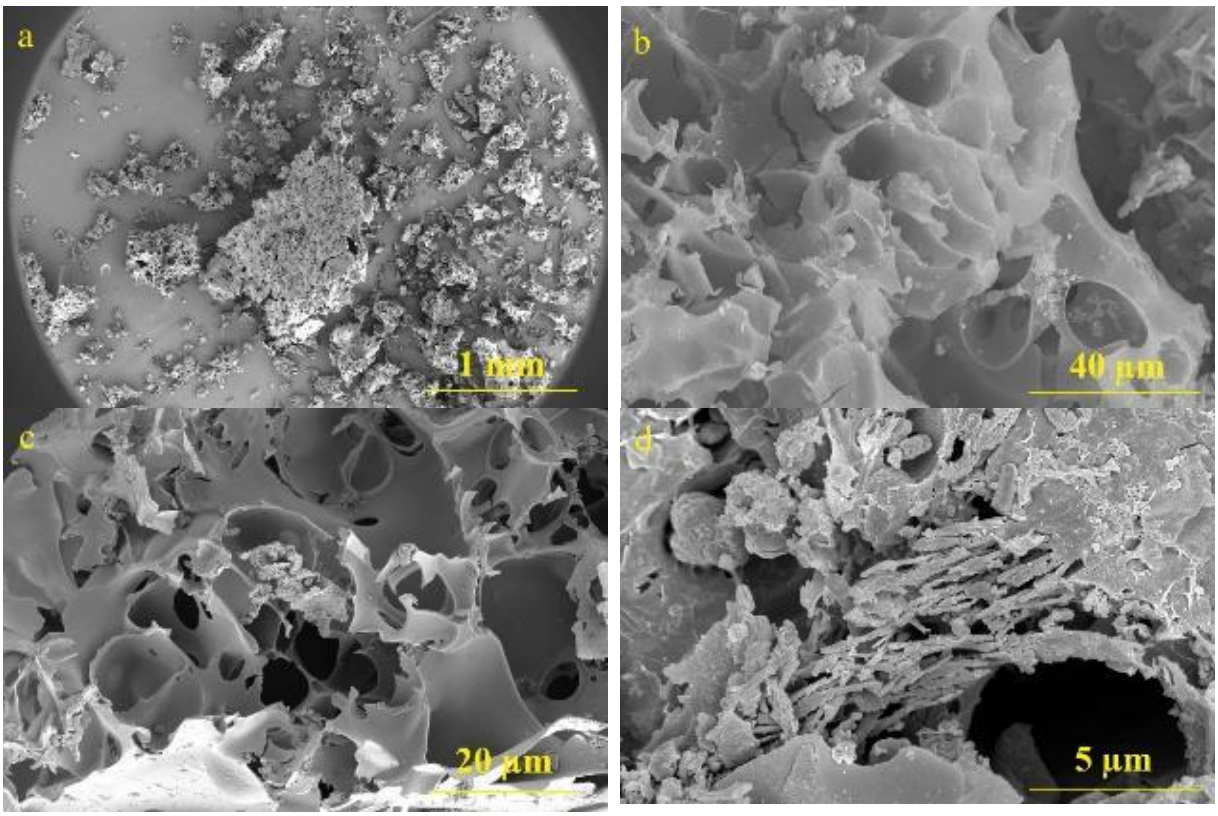

Figure 20 – SEM images of sample Gr(1/5)

The amount of carbon of CRH activated with ratio of KOH 1/5 for two hours is ~82 wt.%, which is similar to carbon in sample Gr(1/4). The presence of elements: C, O, Si, K, Mg, Ca and Fe was confirmed by multipoint analysis of all the points analysed (Fig. 21).

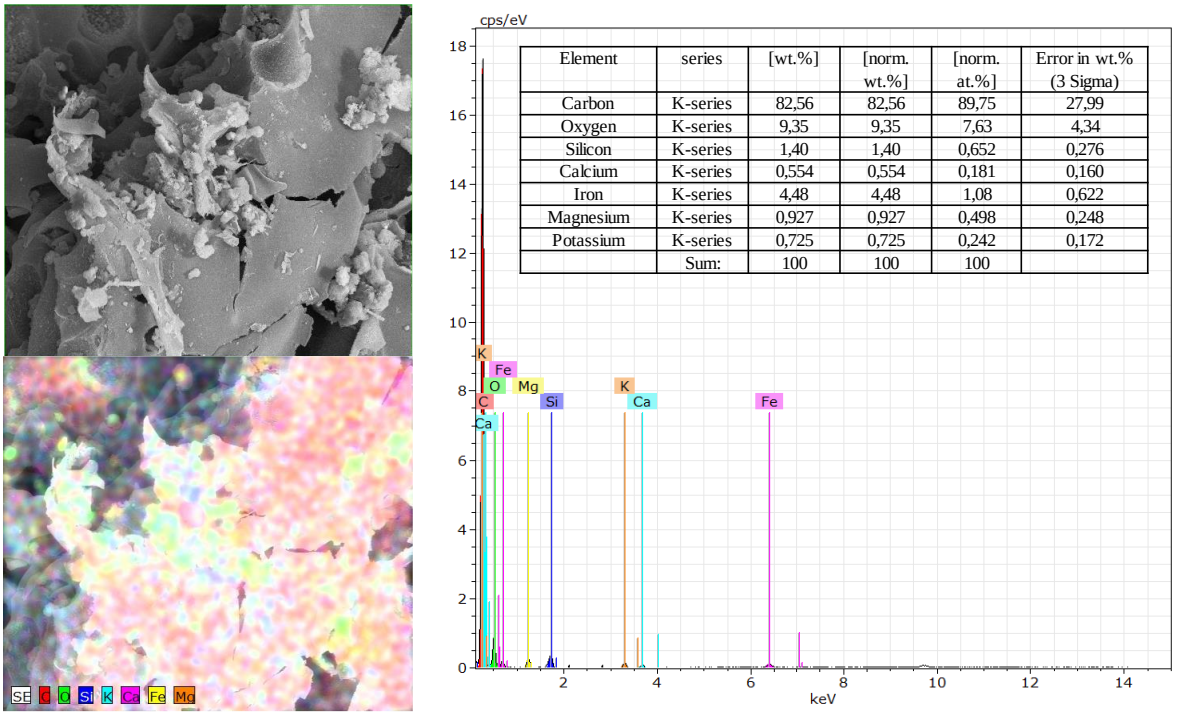

Element	series	[wt.%]	[norm. wt.%]	[norm. at.%]	Error in wt.% (3 Sigma)
Carbon	K-series	82,56	82,56	89,75	27,99
Oxygen	K-series	9,35	9,35	7,63	4,34
Silicon	K-series	1,40	1,40	0,652	0,276
Calcium	K-series	0,554	0,554	0,181	0,160
Iron	K-series	4,48	4,48	1,08	0,622
Magnesium	K-series	0,927	0,927	0,498	0,248
Potassium	K-series	0,725	0,725	0,242	0,172
	Sum:	100	100	100	

Figure 21 – SEM images of sample Gr(1/5)

Overall, from SEM images of Gr(1/4) and Gr(1/5) clearly seen that the Gr(1/4) have more layered structure than Gr(1/5), it is characterized by using desilication processes to Gr(1/4).

3.4.2 Transmission electron microscopy

Transmission electron microscopy (TEM) was used to study the features of the structure and size of particles of synthesized samples. Research was carried out on a JEM-2100 (JEOL, Japan) microscope (at Institute of Nuclear Physics, Almaty, Kazakhstan) with high stability of high voltage and beam current along with an excellent electron-optical system, pole tips HR, equipped with a field emission cathode, accelerating voltage 200 kV, an increase of 40 thousand. TEM involves the study of thin images using a beam of electrons passing through them and interacting with them. Electrons that have passed through the sample focus on the imaging device [90].

TEM images of graphene obtained from CRH using KOH activation are shown in Figure 24.

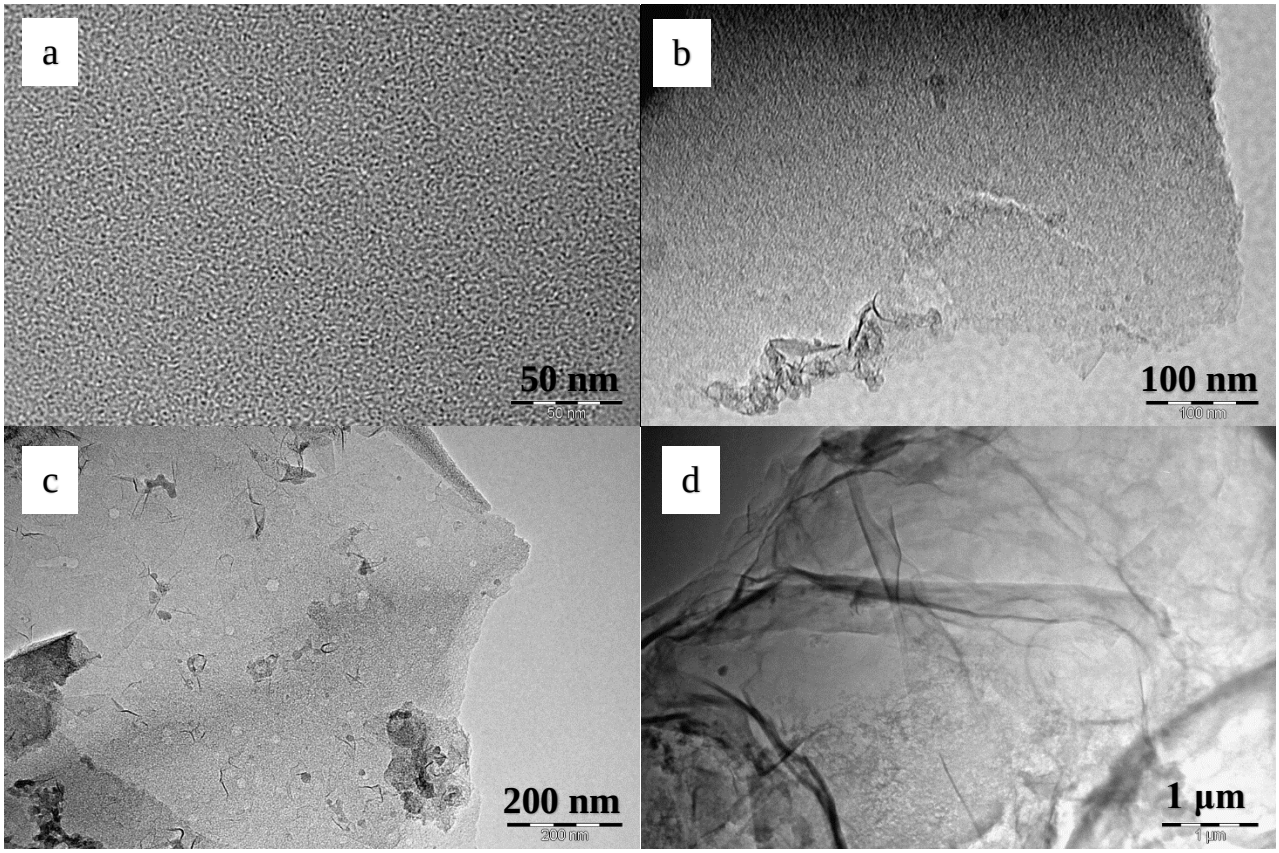

Figure 22 – TEM images of Gr(1/4)

Micrographic images confirmed the synthesis of several graphene layers (Fig. 22b, d). The layers have defects and inclusions of the carbon component (Fig. 22c), however, there are areas without defects with a homogeneous surface structure (Fig. 22a). The general characteristics of raw materials and obtained samples were shown in Table 4.

3.5 Determination of specific surface by BET method

The BET method is based on the sorption of nitrogen at liquid nitrogen temperature. The specific surface is estimated by the amount of inert gas adsorbed by the material and by the air permeability of the layer of powder or porous material. Adsorption methods provide the most reliable data. Samples were investigated on the instrument SORBTOMETR-M. The principle of operation of analyzers is based on the dynamic (thermal desorption) method, which consists in measuring the volume of adsorbed argon or nitrogen, which is in sorption equilibrium and in contact with a dispersed porous material. The results of measurements of the volume of adsorbed argon or nitrogen are used to calculate the specific surface area based on the Brunauer-Emmett-Teller equation (BET) [91-93].

The following table 9 presents the data of the BET analysis of the surface of samples RH, CRH and graphene materials. As follows from the table, the specific surface area of carbonized rice husk is 201.349 m^2/g, the specific pore volume is 0.087 cm^3/g and the average pore size of 1.723 nm, indicate those characteristics of the sorbent that determine its suitability as a raw material for obtaining adsorbents.

Table 9 – Data sorption analysis of the surface of samples

Sample Name	Specific surface area S, m^2/g	Specific pore volume, V, cm^3/g	The average pore size, nm
RH	47.268	0.059	1.723
CRH	201.349	0.087	1.723
Gr(1/5)	2817.774	1.587	26.126

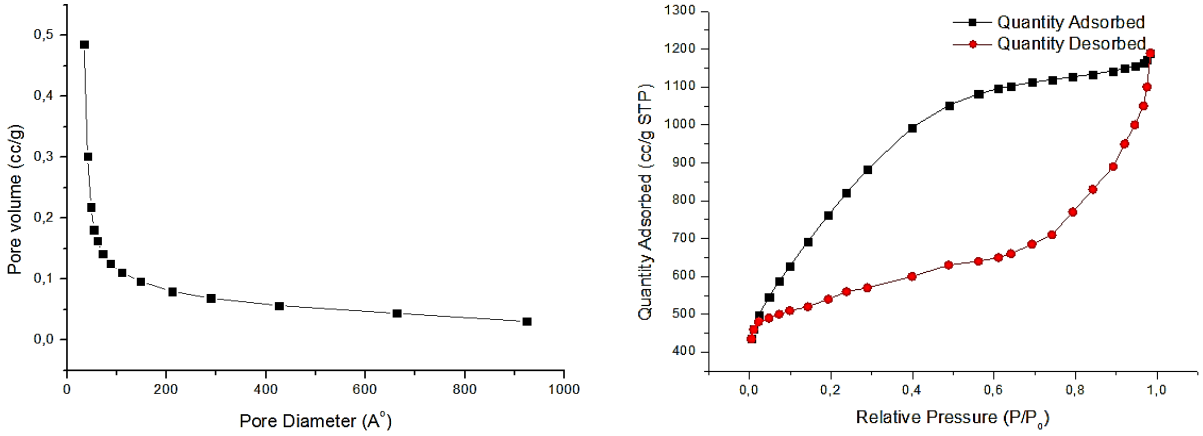

Figure 23 – BET analysis of the Gr(1/5)

Figure 23 shows the results of measurement of microstructure and pore characteristics of the Gr(1/5) sample by using the BET specific surface area analyzer. Specific surface areas of graphene sample was 2817 m^2/g and the average pore diameter was 26.126 nm with a considerable amount of ultrafine pores less than 80 nm being also observed.

3.6 Material spectroscopically properties

3.6.1 Raman spectroscopy

Raman investigation was performed to evaluate the presence of nanostructured carbon, as graphene, and to estimate the number of layers characterizing the nanostructures. Raman spectroscopy of Raman scattering is a molecular spectroscopy to observe inelastic-scattered light and allows the identification of vibrational states (phonons) of molecules. Studies were conducted on the instrument of the National Nanotechnological Laboratory of Open Type by Solver Spectrum (NT-MDT) and at the University of Naples Federico II by Jasco NRS-3100. By using Solver Spectrum (NT-MDT), Raman spectra were obtained by excitation with a blue laser with a wavelength of 473 nm, the signal accumulation time was 30 seconds. The spectral resolution of the grating is 4 cm^{-1}. Another type of Raman microscope (Jasco, NRS-3100) was worked at the 514 nm line of a water cooled Ar+ laser, 4 mW at the sample, was injected into an integrated Olympus microscope and focused to a spot diameter of approximately 2 μm by a 100× objective. A holographic notch filter was used to reject the excitation laser line. Raman scattering was collected by a Peltier-cooled 1024×128 pixel CCD photon detector (Andor DU401BVI). Raman measurements were at least triplicated for scope of reproducibility. Cyclohexane was used for calibration [94].

To study the Raman spectra of the obtained samples, the basic picture of the Raman spectroscopy of graphene and graphite was given (Fig. 24).

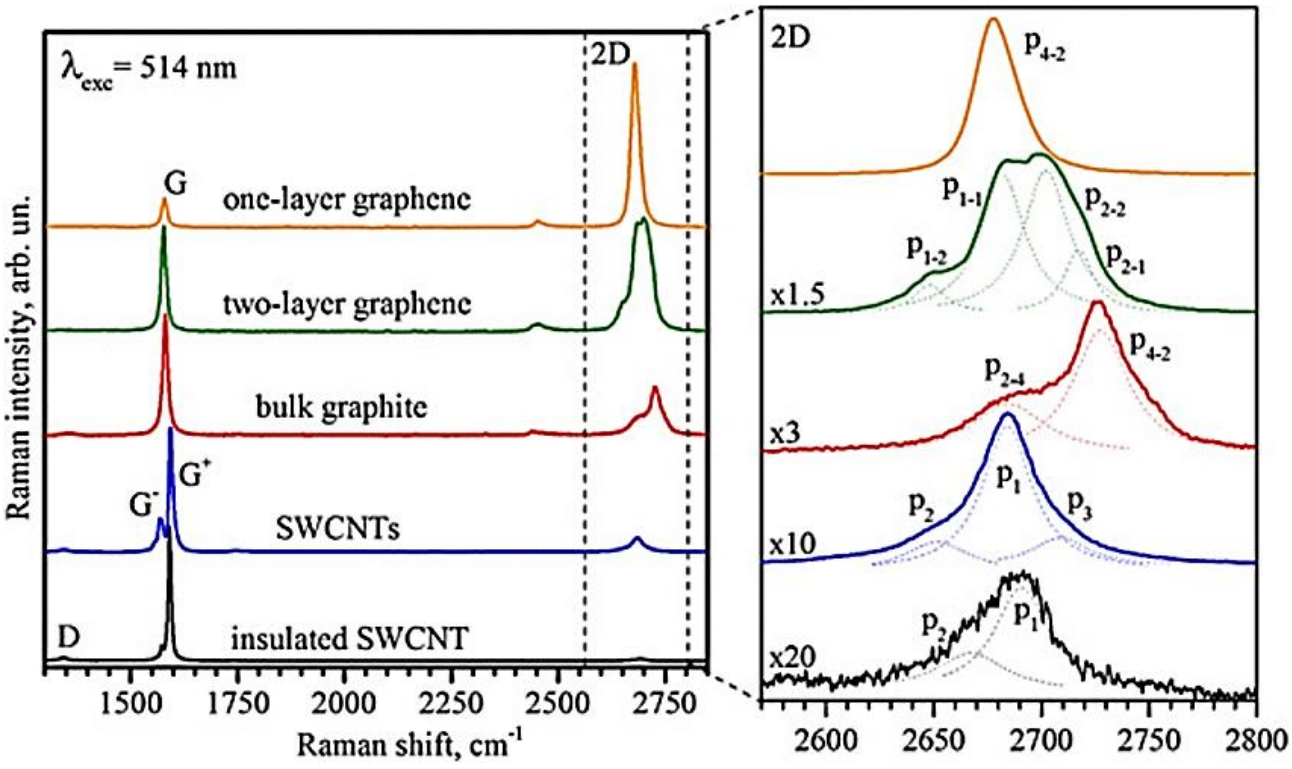

Figure 24 – Raman spectra of single-layer graphene, two-layer graphene, bulk graphite, mixture of SWCNTs, and single SWCNT [95]

In the Raman spectra of one-layer graphene besides allowed in the first-order scattering processes of G band, which is caused by twofold degenerated valence intra-

layer vibrations of C-atoms, intensive single two-phonon 2D band is observed [96]. This band is due to second-order processes for phonons near the K-point [97]. The intensity relation of G and 2D bands (I_{2D}/I_G~5) and uniform contour of 2D band are the typical features of single-layer graphene [96, 98]. The 2D band in the Raman spectra of two-layer graphene consists of four components, which are well approximated by four Lorentz contours [98]. These components are known to be related with the structure of electron bands, which are revealed due to double electron-phonon resonance [96]. The 2D band in the Raman spectrum of monocrystalline Bernal graphite contains only two components, which also reflects the electron band structure.

The real reaction processes and activation mechanisms are variable depending not only on the activation parameters (i.e. amount of KOH, activation temperature, etc.), but also on the reactivity of various carbon sources. To determine the optimal temperature of mixture KOH/CRH for obtaining graphene, were taken three samples and heated at the temperatures of 650°C, 750°C and 850°C. A quick and accurate way to determine the number of layers of graphene is of great importance in accelerating the study of this material. As in the previous works [70-76] we determined the number of graphene layers obtained by employing the proposed method (Table 10).

Table 10 – The investigation of optimal ratio and temperature for obtaining graphene layers

ID sample	Ratio of CRH/KOH, g/g	Temperature, °C	I_G/I_{2D}	I_D/I_G	Number of layers
CRH_1	1/4	650	-	-	
CRH_2	1/4	750	-	-	
CRH_3	1/1.5	850	-	-	
Gr(1/4)	1/4	850	2.06	0.29	7 – 8
Gr(1/5)	1/5	850	1.57	0.39	4 – 5

Samples obtained at temperatures of 650°C (sample CRH_1) and 750°C (sample CRH_2) largely retained the amorphous phase of carbon. A sample obtained at 850°C showed the presence of a graphite phase (sample CRH_3). According to Raman spectra high quality graphene multilayer were not found in samples CRH_1, CRH_2 and CRH_3 (Fig. 24), in contrast to samples Gr(1/4) and Gr(1/5) (Fig. 25).

These results indicate that CRH/KOH ratio of 1/4 and 1/5 at a temperature of 850°C should be used during the preparation of graphene. Calculation data for graphene layers based on Raman spectroscopy indicates a decrease in the number of layers with an increase in the ratio CRH/KOH from 1/4 to 1/5.

Raman investigation allows to distinguish amorphous carbon from graphite or from nanostructured graphene. The main features in the Raman spectra of carbons are the so-called G and D peaks, which lie at around 1560 and 1360 cm^{-1} respectively for visible excitation. Non-amorphous sp^2 carbon structures exhibit an additional G' (or 2D) band as well around 2700 cm^{-1}. Also, the ratio between the intensities of peak *G* I_G and peak 2D I_{2D}, I_G/I_{2D} gives an estimate of the number of layers. For monolayer

graphene, this ratio is less than unity. The ratio between the intensities of peak *D* I_D and peak G I_G, I_D/I_G evaluates the defectiveness of graphene layers.

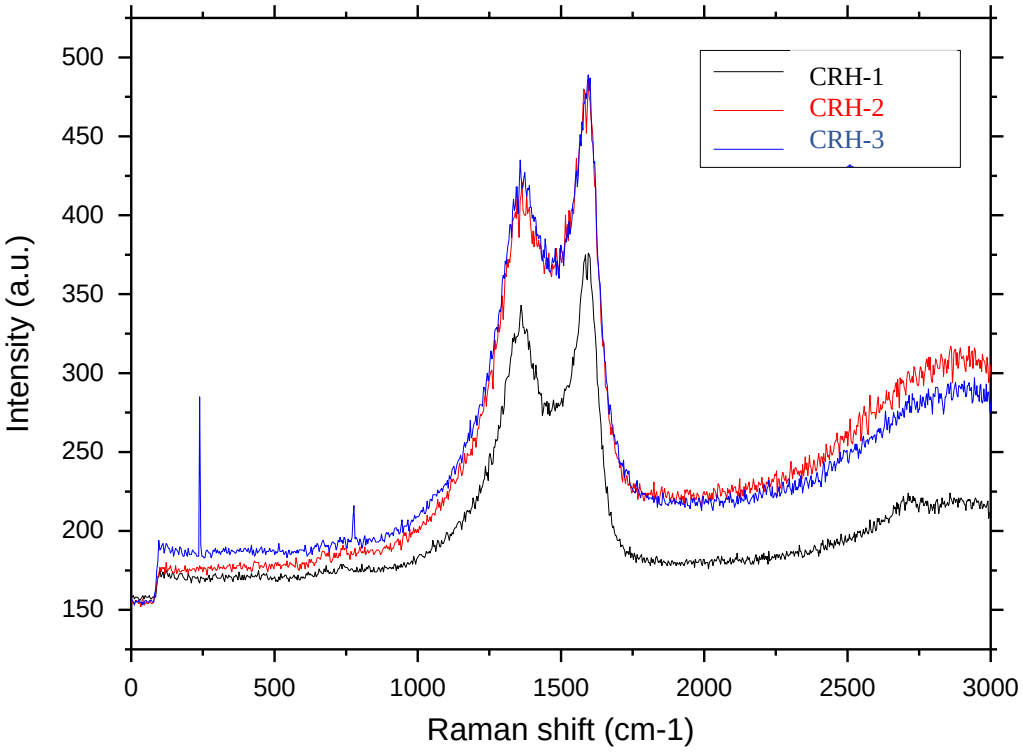

Figure 25 – Raman spectra of samples CRH_1, CRH_2 and CRH_3

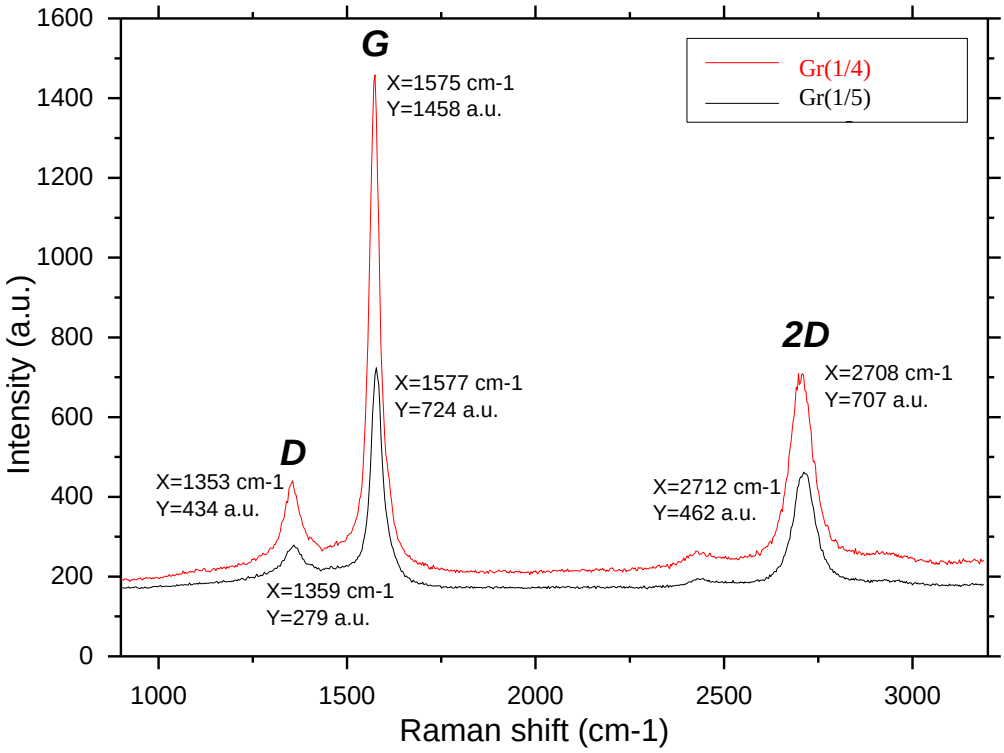

Figure 26 – Raman spectra of sample Gr(1/4) and Gr(1/5)

Figure 26 shows Raman spectra of graphene layers obtained from CRH. The maximum number of graphene layers is less than ten (Table 10), as indicated by the ratio between the peaks' intensities I_G/I_{2D}. It was shown [99] that the ratio of I_G/I_{2D} = 1.3 corresponds to three layers of graphene, whereas the authors of [100] found that I_G/I_{2D} = 1.8-2.4 corresponds to 5-10 layers of graphene.

Also, after washing and functionalization processes of samples, the Raman spectroscopy analysis were performed at the University of Naples Federico II by Jasco NRS-3100. CRH exhibits some fluorescence, along with Raman features related to only amorphous carbon (D and G bands) in all the three treatments with no trace of G' band. Representative Raman spectra were collected for the 3 samples treated in 3 different ways (Figures 27-29).

Raman spectra of Gr(1/5) and Gr(1/4) clearly indicate a mixture of amorphous and graphene entities. The ratio of the two components is spatially variable, so the spectra in Figure 28 and 29 are only representative of the mixture of sample Gr(1/5) and Gr(1/4). Spectra containing only features of amorphous or graphene components were obtained by subtracting to the mixture the contribution of pure amorphous (Fig 30).

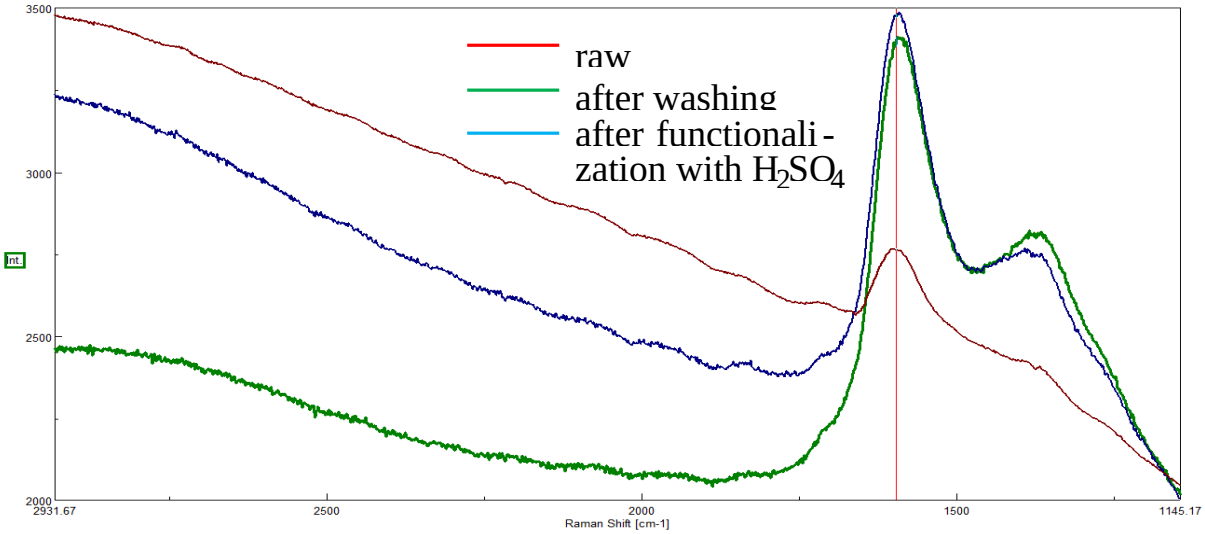

Figure 27 – Raman spectrum of the sample CRH

Both activated samples with ratio 1:4 (Gr(1/4)) and 1:5 (Gr(1/5)) exhibit D, G and G' bands. A significant spatial heterogeneity is detected, but two major components can be isolated: amorphous carbon (with D and G bands around 1352 and 1594 cm^{-1}) and graphene (with detectable D, G and G' bands). We analyzed the ratio $I_G/I_{G'}$ only for those spots were amorphous C was considered negligible. For both samples Gr(1/5) and Gr(1/4), the ratio $I_G/I_{G'}$ is close to 1,56±0,10, suggesting a multilayered structure. Nevertheless, all the Raman spectra showing G' bands exhibit very symmetric line shape, typical of a 1-2 layer graphene.

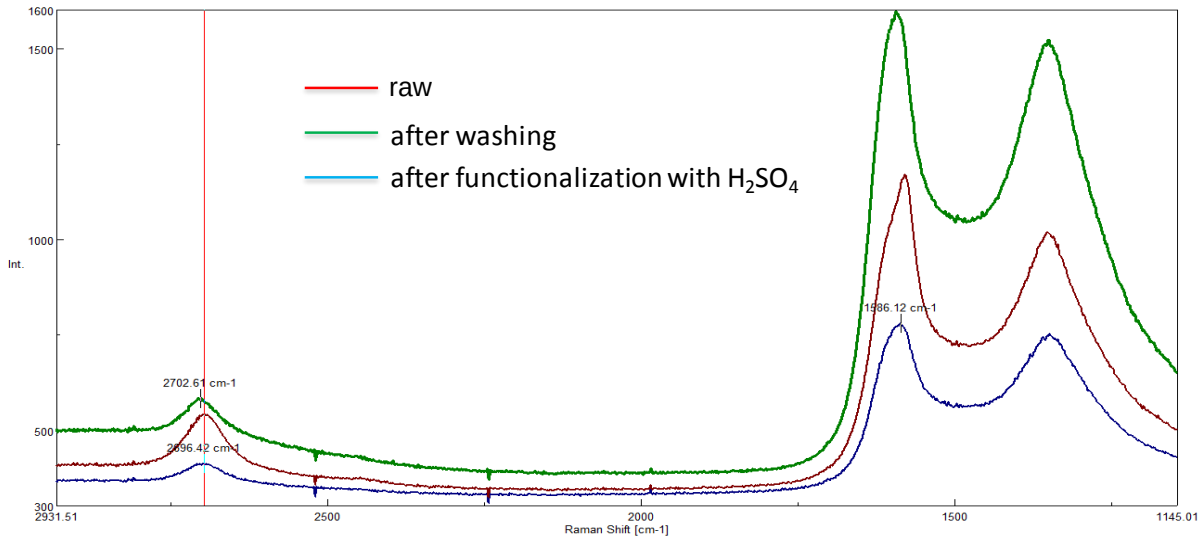

Figure 28 – Raman spectrum of the sample Gr(1/4)

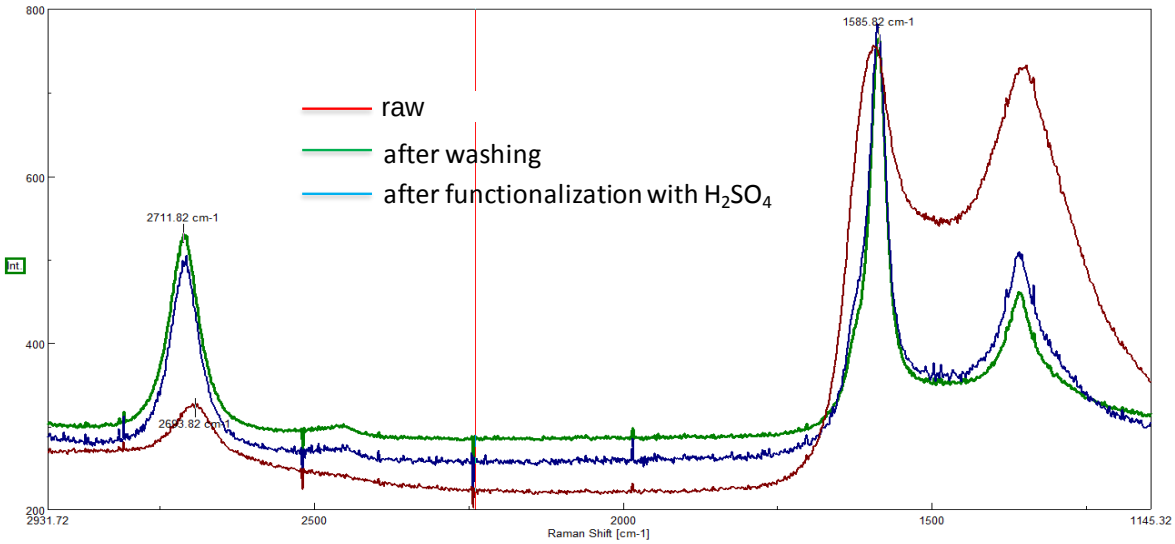

Figure 29 – Raman spectrum of the sample Gr(1/5) (G/G'=2)

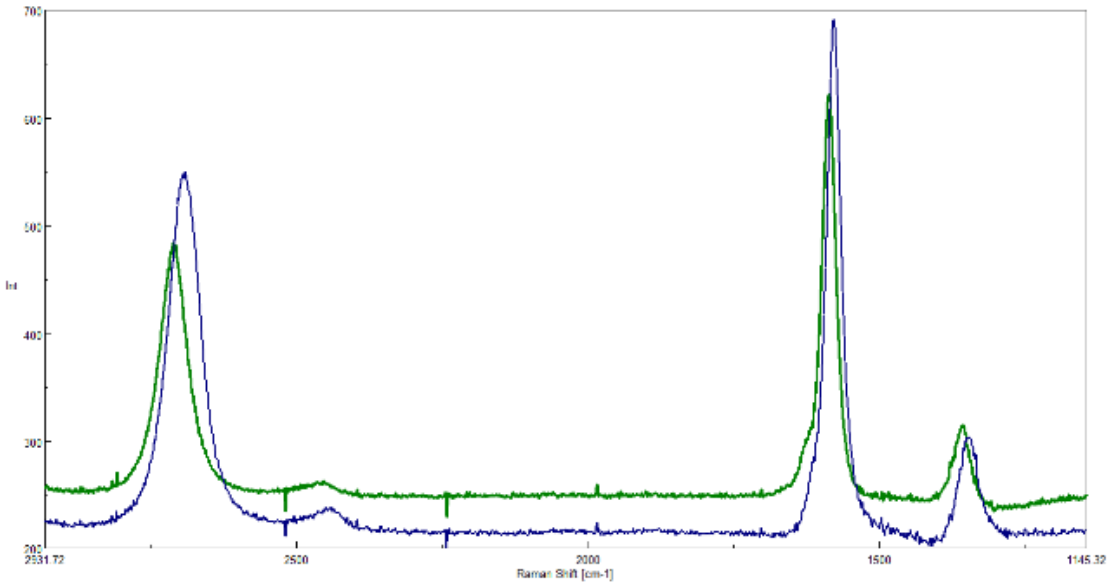

Figure 30 – Raman spectrum of the sample Gr(1/5) (green) and Gr(1/4) (blue)

Whatever is the number of layer (to be confirmed), the ratio and the lineshape in Figures 28 and 29 suggest similar nanostructuring in samples Gr(1/5) and Gr(1/4).

Interestingly, in samples $Gr(1/5)_1$ and $Gr(1/4)_3$, the graphene-related bands are somehow shifted: 1358/1596/2711 cm^{-1} in sample Gr(1/4), and 1350/1579/2694 cm^{-1} in sample Gr(1/5). By comparing sample Gr(1/5) and Gr(1/4) in the limited sampling we have performed, the activation ratio 1:5 provides a higher graphene content than 1:4. No effect of H_2SO_4 was detected via Raman.

Also, the sample obtained from graphite was analyzed by Raman spectroscopy (Fig. 31). Discerning the two-dimensional nature of graphene can be accomplished by contrasting the G′-band features of graphite and the former material. First, the relative intensities between the G and G′ bands are different for graphene and its macroscopic relative graphite. In the case of graphene, the G′-band has a greater intensity than the G-band, which is the case for G-bands illustrated in Figure 24. The G′-band of graphite is also shifted to a higher frequency compared to that of graphene. Thirdly, the overall shape of the G′-band is usually more uniform compared to that of graphite, usually requiring a single Lorentzian to be fitted [101].

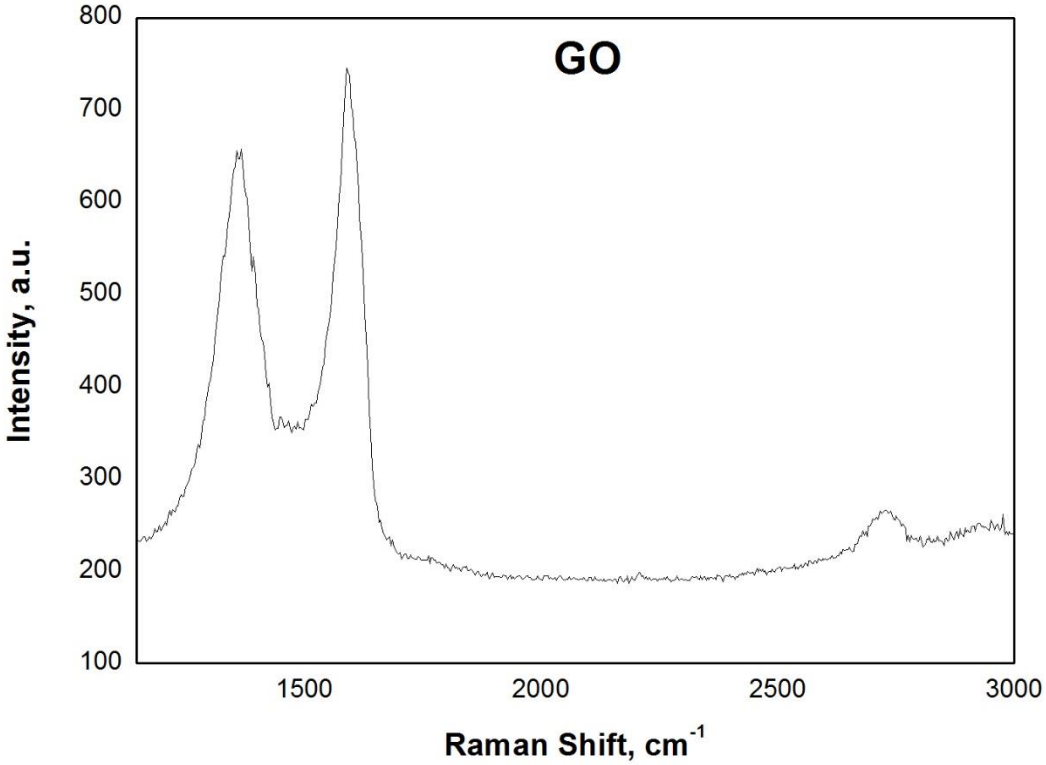

Figure 31 – Raman spectrum of the GO obtained from graphite

The results indicate a mixture of amorphous carbon and graphene entities, which corresponds to three peaks: peak D at 1363 cm^{-1}, peak G at 1588 cm^{-1}, and peak G' at 2725 cm^{-1}.

3.5.2 Fourier-transform infrared spectroscopy

To identify organic, polymeric, and inorganic materials in samples of the RH, CRH and graphene, fourier-transform infrared spectroscopy (FTIR) analysis were

performed at IRC-CNR, on solid sample dispersions prepared by mixing and grinding the powdered materials (0.5-0.8 wt.%) with KBr. Pellets of the solid mixtures were obtained upon compression at 10 Ton for 10 minutes. FTIR spectra in the 3400 - 400 cm^{-1} range were acquired in the transmittance mode using a Nicolet 5700 spectrophotometer. The data of CRH, Gr(1/4), Gr(1/4) and Gr(1/5) after washing and functionalization are reported in figures 32-35.

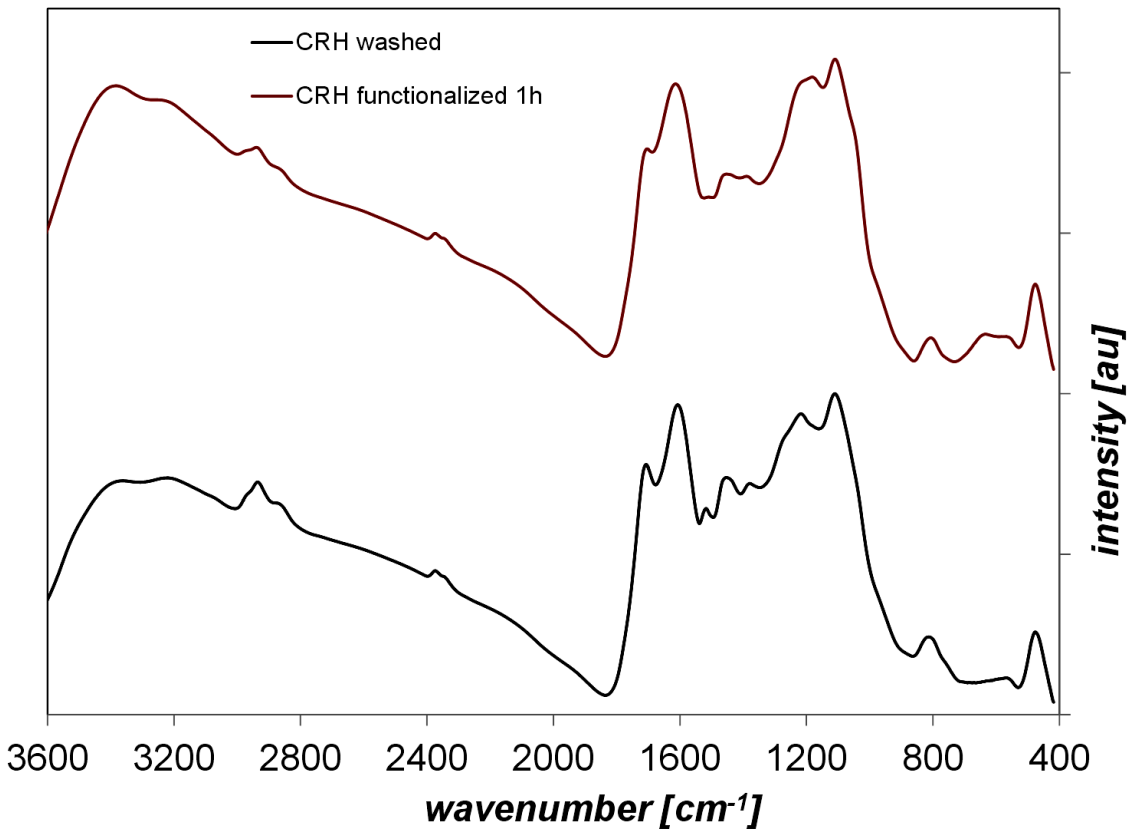

Figure 32 – FTIR spectrum of CRH after washing and functionalization

CRH spectra are characterized by different signals ascribable to various functional groups. Around 3000 cm^{-1}, the low-intense bands are due to the stretching vibrations of aliphatic and aromatic C-H bonds, in the medium-frequency range (1700 and 1000 cm^{-1}) a broad combination of peaks generated by the overlapping of carbon skeleton adsorption bands (C=O, C=C, C-C, C-H- C-O stretching and bending modes) was found.

Gr(1/4) and Gr(1/5) spectra are characterized by the typical broad shape of large condensed aromatic carbon networks. Only the peak due to C=C stretching modes and the overlapped peaks between 900 and 1500 cm^{-1} due to skeleton vibrations are detected.

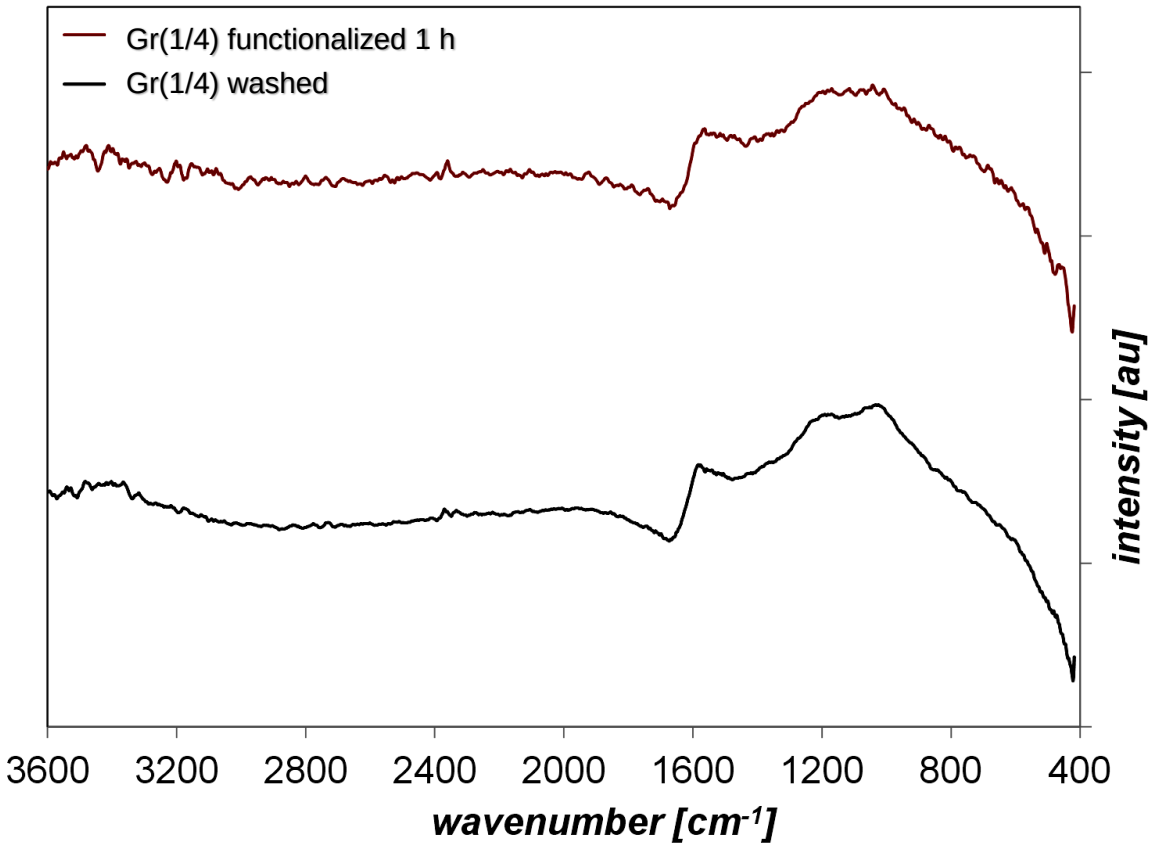

Figure 33 – FTIR spectrum of Gr(1/4) after washing and functionalization

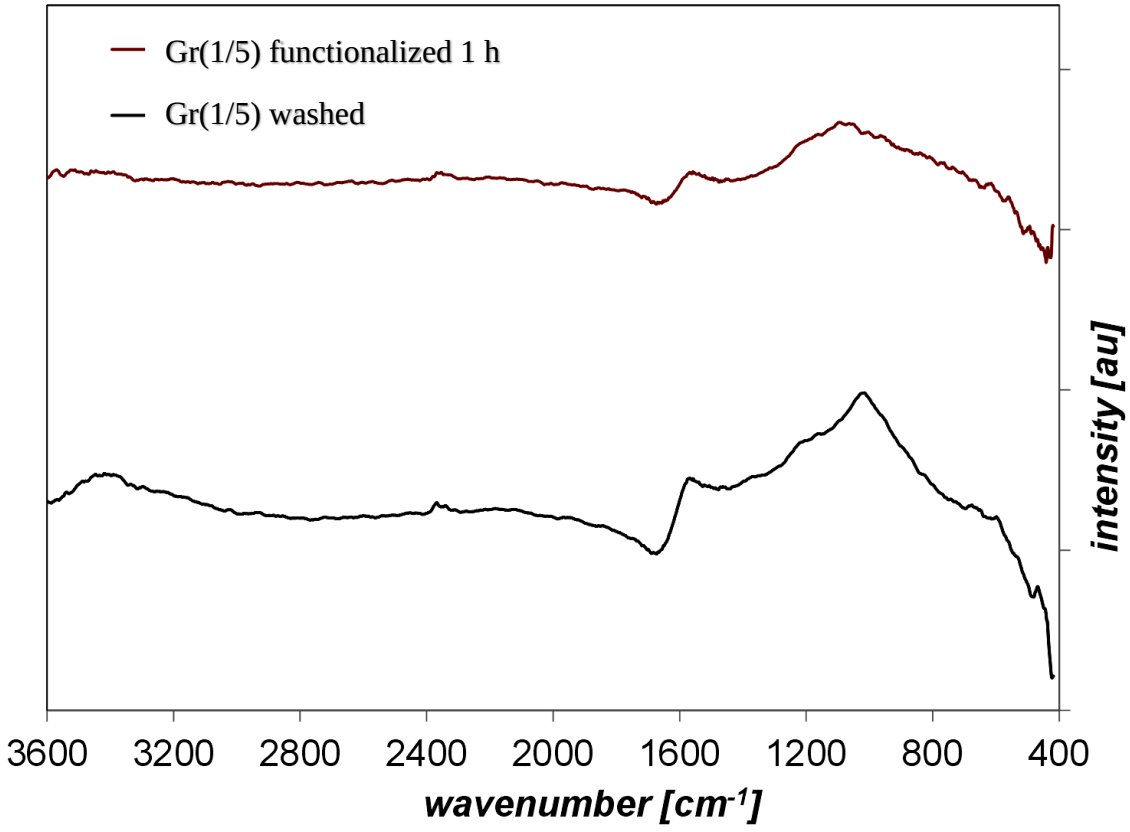

Figure 34 – FTIR spectrum of Gr(1/5) after washing and functionalization

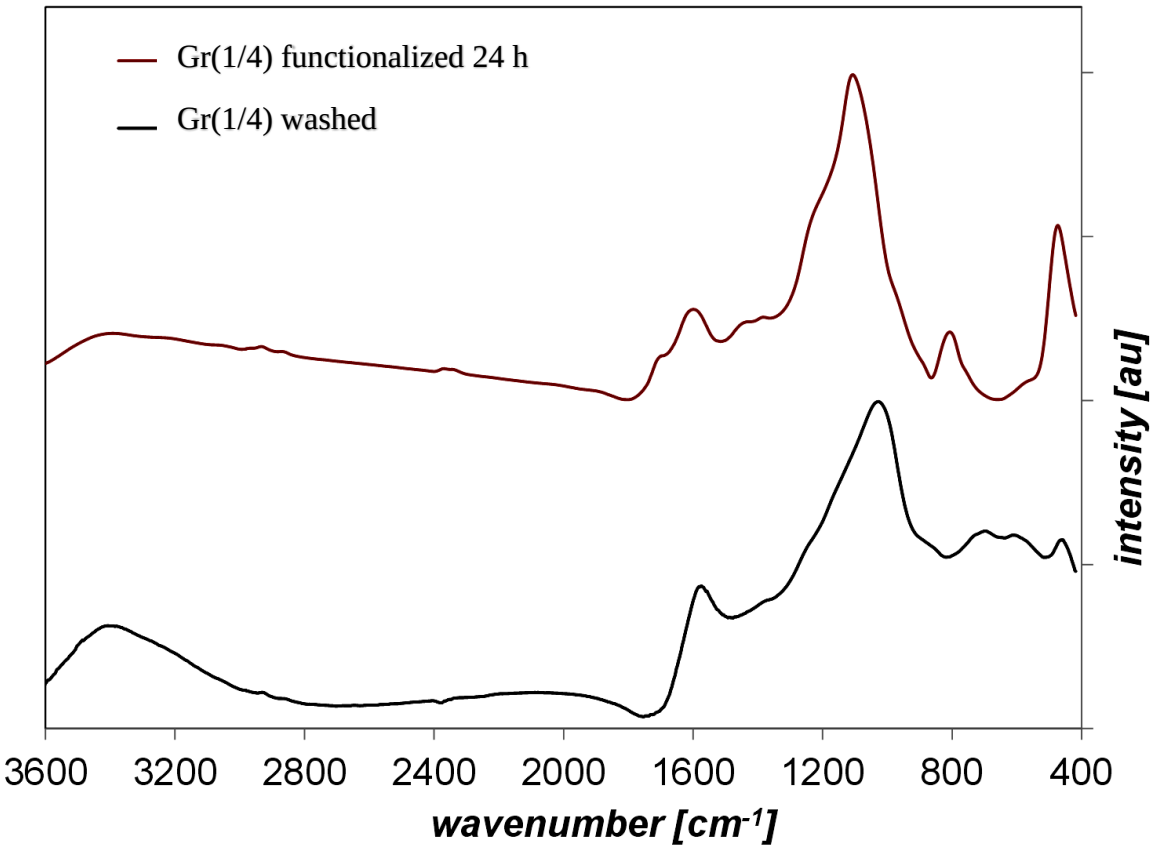

Figure 35 – FTIR spectrum of CRH after washing and functionalization (24 h)

Gr(1/4) spectra are characterized by different signals ascribable to various functional groups. The sample after washing is characterized by a peak due to C=C stretching modes (ca 1600 cm^{-1}) and overlapped peaks between 900 and 1500 cm^{-1} due to skeleton vibrations (C-C, C-H- C-O stretching and bending modes). The sample after 24 hours of functionalization is characterized by a main peak at 1090 cm^{-1} due to sulfoxide groups (Fig. 35).

Overall the FTIR results indicated that the functionalization of 1 hour with H_2SO_4 does not introduce significant change in the samples while that performed for 24 hours successfully allowed the introduction of sulfonic groups.

4 DESALINATION OF SEA WATER

4.1 Membrane preparation

GO membranes were prepared by two methods: vacuum filtration and immersion precipitation method (NIPS technique) [102] in different conditions.

In the first and more conventional method, graphene materials are deposited on the membrane (based on acetates) substrate via vacuum filtration (Figs. 36-37). Polymeric membrane disks were placed in the membrane preparation set and washed thoroughly with deionized water. After the pre-wash, approximately 40 mL of the graphene oxide suspension (0.01 mg/mL) was filtered through the membrane (filtration area 38 mm^2) under -0.8 bar at room temperature (Fig. 36a), forming the graphene oxide membrane composed of a thin GO layer on the membrane support (Fig. 36b). The resultant graphene oxide membrane was vacuum-dried (-0.95 bar) at 40°C for 40 h (Fig. 36).

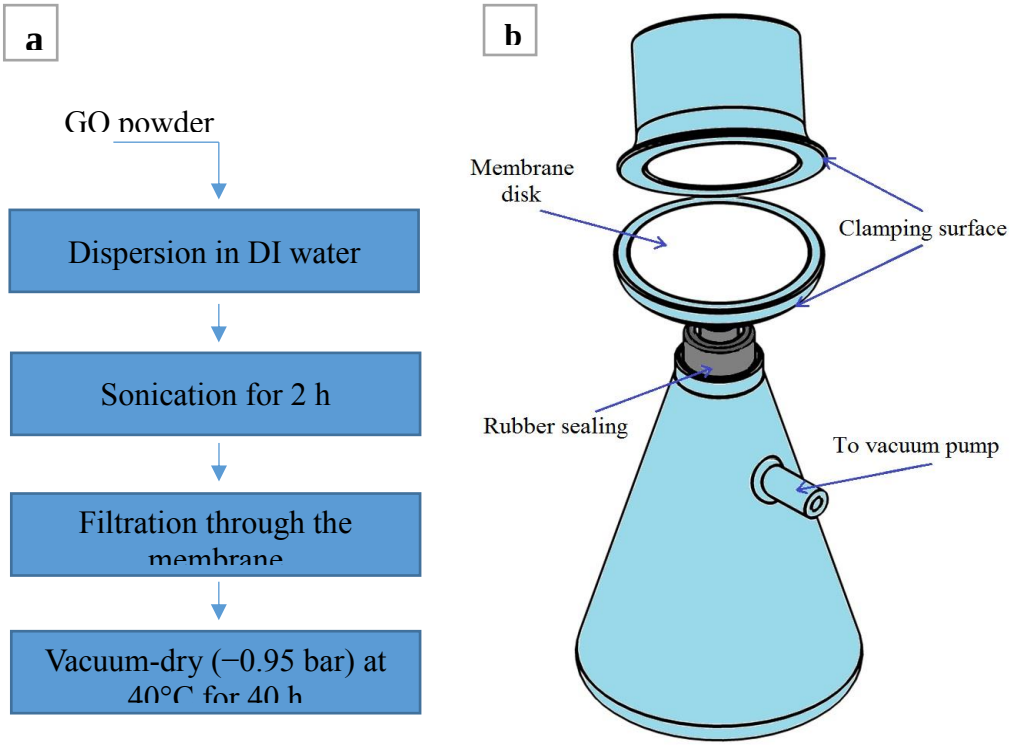

Figure 36 – Membrane synthesis steps (a) and preparation set-up (b)

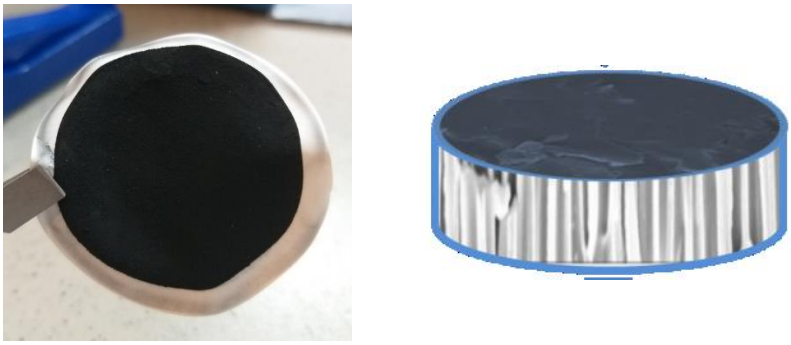

Figure 37 – Picture of membranes obtained by vacuum filtration method

It can be seen that the surface of the membranes is evenly covered by graphenes and does not crumble when turned over.

In the second method, 0,5 g of PVDF and 4 ml of 1-methyl-2-pyrrolidone were added in heat-resistant glass and heated around 50°C by stirring for 1 hour to get homogeneous polymer solution (Fig. 38). Then, 0.1 g of carbon sample was dispersed in a little amount of 1-methyl-2-pyrrolidone (2 mL): it was sonicated for 30 min to obtain a uniform dispersion and added to PVDF suspension. After that, 0.1 g of polyvinylpyrrolidone (PVP) was added to the dispersed suspension of PVDF/GO and gently stirred for 1 hour to get homogeneous suspension. The resulting suspension was degasified by sonication to eradicate trapped air bubbles. The homogeneous casting solution was cast over a glass plate (adjusting the thickness at 400 microns) and immersed in the coagulation bath containing water as non-solvent. The resulting membrane was kept in coagulation bath for 24 hours to ensure the complete phase inversion. The overview of the composition of casting solution was reported in Table 11.

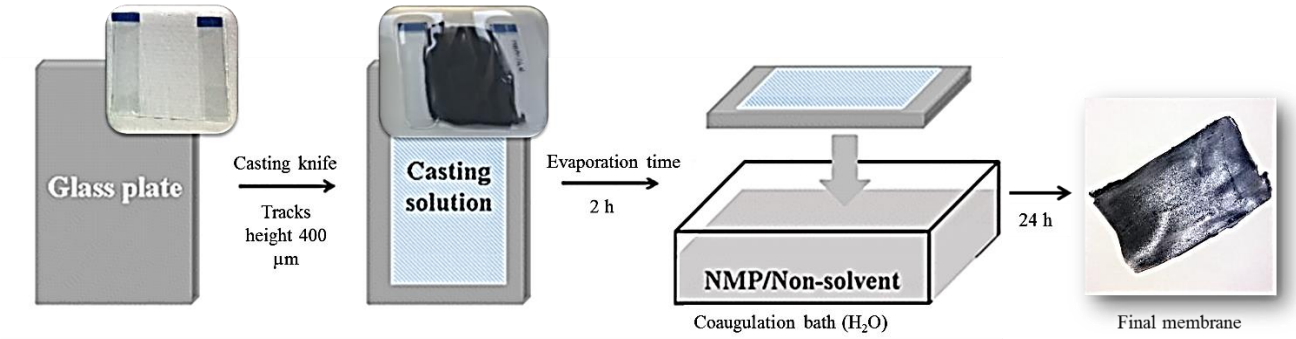

Figure 38 – Schematic of membrane preparation by non-solvent induced phase inversion (NIPS) technique

Table 11 – The composition of membrane

Sample	NMP (ml)	PEI (g)	PVP (g)	Gr(1/4) washed (g)	Gr(1/4) washed and functionalized (g)	Car-bon black (g)	Size, µm
M PVP/PEI	1,95	0,41	0,1	-	-	-	150
M PVP/PEI/AC(1/4)w	1,95	0,41	0,1	0,1	-	-	340
M PVP/PEI/AC(1/4)f	1,95	0,41	0,1	-	0,1	-	228
M PVP/PEI/CB	1,95	0,41	0,1	-	-	0,1	312

The Figure 39 represents the images of nanocomposite membrane matrix with a different amount of additive dosage. All the membranes displayed asymmetric structure with dense top layer followed by porous sublayer with fully developed macro-pores, which is the typical morphology of membrane fabricated via the phase inversion process.

Figure 39 – Picture of membranes synthesized by NIPS technique

Overall, vacuum filtration method and NIPS technique allowed preparing a thin layer of cross-linked graphene. To study the desalination properties of membranes, 3 main types of membranes were selected, which their production conditions and other characteristics are described in table 12.

Table 12 – Type of graphene based membranes

ID sample	Label	Conditions for obtaining samples	General characteristics by SEM analysis
Graphene oxide (commercial) membrane	GOM	Dispersed, sonicated, vacuum dried	Microporous film material. Friable sample.
Graphene (obtained from CRH) membrane	GM	Dispersed, sonicated, vacuum dried	Microporous membrane modified by graphene. Graphene was synthesized from rice husk. The sample is fragile, easily break.
Graphene based PVDF filter	GF	Evaporated of mixture of PVDF, 1-methyl-2-pyrrolidone, PVP and graphene	Macroporous filter. Particles of the same size and fragile aggregates. Sheet-like particles are very fragile. Crumbly fragments

4.2 Membranes characterization

The variation in cross sectional morphology of membranes obtained by vacuum filtration and immersion precipitation (washed and functionalized Gr(1/4)) and carbon black additive into membrane matrix was analysed by SEM (FEI Inspect™ S50 Scanning Electron Microscope) analysis. Prior to SEM analysis, the dry membrane was cryogenically fractured in liquid water and a thin layer of gold was coated using a sputtering apparatus. SEM analysis was conducted on the best performing membranes from each GO membrane synthesis method to understand how differences in synthesis method impact membrane morphology, and therefore performance. The surface and cross-section morphologies of the membranes influence the permeability and selectivity of the membranes. Therefore, the surface roughness and surface topography were evaluated and are shown in Figures 40-43.

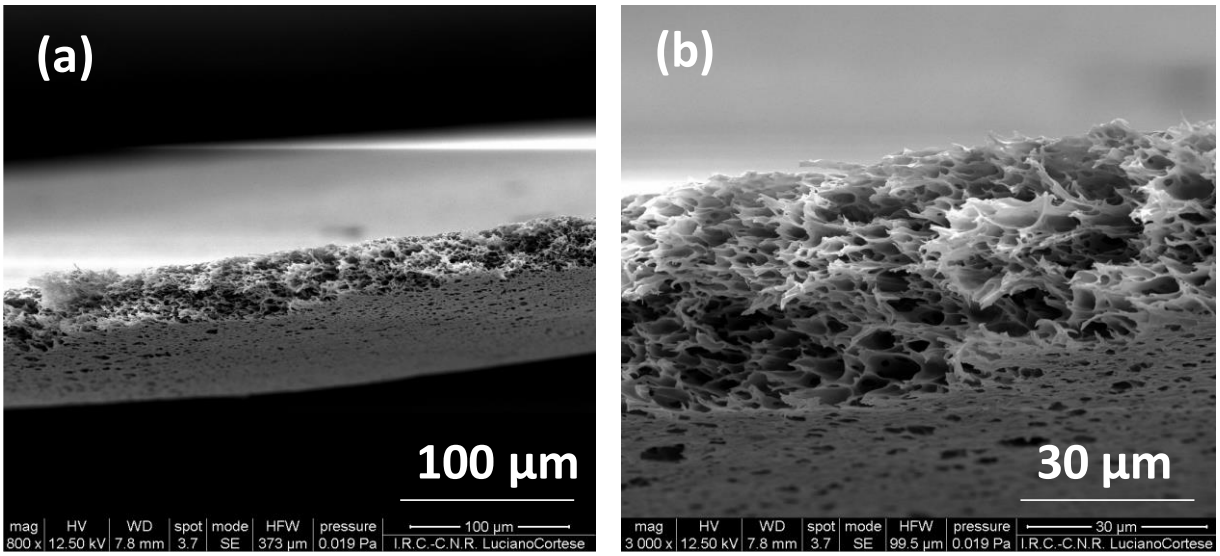

Figure 40 – SEM images of raw PVP/PEI filter obtained by NIPS technique

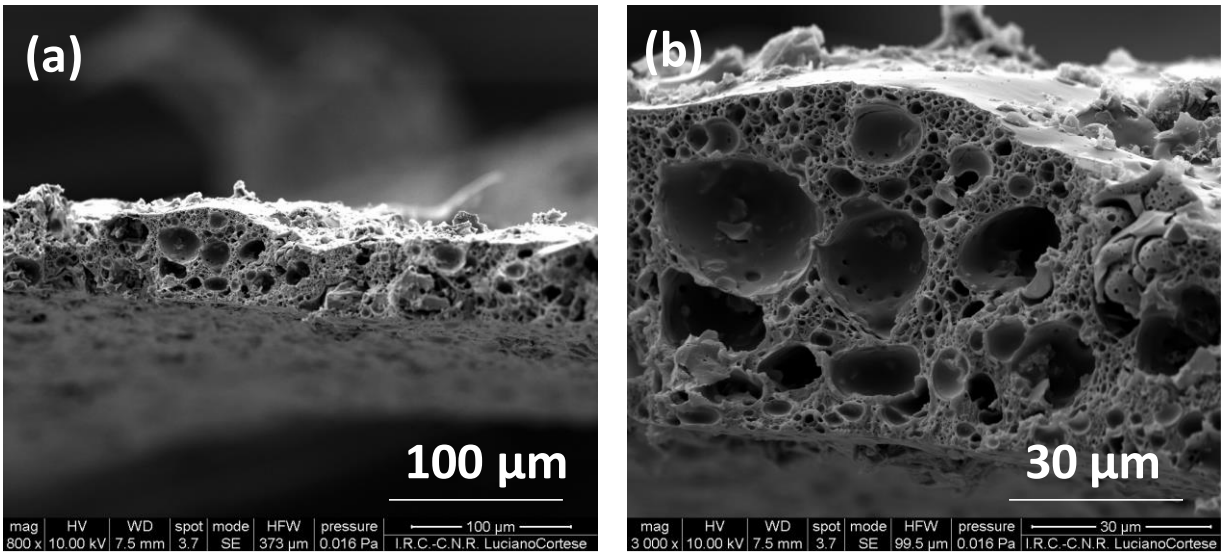

Figure 41 – SEM images of PVP/PEI filter with graphene obtained by NIPS technique

The PVP/PEI membrane was used as a reference for the GO set. At larger scan areas the graphene membranes showed a rougher surface than the control membrane as displayed in Figure 40, which was consistent with previous reports of MMMs [103, 104]. GO membranes showed the roughest surface, followed by CB and then GF. A rough surface is desirable, as an increased roughness value has been linked to an increase in flux [105]. However, at the finest scan area the localized roughness was lower, with GF having the smoothest membrane surface. The difference in behavior for GO at the largest and smallest scan areas could possibly be influenced by the larger GO sheet size associated with the GO synthesis method.

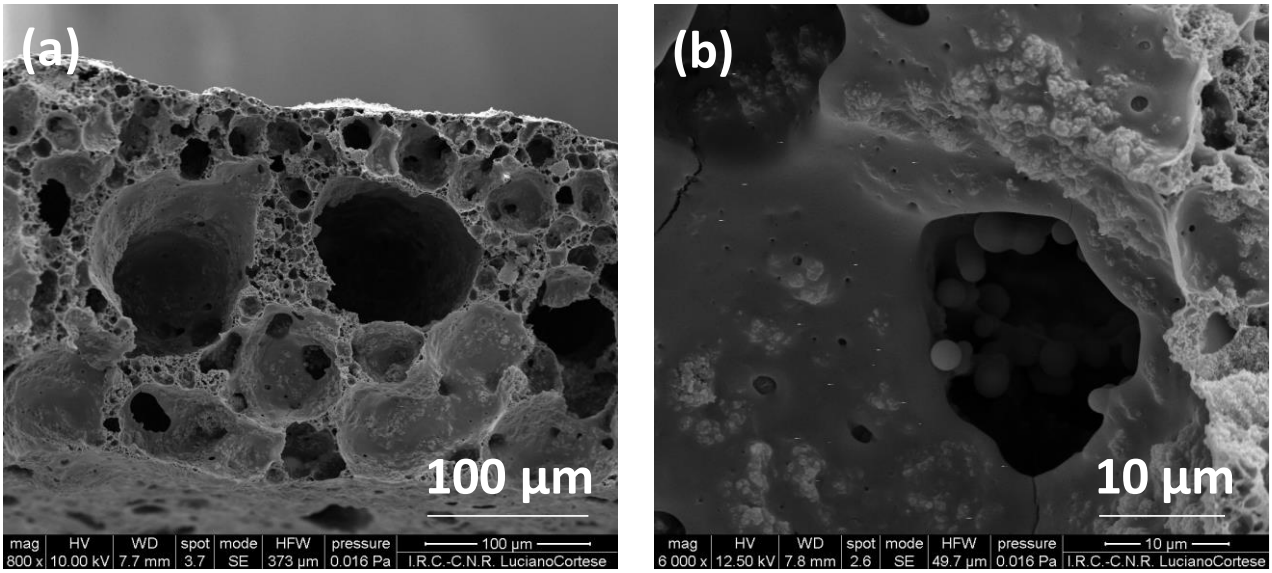

Figure 42 – SEM images of PVP/PEI filter with carbon black obtained by NIPS technique

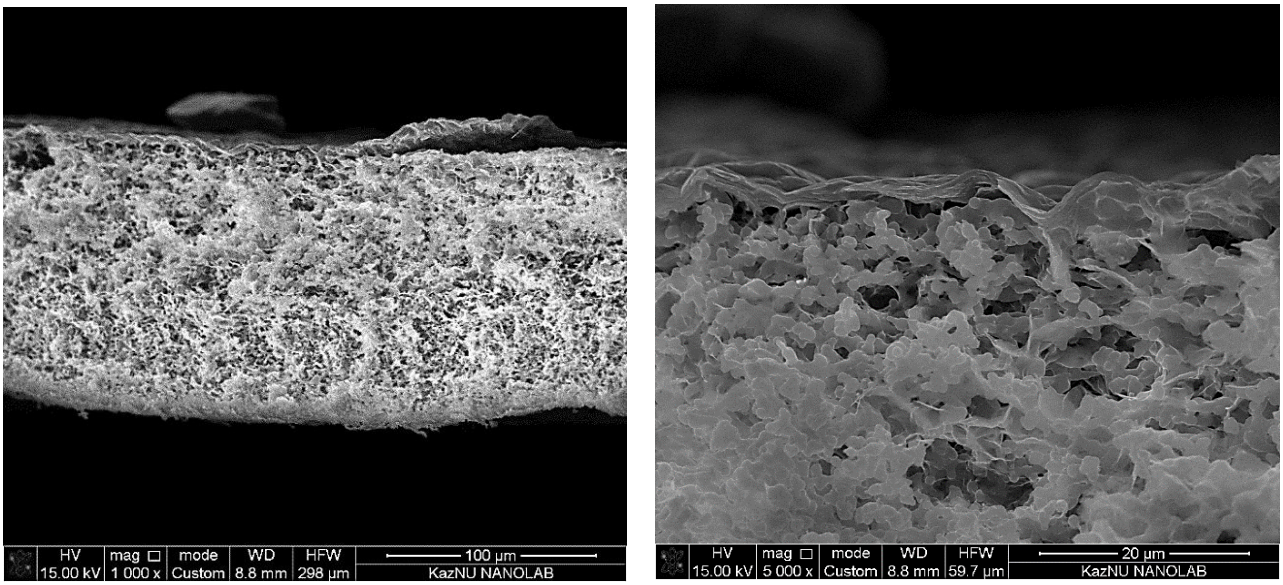

Figure 43 – SEM images of GF membranes obtained by vacuum filtration

Overall, the membranes displayed asymmetric structure with dense top layer followed by porous sublayer with fully developed macro-pores, which is the typical morphology.

4.3 GO membrane desalination tests

The GOM, GM and GF membrane and filtration of five salt liquids (NaCl, KCl, $MgCl_2$, $CaSO_4$ and $MgSO_4$) were tested using a usual filtration system (Fig. 44) at room temperature. Feed solution was loaded into a stirred cell with an effective membrane area of 38 mm^2 an 300 mL feed tank. The volume of the feed solution was 200 mL in total by taking into account both the volumes of the stirred cell and the feed tank. The filtration pressure was provided and controlled by a pump. The fabricated membranes were used for each filtration test. The stable DI water flux was measured and compared between different membrane samples to check the repeatability of our membrane fabrication technique.

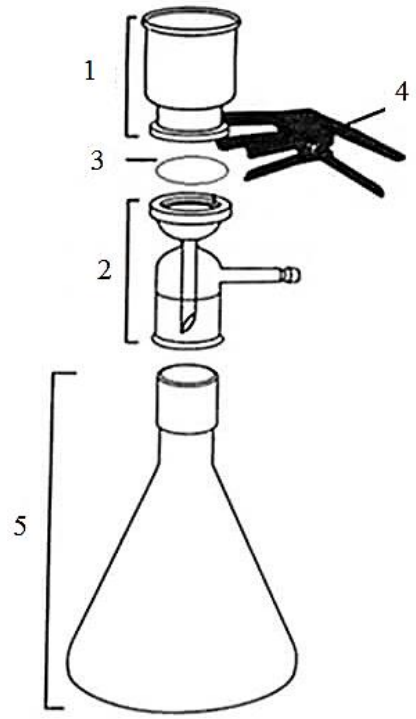

1 – 300 ml filtering cup, 2 – filtering head, 3 – filtering membrane, 4 – clamp, 5 – 500 ml conical flask

Figure 44 – Laboratory vacuum filtration apparatus

The salt rejection tests of membranes were performed on atomic absorption flame emission spectrophotometer (Shimadzu AA-6200) at the Center for Physical and Chemical Research and Analysis (Almaty, Kazakhstan). Atomic absorption flame emission spectrophotometer made use of the absorption of light by these elements in order to measure their concentration. The sampling modes are as follows: optical system - two-beam, monochromator - Cherni-Turner, spectral range - 190-900 nm, spectral gap - 0.2, 0.7 nm (manual switching), background corrector - deuterium,

simultaneous switching on (one works, another - warms up). Atomizers: flame, hydride or mercury prefixes. Flame atomizer - titanium burner, Pt/Ir capillary, ceramic impactor, corrosion-resistant spray chamber, high-temperature flame burner C_2H_2 - N_2O [106].

The desalination properties of membranes were tested for NaCl, KCl, $MgCl_2$, $CaSO_4$ and $MgSO_4$ using a calibrated Atomic Absorption Flame Emission Spectrophotometer. The initial composition of the salt (35 g/L) solution (sample of seawater) was as follows: NaCl (78.8%), KCl (2.1%), $MgCl_2$ (9.1%), $CaSO_4$ (3.5%) and $MgSO_4$ (6.5%). The desalination data before and after filtration and permeable characteristics are given in Table 13.

Table 13 – Desalination and permeable characteristics of samples

Membrane	Salts, g/L		Salt rejection (average), %	Permeability (average), ml/min (under vacuum)	
	Before filtration	After filtration		DI water	Salt water (35 g/L)
GOM	35	0,5	99	4	3
GM	35	1	98	5	4
GF	35	32	8.5	30	30

The concentration of salts before and after filtration shown in Fig. 45. The initial concentration of salts were: NaCl – 27.3 g/L, KCl – 0.7 g/L, $MgCl_2$ – 2.275 g/L, $CaSO_4$ – 1.225 g/L and $MgSO_4$ – 2.275 g/L.

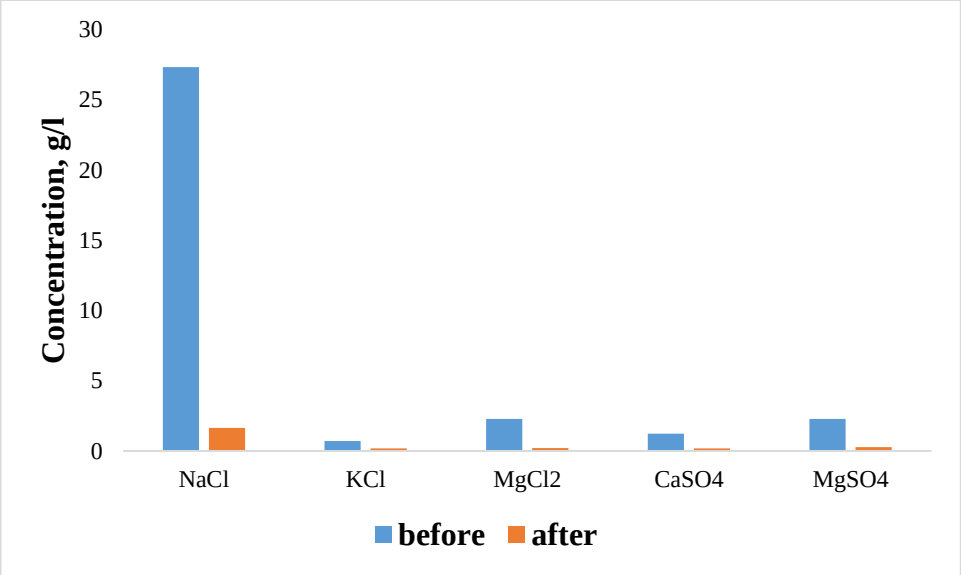

Figure 45 – The concentration of salts before and after filtration

After filtration of this solution through GO membranes, the concentration of salts decreases up to: NaCl – 1.647 g/L, KCl – 0.1891 g/L, $MgCl_2$ – 0.1994 g/L, $CaSO_4$ – 0.1828 g/L and $MgSO_4$ – 0.2665 g/L. From Table 14, we can infer that the permeability plays a big role on the salt rejection: to a slower process corresponds a better filtration

capability. The sodium chloride rejection in RO for GF membranes was below the 50% mark and significant variations of the experimental results were observed. In addition, the poor salt rejection of GF compared to the other two membranes makes it clear that the preparation from graphene oxide (both commercial or from rice husk) by vacuum filtration is much more effective for the production of filtering membranes.

Finally, all GF membranes prepared by NIPS technique showed lower water permeability and salt rejection when compared to the performance control membranes prepared by vacuum filtration.

4.4 X-ray diffraction analysis

To probe the extent of oxidation and changes in GO structure due to the differences in oxidation conditions, XRD was used to evaluate the interlayer distance between GO particles as well as the crystal structure. X-ray diffraction measurements were performed on a diffractometer DRON-4 (at the Institute of Combustion problems) in digital form using copper radiation. The sampling modes are as follows: the voltage on the X-ray tube is 35 kV, the tube current is 20 mA, the goniometer movement step is 0.05°2θ, and the intensity measurement time at the point is 1.5 sec/point. During irradiation, the sample was rotated in its own plane at a speed of 60 rpm. Pre-processing of radiographs to determine the angular position and intensity of the reflections was carried out by the F-peak program. During the phase analysis, the PCPDFWIN program with the PDF-2 diffractometric database was used [107].

X-ray diffraction analysis on the dry membranes showed a characteristic diffraction peak at about 10° and 20°, from which it was calculated that the distance between the nanosheets for dry membranes are 4,145 Å, 3,930 Å and 3,739 Å for GOM, GM and GF samples, respectively. The XRD measurements on GOM, GM and GF after modification of GO (after salt filtration) on the surface of membrane and after filtration tests to different salts are shown in figures 46-47.

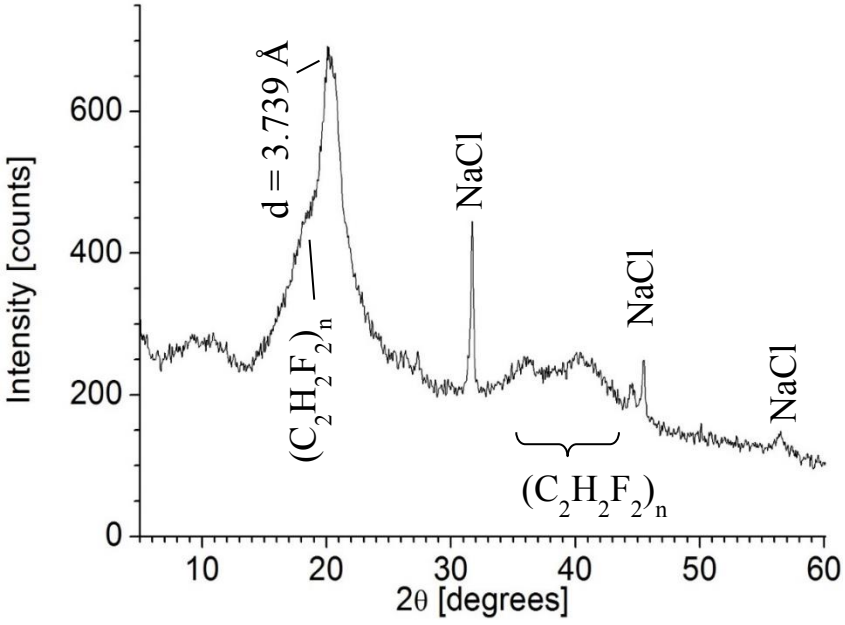

Figure 46 – The XRD pattern of the GF obtained by NIPS technique

The pattern on GF sample (Fig. 46) contains the lines $(C_2H_2F_2)_n$. Carbon is present in a large amount and NaCl in an amount of approximately 4.6%.

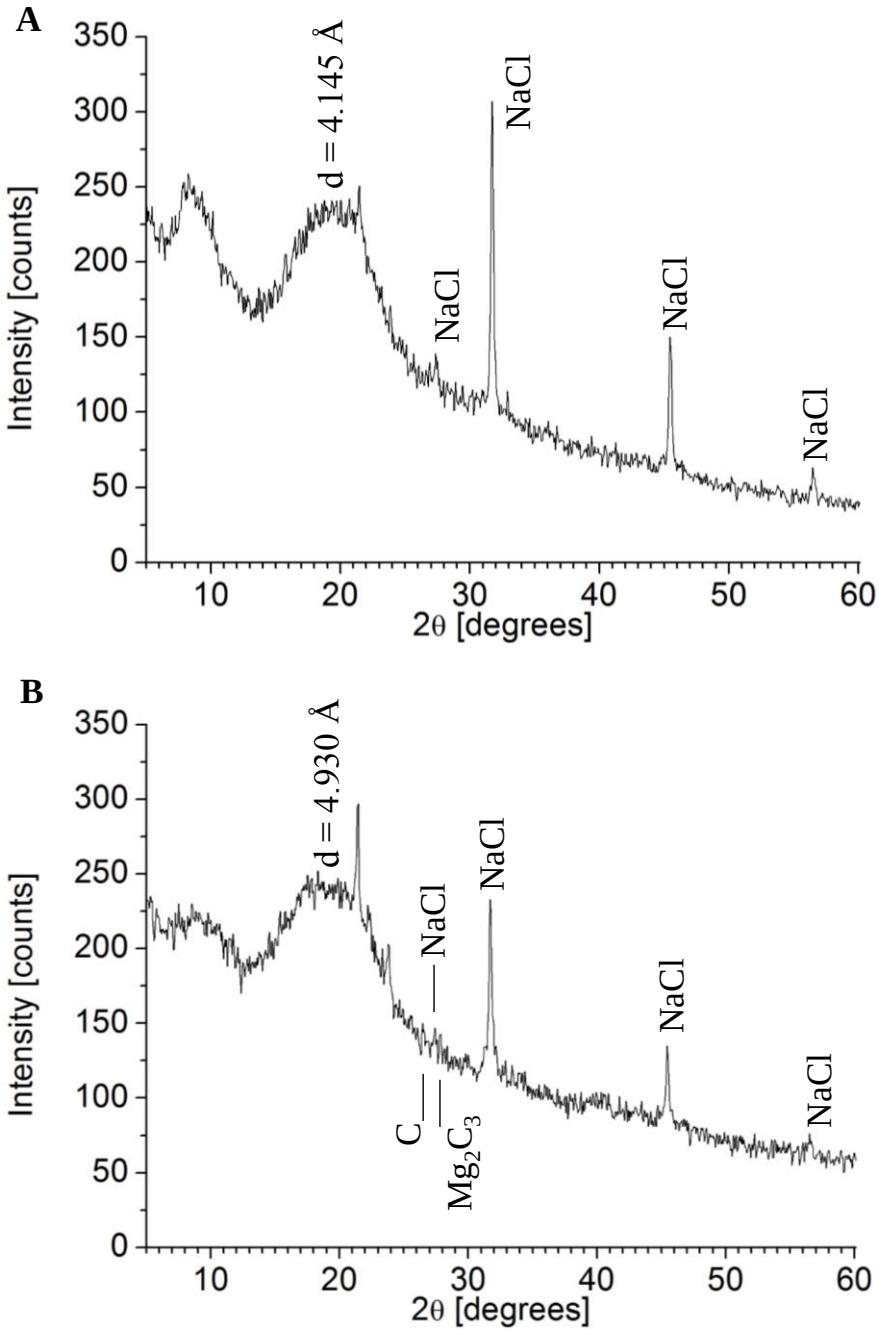

Figure 47 – The XRD pattern of the GOM (a) and GM (b) three membranes obtained by vacuum filtration

Diffraction peaks associated to carbon are present in all samples, corresponding to interlayer distances d=4.145 Å in GOM, d=4.930 Å in GM and d=3.739 Å in GF. The XRD pattern on GOM membrane (Fig. 47(a)) exhibits polymer lines and NaCl diffraction lines. In order to determine the approximate NaCl content in the sample, an X-ray image of NaCl was obtained under the same conditions as the sample. Using this

X-ray as an external standard, the NaCl content in the samples was determined as about 5.0%. From XRD pattern on GM (Fig. 47(b)), we estimated the content of NaCl as approximately 2.5%, while a small amount of carbon and MgCl cannot be excluded.

4.5 IR spectroscopy

The nature of functional groups on the surface of membranes was studied by IR spectroscopy at the Institute of Catalysis named after G.K. Boreskova SB RAS, Novosibirsk, by recording spectra on a Cary-660 FTIR spectrometer (Agilent Technologies, USA) in the diffuse reflection mode on a DiffusIRTM (Pike Technology, USA) prefix in the frequency range 4500-500 cm^{-1} with a resolution of 4 cm^{-1} and an accumulation of 256 scans (to improve the quality of the spectra and the signal/noise). IR diffuse reflectance spectra (IR-DR) are presented in the coordinates: Kubelka – Munk function, F(R) – wave number, without adjusting the baseline [108].

For the study of desalination properties were provided 3 samples, preparation conditions and general characteristics of which are given in Table 13.

IR-DR spectra of membrane samples are shown in Figures 48 and 49; for convenience of analysis, the spectra are arranged taking into account the intensity of the observed absorption bands (ppt).

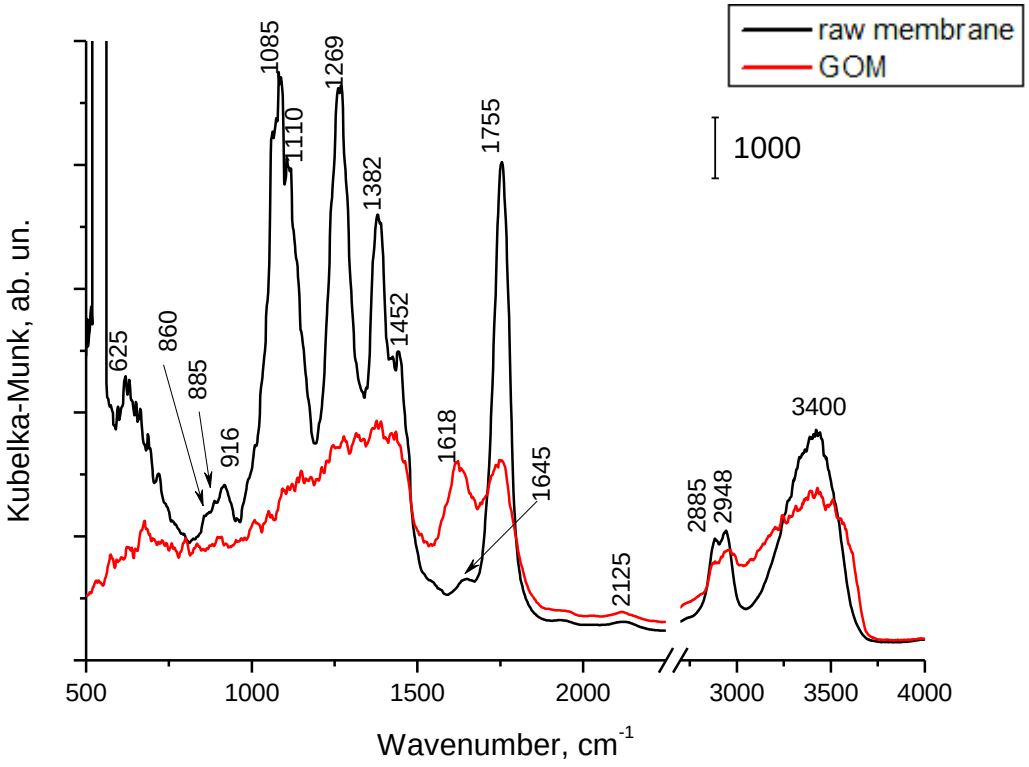

Figure 48 – IR-DR samples of raw membrane (commercial membrane, based on a mixture of acetates) and GOM (commercial membrane with deposited commercial graphene oxide)

The IR spectrum of the raw membrane contains intense bands 3400, 2885, 2948, 1755, 1452, 1382, 1269, 1085-1110, 860-916, 625 cm^{-1}, which fully describe the

vibrations of individual groups of acetates [109, 110]. So, 1755 cm^{-1} refers to the stretching vibrations of non-ionized COOH groups, while the proportion of ionized COO-groups is very small (points 1645 cm^{-1}). 2885 and 2948 cm^{-1}, which are characteristic of symmetrical and asymmetric stretching vibrations of the C-H bond in the CH_3-fragments [111] of acetate, also indicate the presence of acetate groups in the composition of the material. Additional bands of 1452, 1382 and 1085-1110 cm^{-1} in the spectrum of the material belong to asymmetric, symmetric and rotational deformation vibrations of H-C-H in CH_3 groups of acetate, respectively. The 3400 (wide) and 1385 cm^{-1} bands correspond to the stretching and deformation vibrations of OH in free, and 915-885 cm^{-1} (broad) in hydrogen bonded (denoted as OH ... H) COOH-groups of acetic acid. 1265-1205 and 1190-1075 cm^{-1} are due to valence and deformation, respectively, fluctuations of the C-O bond in COO groups, 665-590 cm^{-1} – deformation oscillations of C=O.

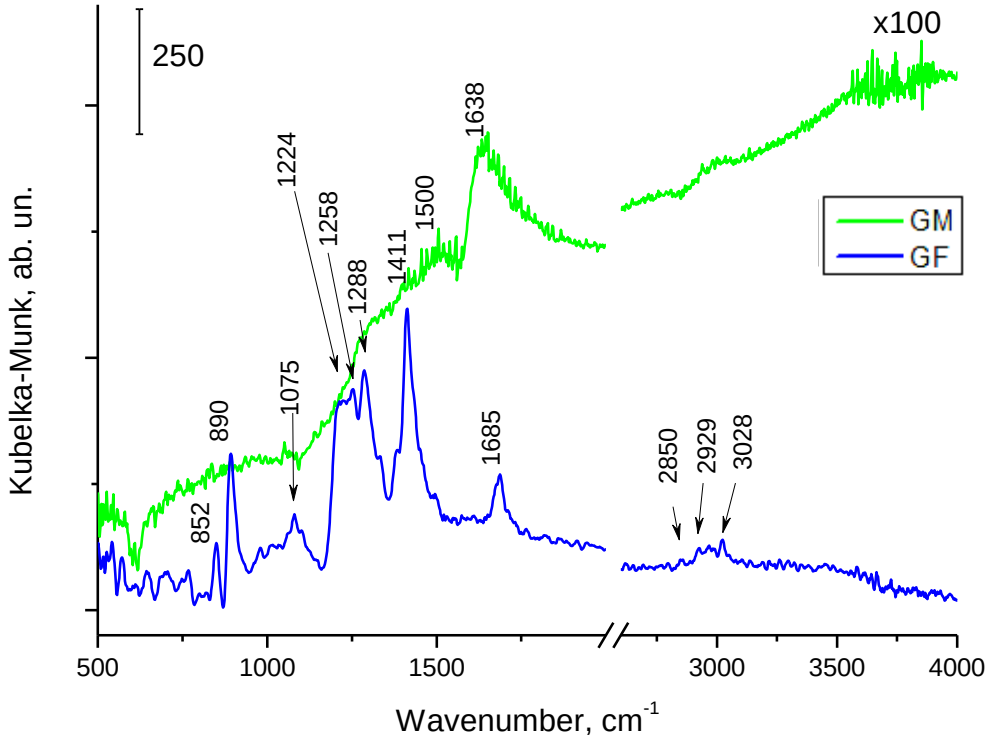

Figure 49 – IR-DR samples of GM membranes (commercial membrane coated with graphene oxide obtained from rice husk) and GF (filter based on a mixture of PVDF (polyvinylidene difluoride), polyvinylpyrrolidone with graphene oxide and graphene)

The IR-spectrum of a microporous membrane coated with graphene oxide (Fig. 48, GOM) contains bands characteristic of the initial membrane (GOM): 3400, 2885, 2948, 1755, 1452-1050 and 625 cm^{-1}, but their intensity is significantly reduced and splitting of bands in the region of 1452-1050 cm^{-1} disappears. This indicates the interaction of carbon material deposited on the surface of the membrane with its functional groups. In addition to these bands, a new band at 1618 cm^{-1} appears in the

spectrum of sample GOM. According to [112], the band in the region of 1560-1600 cm^{-1} corresponds to the E1u mode in graphite structures; however, the second ppt in the spectrum of sample GOM is absent in the region of 820-860 cm^{-1}, corresponding to the A2u vibrational mode of graphite. 1618 cm^{-1} can also be associated with functional groups of graphene oxide, for example, the valence vibrations of the C=C bond in polyaromatic (naphthalene, anthracene [109]) structures or with the C=O bond in quinoline-like structures are in the 1620-1580 cm^{-1} and 1690-1655 cm^{-1} [109], respectively.

Sample GM was out to be the most unfortunate for the analysis of its functional groups by IR spectroscopy. Its spectrum had the lowest intensity, probably due to the high dispersion of graphene particles. Note that in sample GM, graphene was used, obtained by activating rice husk with KOH at a temperature of 850°C, which probably leads to a high degree of graphitization of graphene. The spectrum contains only two ppt. 1638 and ~500 cm^{-1}, which can be analyzed. These bands are most likely due to the stretching vibration of -C=C bonds in polyaromatic [109] or graphite-like [112] structures (Fig. 49).

The IR spectrum of the GF membrane, which is obtained by mixing graphene oxide and graphene with polyvinylpyrrolidone, contains intense bands at 852, 890, 1025, 1224, 1258, 1288, 1411, 1685, 2850, 2929, 2965, and 3028 cm^{-1} (Fig. 49). 1685 and 852-890 cm^{-1} are in the region, as discussed above, of the E1u and A2u vibrational modes of graphite-like structures [112]. At the same time, 1224, 1258, and 1288 cm^{-1} may be due to the defectiveness of the graphite-like structure [180]. A wide band in the region of 1220-1290 cm^{-1} was observed in the spectrum of N-containing carbon nanotubes and nanofibers and was associated by the authors with violation of the translational symmetry of the defective graphite-like structure. Pair of 2850 and 2965 cm^{-1} is characteristic of CH_3-groups and corresponds to symmetric and asymmetric (respectively) valence vibrations of C-H bonds in them. Additional bands at 1411 and 1025 cm^{-1} in the spectrum of the GF membrane are related to the deformation and rotational vibrations of H-CH-H in CH_3 groups [112], respectively. These bands indicate the presence of carbon with sp^3 hybridization in the membrane. Pair of 2929 and 3028 cm^{-1} are characteristic of CH_2-groups and =C-H groups in acyclic and aromatic compounds, respectively. For the last sample, only ppt in the region of 1025 (C = O) and 1224-1288 (CO-O [115]) cm^{-1} can be associated with oxygen-containing graphene oxide groups, but they are in the region of C-H vibrations from CH_3-groups and defects of graphite-like structures.

4.6 Permeation properties and mechanism

The porosity and hydrophilicity are the two important factors, which decides the permeation properties of the membranes. Table 15 gives dependent pure water and salt-water (35 g/L) fluxes of the membranes with different amount of modified graphene based carbon content. From the experimental observation, the inclusion of modified graphene based carbon additive in the membrane matrix has a synergistic effect on the physicochemical and hydrodynamic permeation behavior of nanocomposite

membrane. Here, the pure water fluxes of the nanocomposite membrane showed a similar trend that of porosity and hydrophilicity.

Many mechanistic models have been proposed to describe desalination by membranes. Some of these descriptions rely on relatively simple concepts while others are far more complex and require sophisticated solution techniques. Models of systems can be divided into three types:

Table 14 – Permeable characteristic of samples

Sample	Water	Salt water (35 g/L)
M PVP/PEI	fast	-
M PVP/PEI/Gr(1/4)$_{1w}$	slow	slow
M PVP/PEI/Gr(1/4)$_{1f}$	fast	fast
M PVP/PEI/CB	fast	fast

1. Irreversible thermodynamics models. In this model, the membrane is considered as a black box, irreversible thermodynamics models assume the membrane is not far from equilibrium and so fluxes can be described by phenomenological relationships.

2. Solution-Diffusion Model (non-porous models). In 1965, Lonsdale proposed the solution-diffusion model at the first time, this model assumes that the RO membrane has a nonporous diffusion surface layer, solvent and solute molecules dissolve into this layer and then disuse through it by a solid or liquid diffusion mechanism. The diffusion of solution dissolves is caused by chemical potential gradient, which are the result of the concentration and pressure differences across the membrane.

3. Preferential sorption-capillary flow model (porous models). This model assumes that the mechanism of separation is determined by both surface phenomena and fluid transport through pores in the RO membrane. In contrast to the solution-diffusion model, the membrane is assumed to be microporous. The model states that the membrane barrier layer has chemical properties such that it has a preferential sorption for the solvent or preferential repulsion for the solutes of the feed solution. As a result, a layer of almost pure solvent is preferentially sorbed on the surface and in the pores of the membrane. Solvent transport occurs as solvent from this layer is forced through the membrane capillary pores under pressure.

4.7 Fouling of membranes

Fouling is a phenomenon in which the membrane adsorbs or interacts in some manner with some materials in the feed stream, resulting in a decrease in membrane performance (lowering the flux and/or increase in rejection of solutes) when all operating parameters are kept constant, fouling decreases the membranes performance. RO membrane elements are subject to fouling by suspended or sparingly soluble materials that may be present in the feed water, Common examples of foulants are:

- Metal oxides
- Calcium carbonate scale
- Sulfate scale of calcium, barium or strontium
- Colloidal foulants
- NOM organic material (Natural Organic Matter).

CONCLUSIONS

The results of research work allow to make the following conclusions:

1. Graphene materials were obtained from rice husk. It was found that carbonization/activation of rice husk leads to the formation of a mixture of graphene layers and amorphous carbon. At the maximum ratio of rice husk and activating reagent (1:5), the relative amount of the graphene component increases, the number of layers remains unchanged. For both samples, Gr(1/5) and Gr(1/4), the I_G/I_{2D} ratio is close to 1.56 ± 0.10, which proves the 4-5-layer structure of graphene.

2. The physicochemical properties of the obtained graphene materials were successfully studied, it was found that the obtained material is highly porous with an average pore size <100 nm, contains 80-90% C (scanning electron microscopy) and have a specific surface area of 2500-3000 m^2/g (by BET method).

3. The graphene membranes were prepared by vacuum filtration and immersion precipitation methods. It was found that GOM, GM membranes which prepared by vacuum filtration method have a more microporous and nanoporous structure with a dense upper layer than the GF membranes which prepared by immersion precipitation method, therefore their water permeability are 4, 5 and 30 ml/min correspondingly.

4. The desalination effects of graphene membranes were tested for NaCl, KCl, $MgCl_2$, $CaSO_4$ and $MgSO_4$. It was revealed that after filtration of this solution through graphene membranes, the concentration of salts decreases up to: NaCl – 99.5%, KCl – 99.8%, $MgCl_2$ – 99.5%, $CaSO_4$ – 77.6% and $MgSO_4$ – 99.3%.

Assessment of the completeness of the solutions to the tasks. The tasks set in the work are completely solved. Graphene materials are obtained from rice husks and used as membranes for desalination of seawater. The results are reliable and reasonable, since all measurements were carried out on calibrated instruments using standard methods.

Part of the study was performed at the University of Naples “Federico II” in Naples (Italy) inside the group of prof. Marco Trifuoggi and under the foreign scientific supervisor, PhD, Professor Roberto Di Capua: performing scanning electron microscopy (SEM) coupled with energy dispersive x-ray Analysis (EDAX) detector, ICP Mass Spectroscopy, elemental analysis, Raman Spectroscopy on samples. The second part of study was performed in laboratories of Institute of research for combustion, under the continuous supervision of Dr. Michela Alfe and Dr. Valentina Gargiulo: purification and functionalization (to add sulfonic groups) processes of the sample, and then in the preparation and first characterizations of prototypes membranes for desalination purposes by using instrumental analytical techniques such as EDAX-SEM, ICP-MS, elemental analysis, thermogravimetric analysis (TGA) and infrared spectroscopy (FTIR).

Assessment of technical and economic efficiency proposed in the dissertation. The results obtained in the framework of this dissertation can be proposed for producing graphene membranes synthesized based on rice husks. An advantage of the proposed method for the synthesis of graphenes is the relative availability of the initial

reagent - rice husk. Rice husk-based graphene materials can also be used as sorbents and filters of treatment facilities, for the manufacture of supercapacitor electrodes.

Assessment of the scientific level of the work performed in comparison with the best achievements in this field. Currently, most researchers use commercial graphene for desalination of seawater, which is one of the most expensive materials from a commercial point of view (the cost of 1 g of graphene oxide is $ 160). This work may open up prospects for the production of domestic materials based on graphene from rice husks as affordable, cheap and effective sorbents for wastewater treatment. The results obtained are of practical interest for obtaining new improved nanomaterials for the purification and desalination of water.

In addition, the scientific level of the presented dissertation complies with international standards for research conducted in the selected field. This is evidenced by a fairly good level of publications, the presentation and discussion of the results of work at international symposia and conferences.

REFERENCES

1. Chester, Jickells, Roy, Tim (2012) Marine Geochemistry. Blackwell Publishing. ISBN 978-1-118-34907-6.

2. Millero, Frank J.; Feistel, Rainer; Wright, Daniel G.; McDougall, Trevor J. (January 2008). "The composition of Standard Seawater and the definition of the Reference-Composition Salinity Scale". Deep Sea Research Part I: Oceanographic Research Papers. 55 (1): 50–72. doi:10.1016/j.dsr.2007.10.001.

3. Yan Dong, Ralph K. Rosenbaum, and Michael Z. Hauschild Assessment of Metal Toxicity in Marine Ecosystems: Comparative Toxicity Potentials for Nine Cationic Metals in Coastal Seawater. Environmental Science & Technology 2016, 50 (1), 269-278. DOI: 10.1021/acs.est.5b01625..

4. Nayar, Kishor G.; Sharqawy, Mostafa H.; Banchik, Leonardo D.; Lienhard V, John H. (July 2016). "Thermophysical properties of seawater: A review and new correlations that include pressure dependence". Desalination. 390:1-24 doi:10.1016/j.desal.2016.02.024.

5. Kristoff Gibbon-Walsh, Pascal Salaün, and Constant M.G. van den Berg . Pseudopolarography of Copper Complexes in Seawater Using a Vibrating Gold Microwire Electrode. The Journal of Physical Chemistry A 2012, 116 (25), 6609-6620. DOI: 10.1021/jp3019155.

6. "Thermophysical properties of seawater". Department of Mechanical Engineering, Massachusetts Institute of Technology. Retrieved 24 February 2017.

7. "Ocean Microbe Census Discovers Diverse World of Rare Bacteria". ScienceDaily. 2006. Retrieved 13 May 2013

8. Hogan, C. Michael (2010). "Calcium", eds. A. Jorgensen, C. Cleveland. Encyclopedia of Earth. Some evidence shows the potential for fairly regular ratios of elements maintained across surface oceans in a phenomenon known as the Redfield Ratio. National Council for Science and the Environment.

9. Elentron literature https://en.wikipedia.org/wiki/Seawater#cite_note-16 .

10. Doney, Scott C.; Fabry, Victoria J.; Feely, Richard A.; Kleypas, Joan A. (1 January 2009). "Ocean Acidification: The Other CO_2 Problem". Annual Review of Marine Science. 1 (1): 169–192.

11. Doney, Scott C. (18 June 2010). "The Growing Human Footprint on Coastal and Open-Ocean Biogeochemistry". Science. 328(5985): 1512–1516. doi:10.1126/science.1185198. PMID 20558706.

12. "Desalination" (definition), The American Heritage Science Dictionary, Dunder Mifflin Company, via dictionary.com. Retrieved August 19, 2007.

13. "Australia Aids China in Water Management Project. People's Daily Online, 2001-08-03, via english.people.com.cn. Retrieved August 19, 2007.

14. Panagopoulos, Argyris; Haralambous, Katherine-Joanne; Loizidou, Maria (November 25, 2019). "Desalination brine disposal methods and treatment technologies - A review". The Science of the Total Environment. 693: 133545. doi:10.1016/j.scitotenv.2019.07.351. ISSN 1879-1026. PMID 31374511.

15. Fischetti, Mark (September 2007). "Fresh from the Sea". Scientific American. 297(3): 118–119. Bibcode:2007SciAm.297c.118F.

16. Ebrahimi, Atieh; Najafpour, Ghasem D; Yousefi Kebria, Daryoush (2019). "Performance of microbial desalination cell for salt removal and energy generation using different catholyte solutions". Desalination. 432:1. doi:10.1016/j.desal.2018.01.002

17. Singleton, M.; et., al. (2011). "Optimization of ramified absorber networks doing desalination". Phys. Rev. E. 83:16308. Bibcode:2011PhRvE..83a6308S. doi:10.1103/PhysRevE.83.016308.

18. Koutroulis, E.; et., al. (2010). "Design optimization of desalination systems power-supplied by PV and W/G energy sources". Desalination. 258: 171. doi:10.1016/j.desal.2010.03.018.

19. K. V. Reddy and N. Ghaffour, Desalination 205(1), 340 (2007). https://doi.org/10.1016/j.desal.2006.03.558

20. M. Nair and D. Kumar, Desalination Water Treat. 51(10-12), 2030 (2013). https://doi.org/10.1080/19443994.2013.734483

21. J. E. Miller, Review of Water Resources and Desalination Technologies. Sandia National Labs Unlimited Release Report SAND-2003-0800 (2003).

22. P. Palomar and I. J. Losada, Desalination 255(1), 97 (2010). https://doi.org/10.1016/j.desal.2010.01.008

23. Joanna Kujawa, Sophie Cerneaux, Stanisław Koter, and Wojciech Kujawski. Highly Efficient Hydrophobic Titania Ceramic Membranes for Water Desalination. ACS Applied Materials & Interfaces 2014, 6 (16), 14223-14230. DOI: 10.1021/am5035297.

24. S. Rybar, M. Vodnar, F. L. Vartolomei, R. L. Méndez, and J. B. L. Ruano, Experience with Renewable Energy Source and SWRO Desalination in Gran Canaria - SP05-100 International Desalination Association World Congress (2005).

25. Global Water Intelligence/Water Desalination Report (GWI/WDR), 2015.

26. N. Ghaffour, T.M. Missimer, G.L. Amy, Technical review and evaluation of the economics of water desalination: current and future challenges for better water supply sustainability, Desalination 309 (2013) 197–207.

27. N. Voutchkov, Considerations for selection of seawater filtration pretreatment system, Desalination 261 (2010) 354–364.

28. L.O. Villacorte, A.A. Tabatabai, D.M. Anderson, G.L. Amy, J.C. Schippers, M.D. Kennedy, Seawater reverse osmosis desalination and (harmful) algal blooms, Desalination 360 (2015) 61-80.

29. T.M. Missimer, N. Ghaffour, A.H.A. Dehwah, R.G. Maliva, G. Amy, Subsurface intakes for seawater reverse osmosis facilities: capacity limitation, water quality improvement, and economics, Desalination 322 (2013) 37–51.

30. K. Rahmawati, N. Ghaffour, C. Aubry, G.L. Amy, Boron removal efficiency from Red Sea water using different SWRO/BWRO membranes, J. Membr. Sci. 423-424 (2012) 522-529.

31. http://www.iwa-network.org/desalination-past-present-future/ Last Login Date: 18.11.2019

32. Abdulkerimov S.A., Bogdanov V.P., Godin S.M. Experimental studies of the energy-informational effects of radiation of a longitudinal electromagnetic wave generator with water // Electrodynamics and microwave and high-frequency technology, No. 3 (8) / 2000.

33. Schaschke C., 2014. A Dictionary of Chemical Engineering. Oxford University Press.

34. Distillation: The Historical Symbol of Chemical Engineering. (2019) The University of Toledo. URL https://www.utoledo.edu/engineering/chemical-engineering/distillation.html.

35. Products made from petroleum. Ranken Energy Corporation. 2017. URL https://www.ranken-energy.com/index.php/products-made-from-petroleum/.

36. Mosin O.V. Magnetic water treatment systems. The main prospects and directions // Plumbing, No. 1. 2011.

37. Jovan Kamcev, Donald R. Paul, Gerald S. Manning, Benny D. Freeman. Ion Diffusion Coefficients in Ion Exchange Membranes: Significance of Counterion Condensation. Macromolecules 2018, 51 (15), 5519-5529. DOI: 10.1021/acs.macromol.8b00645.

38. Ryan S. Kingsbury, Sophie Flotron, Shan Zhu, Douglas F. Call, Orlando Coronell. Junction Potentials Bias Measurements of Ion Exchange Membrane Permselectivity. Environmental Science & Technology 2018, 52 (8), 4929-4936. DOI: 10.1021/acs.est.7b05317

39. Zhen Zhang, Xin Sui, Pei Li, Ganhua Xie, Xiang-Yu Kong, Kai Xiao, Longcheng Gao, Liping Wen, and Lei Jiang . Ultrathin and Ion-Selective Janus Membranes for High-Performance Osmotic Energy Conversion. Journal of the American Chemical Society 2017, 139 (26), 8905-8914. DOI: 10.1021/jacs.7b02794

40. https://www.amtaorg.com/Water_Desalination_Processes.html. Last Login Date: 18.11.2019

41. Ying Mei, Lei Liu, Yi-Chun Lu, Chuyang Y. Tang. Reverse Electrodialysis Chemical Cell for Energy Harvesting from Controlled Acid–Base Neutralization. Environmental Science & Technology 2019, 53 (8), 4640-4647. DOI: 10.1021/acs.est.8b06361.

42. Panagopoulos, Argyris; Haralambous, Katherine-Joanne; Loizidou, Maria (2019-11-25). "Desalination brine disposal methods and treatment technologies - A review". Science of the Total Environment. 693: 133545. Bibcode:2019ScTEn.693m3545P. doi:10.1016/j.scitotenv.2019.07.351. ISS N 0048-697. PMID 31374511.

43. Eugene S. Beh, Michael A. Benedict, Divyaraj Desai, Jessy B. Rivest. A Redox-Shuttled Electrochemical Method for Energy-Efficient Separation of Salt from Water. ACS Sustainable Chemistry & Engineering 2019, 7 (15) , 13411-13417. DOI: 10.1021/acssuschemeng.9b02720.

44. Warsinger, David M.; Tow, Emily W.; Nayar, Kishor G.; Maswadeh, Laith A.; Lienhard V, John H. (2016). "Energy efficiency of batch and semi-batch (CCRO) reverse osmosis desalination". Water Research. 106: 272–282.

45. Amanda N. Quay, Tiezheng Tong, Sara M. Hashmi, Yu Zhou, Song Zhao, Menachem Elimelech.Combined Organic Fouling and Inorganic Scaling in Reverse Osmosis: Role of Protein–Silica Interactions. Environmental Science & Technology 2018, 52 (16), 9145-9153. DOI: 10.1021/acs.est.8b02194

46. Dipak Ankoliya, Bhargav Mehta, Hiren Raval. Advances in surface modification techniques of reverse osmosis membrane over the years. Separation Science and Technology 2019, 54 (3), 293-310. DOI: 10.1080/01496395.2018.1483404.

47. Yanmei Jiao, Chun Yang, and Yuejun Kang. Energy Conversion from Salinity Gradients by Forward Osmosis–Electrokinetics. The Journal of Physical Chemistry C 2014, 118 (20), 10574-10583. DOI: 10.1021/jp412032b

48. Williams P, Ahmad M, Connolly B, Radcliffe D. Technology for freeze concentration in the desalination industry. Desalination 2015; 356: 314–327.

49. Kuichang Zuo, Zhen Wang, Xi Chen, Xiaoyuan Zhang, Jiaolan Zuo, Peng Liang, and Xia Huang . Self-Driven Desalination and Advanced Treatment of Wastewater in a Modularized Filtration Air Cathode Microbial Desalination Cell. Environmental Science & Technology 2016, 50 (13) , 7254-7262. DOI: 10.1021/acs.est.6b00520.

50. O. K. Buros, The ABCs of Desalting Topsfield, MA: International Desalination Association, (2000). pp. 30

51. Chanhee Boo, Seungkwan Hong, Menachem Elimelech. Relating Organic Fouling in Membrane Distillation to Intermolecular Adhesion Forces and Interfacial Surface Energies. Environmental Science & Technology 2018, 52 (24), 14198-14207. DOI: 10.1021/acs.est.8b05768.

52. Nick Guan Pin Chew, Shanshan Zhao, Rong Wang. Recent advances in membrane development for treating surfactant- and oil-containing feed streams via membrane distillation. Advances in Colloid and Interface Science 2019, 273, 102022. DOI: 10.1016/j.cis.2019.102022.

53. J. Hou, G. Dong, Y.Ye, V. Chen, Enzymatic degradation of bisphenol-A with immobilized laccase on TiO_2 sol-gel coated PVDF membrane. Membrane Science. 2014. 19–30

54. A.W. Mohammad, Y.H. Teow, W.L. Ang etc. Nanofiltration membrane review: Recent advances and future prospects. Desalination. 2015. 226–254.

55. Maria del Rayo Chavez-Castillo, Mario Alberto Rodríguez-Meza and Lilia Meza-Montes. Graphene and Silicene: a new life thanks to the subtlety of two-dimensional materials. Science. 2003. 148-152.

56. Arash Aghigh, Vahid Alizadeh, H.Y. Wong etc. Recent advances in utilization of graphene forfiltration and desalination of water. Desalination. 2015, 389–397

57. Wang, E. N. & Karnik, R. Water desalination: Graphene cleans up water. Nat. Nanotechnol. 7, 552-554 (2012).

58. Rasel Das, Md. Eaqub Ali, SharifahBeeAbdHamid etc. Carbon nanotube membranes for water purification: A bright future inwater desalination. Desalination. 2014, 97–109.

59. Veera Gnaneswar Gude. Desalination and sustainability – An appraisal and current perspective. Water Research. 2016, № 89. 87–106.

60. Water technology, 2015a. http://www.water-technology.net/projects/-ras-al-khairdesalinationplant/

61. Water technology, 2015b. http://www.water-technology.net/projects/perth

62. Weiwei Mo, Ranran Wang, and Julie B. Zimmerman. Energy–Water Nexus Analysis of Enhanced Water Supply Scenarios: A Regional Comparison of Tampa Bay, Florida, and San Diego, California. Environ. Sci. Technol., 2014, 48 (10), p. 5883–5891.

63. Water technology, 2015c http://www.water-technology.net/projects/tampa Last Login Date: 18.11.2019

64. Ioannis Karagiannis, Petros G. Soldatos Water Desalination Cost Literature: Review and Assessment (2008) Desalination 223(1-3):448-456 DOI:10.1016/j.desal.2007.02.071.

65. G. Fiorenza, V.K. Sharma and G. Braccio, Technoeconomic evaluation of a solar powered water desalination plant, Ener. Conv. Manag., 44 (2003) 2217–2240.

66. AMTA (American Membrane Technology Association), Desalting Facts: How Much Does Desalted Water Cost? (2001) Available: http://www.membranes-amta.org/media/pdf/desaltingcost.pdf. [2019, October 28].

67. D. Voivontas, K. Misirlis, E. Manoli, G. Arampatzis, D. Assimacopoulos and A. Zervos, A tool for the design of desalination plants powered by renewable energies, Desalination, 133 (2001) 175–198.

68. D. Zejli, R. Benchrifa, A. Bennouna and K. Zazi, Economic analysis of wind-powered desalination in the south of Morocco, Desalination, 165 (2004) 219–230.

69. Mohamed A. Dawoud, Mohamed M. Al Mulla Environmental Impacts of Seawater Desalination: Arabian Gulf Case Study // International Journal of Environment and Sustainability. Vol. 1 No. 3, pp. 22-37.

70. Seitzhanova M.A., Chenchik D.I., Yeleuov M.A., Mansurov Z.A., Capua R.D., Elibaeva N.S. Synthesis and characterization of graphene layers from rice husks // Chem Bull Kazakh Univ. 2018 2(89):12-18

71. Seitzhanova M.A., Mansurov Z.A., Chenchik D.I., Azat S., Jandosov J.M., Galin A.G. Obtaining graphene oxide from rice husk // 3rd International Conference on Surfaces, Coatings and Nanostructured Materials – ASIA, City University of Hong Kong, Hong Kong SAR, PR China. 4-7 December 2017. P. 21

72. Seitzhanova Makpal Azizovna, Yeleuov Mukhtar Auezovich, Chenchik Dmitry Ivanovich, Mansurov Zulkhair Aimuhametovich and Roberto Di Capua Synthesis of graphene from rice husk and its application as desalination membrane // 9th International Conference and Expo on Separation Techniques. September 13-14, 2018 | Zurich, Switzerland. p. 89

73. Seitzhanova M.A., Mansurov Z.A., Chenchik D.I., Roberto Di Capua Synthesis of graphene from rice husk and its application in desalination of seawater // Proceedings of III Conference of students and young scientists “Chemical physics and nanomaterials” dedicated to the memory of Mansurov Batyr. 15 March 2018. p. 36.

74. Seitzhanova M.A., Michela Alfe, Valentina Gargiulo, Luciano Cortese, Zulhair Mansurov, Roberto Di Capua Obtaining graphene-based membranes // X International Symposium «The physics and chemistry of carbon and nanoenergetic materials», September 12-14, 2018, Almaty, Kazakhstan, p. 37-40.

75. Seitzhanova M.A., Chenchik Dmitry Ivanovich, Mansurov Zulkhair Aimuhametovich, Roberto Di Capua Development of a method of obtaining graphene layers from rice husk // Functional nanostructures proceedings. 2018. p. 6-8

76. Seitzhanova M.A., Yeleuov Mukhtar, Mansurov Zulkhair Aimuhametovich, Valentina Roviello, Roberto Di Capua The characteristics of graphene obtained from rice husk and graphite // Eurasian Chemico-Technological Journal, 21 (2019) 149-156.

77. Utility Model Patent No. 4343. 2019 / 0426.2 dated 05/04/2019. A method of manufacturing membranes for desalinization based on graphene oxide. Seitzhanova M.A., Chenchik D.I., Yeleuov M.A., Mansurov Z.A., Capua R.D.

78. I. Pinnau, B.D.Freeman, Book "Membrane Formation and Modification", Publ. American Chemical Society, 2000, 376 p.

79. Yang Qin, Hu Yang, Zhenliang Xu, Feng Li Surface Modification of Polyacrylonitrile Membrane by Chemical Reaction and Physical Coating: Comparison between Static and Pore-Flowing Procedures // ACS Omega 2018, 3, 4, 4231-4241 Publication Date:April 16, 2018 https://doi.org/10.1021/acsomega.7b02094.

80. Shen, Y.; Zhao, P.; Shao, Q. Porous silica and carbon derived materials from rice husk pyrolysis char. Microporous Mesoporous Mater. 2014, 188, 46– 76, DOI: 10.1016/j.micromeso.2014.01.005.

81. Sukharnikov Yu., Efremova S. Obtaining a silicon-carbon composite and an organic product from rice husk and their application in various branches of technology and agriculture // Industry of Kazakhstan. - 2009. - No. 8. - S. 43-50.

82. Haoran Chen, Weixing Wang, Jarett C. Martin, Adam J. Oliphant, Paige A. Doerr and etc. Extraction of Lignocellulose and Synthesis of Porous Silica Nanoparticles from Rice Husks: A Comprehensive Utilization of Rice Husk Biomass // ACS Sustainable Chem. Eng. 2013, 1, 2, 254-259 Publication Date:December 17, 2012 https://doi.org/10.1021/sc300115r

83. Voronkov M.G., Zelchan G.I., Lukevits E.Ya. Silicon and life. Riga: Zinatne, 1978. 587 p.

84. Hongjun Chen, Guoping Wang, Xianguo Lu, Ming Jiang, Irving A. Mendelssohn Balancing the Needs of China's Wetland Conservation and Rice Production // Environ. Sci. Technol. 2015, 49, 11, 6385-6393 Publication Date:May 8, 2015 https://doi.org/10.1021/es505988z.

85. Efremova S. Structural transformations of rice husk and its constituent components during pyrolysis // Industry of Kazakhstan. 2008. No.8. p. 62-65;

86. Efremova S. Physico-chemical fundamentals and technology of rice husk processing. Almaty, 2011. 150 p.

87. Maria Irakli, Fotis Kleisiaris, Kalliopi Kadoglidou, Dimitrios Katsantonis. Optimizing Extraction Conditions of Free and Bound Phenolic Compounds from Rice By-Products and Their Antioxidant Effects. Foods 2018, 7 (6), 93. DOI: 10.3390/foods7060093.

88. Jandosov JM, Shikina NV, Bijsenbayev MA, Shamalov ME, Ismagilov ZR, Mansurov ZA (2009) Eurasian Chem Tech J 11:245-252

89. Wang J, Kaskel S (2012) J Mater Chem 22:23710-23725. http://doi.org/10.1039/C2JM34066F

90. James R. McBride, Andrew R. Lupini, Michael A. Schreuder, Nathanael J. Smith, Stephen J. Pennycook, Sandra J. Rosenthal Few-Layer Graphene as a Support Film for Transmission Electron Microscopy Imaging of Nanoparticles // ACS Appl. Mater. Interfaces 2009, 1, 12, 2886-2892 Publication Date:November 3, 2009 https://doi.org/10.1021/am900608j

91. Hanaor, D. A. H.; Ghadiri, M.; Chrzanowski, W.; Gan, Y. (2014). "Scalable Surface Area Characterization by Electrokinetic Analysis of Complex Anion Adsorption" (PDF). Langmuir. 30 (50):15143-15152. doi:10.1021/la503581e. PMID 25495551.

92. Rouquerol, J.; Llewellyn, P.; Rouquerol, F. (2007), "Is the bet equation applicable to microporous adsorbents?", Studies in Surface Science and Catalysis, Elsevier, 160, p. 49-56, doi:10.1016/s0167-2991(07)80008-5, ISBN 9780444520227

93. Sathre, Roger; Masanet, Eric (2013-03-18). "Prospective life-cycle modeling of a carbon capture and storage system using metal–organic frameworks for CO2 capture". RSC Advances. 3 (15): 4964. doi:10.1039/C3RA40265G. ISSN 2046-2069.

94. George Devitt, Kelly Howard, Amrit Mudher, Sumeet Mahajan Raman Spectroscopy: An Emerging Tool in Neurodegenerative Disease Research and Diagnosis // ACS Chem. Neurosci. 2018, 9, 3, 404-420 Publication Date:January 8, 2018 https://doi.org/10.1021/acschemneuro.7b00413

95. Yurii Stubrov, Viktor Gubanov, V. V. Strelchuk Manifestation of Structure of Electron Bands in Double-Resonant Raman Spectra of Single-Walled Carbon Nanotubes. (2019) Nanoscale Research Letters 11(1).

96. Ferrari AC, Meyer JC, Scardaci V, Casiraghi C, Lazzeri M, Mauri F, Piscanec S, Jiang D, Novoselov KS, Roth S, Geim AK (2006) Raman spectrum of graphene and graphene layers. Phys Rev Lett 97:187401

97. Aitor García-Ruiz, Sergey Slizovskiy, Marcin Mucha-Kruczyński, Vladimir I. Fal'ko Spectroscopic Signatures of Electronic Excitations in Raman Scattering in Thin Films of Rhombohedral Graphite // Nano Lett. 2019, 19, 9, 6152-6156 Publication Date:July 30, 2019 https://doi.org/10.1021/acs.nanolett.9b02196

98. Malard LM, Pimenta MA, Dresselhaus G, Dresselhaus MS (2009) Raman spectroscopy in graphene. Phys Rep 473:51–87

99. Prikhod'ko N.G., Mansurov Z.A., Auelkhankyzy M., Lesbaev B.T., Nazhipkyzy M., Smagulova G.T. Flame synthesis of graphene layers at low pressure // Russian Journal of Physical Chemistry B. – 2015. – Vol.9, Is.5. – P.743-747.

100. Umber Kalsoom, M. Shahid Rafique, Shamaila Shahzadi, Khizra Fatima, Rabia Shaheen Bi- tri- and few-layer graphene growth by PLD technique using Ni as catalyst // Materials Science-Poland, 35(4), 2017, pp. 687-693 http://www.materialsscience.pwr.wroc.pl/ DOI: 10.1515/msp-2017-0099.

101. Yingfang Xie, Jinglin You, Liming Lu, Min Wang, Jian Wang. Raman Spectroscopic Study of Coal Samples during Heating. Applied Sciences 2019, 9 (21), 4699. DOI: 10.3390/app9214699.

102. Raghavendra S. Hebbar, Arun M. Isloor, Balakrishna Prabhu, Inamuddin, Abdullah M. Asiri & A. F. Ismail Removal of metal ions and humic acids through polyetherimide membrane with grafted bentonite clay // SCIENTIFIC REPORTS | (2018) 8:4665 | DOI:10.1038/s41598-018-22837-1.

103. Nasseri S., Ebrahimi S., Abtahi M., Saeedi R. Synthesis and characterization of polysulfone/graphene oxide nano-composite membranes for removal of bisphenol A from water. J. Environ. Manag. 2018. 205:174–182. doi: 10.1016/j.jenvman.2017.09.074.

104. Akin I., Zor E., Bingol H., Ersoz M. Green Synthesis of Reduced Graphene Oxide/Polyaniline Composite and Its Application for Salt Rejection by Polysulfone-Based Composite Membranes. J. Phys. Chem. B. 2014 118:5707–5716. doi: 10.1021/jp5025894.

105. Emadzadeh D., Lau W.J., Matsuura T., Rahbari-Sisakht M., Ismail A.F. A novel thin film composite forward osmosis membrane prepared from PSf–TiO_2 nanocomposite substrate for water desalination. Chem. Eng. J. 2014 237:70–80. doi: 10.1016/j.cej.2013.09.081.

106. Clarice C. Leite, Alexandre de Jesus, Mariana L. Potes, Mariana A. Vieira, Dimitrios Samios, Márcia M. Silva Direct Determination of Cd, Co, Cu, Fe, Mn, Na, Ni, Pb, and Zn in Ethanol Fuel by High-Resolution Continuum Source Flame Atomic Absorption Spectrometry // Energy Fuels 2015, 29, 11, 7358-7363 Publication Date:October 20, 2015 https://doi.org/10.1021/acs.energyfuels.5b01796

107. Cong Qiuzi, Yu Xiang and He Li Fundamentals of X-Ray Phase Analysis. In book "Multifunctional Two- and Three-Dimensional Polycrystalline X-Ray Diffractometry" Pp. 34-41. DOI: 10.2174/978160805076511101010034 eISBN: 978-1-60805-076-5, 2011 ISBN: 978-1-60805-625-5

108. Griffiths P.; de Hasseth J. A. (18 May 2007). Fourier Transform Infrared Spectrometry (2nd ed.). Wiley-Blackwell. ISBN 0-471-19404-2.

109. Socrates G. Infrared and Raman Characteristic Group Frequencies. Tables and Charts. Third Edition. John Wiley& Sons Ltd. 2001.

110. Amy M. Balija, Layne A. Morsch Inquiry-Based IR-Spectroscopy Activity Using iSpartan or Spartan for Introductory-Organic-Chemistry Students // J. Chem. Educ. 2019, 96, 5, 970-973 Publication Date:March 25, 2019 https://doi.org/10.1021/acs.jchemed.8b00456

111. Antonio B. Fuertes, Marta Sevilla Hierarchical Microporous/Mesoporous Carbon Nanosheets for High-Performance Supercapacitors // ACS Appl. Mater. Interfaces 2015, 7, 7, 4344-4353 Publication Date:February 12, 2015 https://doi.org/10.1021/am508794f

112. Ismagilov Z.R., Shalagina A.E., Podyacheva O.Yu., Ischenko A.V., Kibis L.S., Boronin A.I., Chesalov Y.A., Kochubey D.I., Romanenko A.I., Anikeeva O.B., Buryakov T.I., Tkachev E.N. // Carbon. 2009. V. 47. P, 1922.